Inaugural dissertation for
obtaining the doctoral degree of the
Combined Faculty of Mathematics,
Engineering and Natural Sciences of the
Ruprecht - Karls - University
Heidelberg

Presented by
M. Sc. Karel Mocaer
Born in Paris, France
Oral examination 7th of December 2023

Ultrastructural characterization of dinoflagellates from heterogeneous marine environmental samples

Referees:
Prof. Dr. Gáspár Jékely
Dr. Rainer Pepperkok

Acknowledgments

First of all I would like to thank my supervisor Yannick Schwab for giving me the opportunity to work on a fascinating project, and for the support he gave me during these years as a PhD student. I feel privileged to have had the chance of learning from your wide expertise and discovering the new field of environmental science by your side.

Thank you, to my thesis committee for their guidance and valuable advice on my project throughout these last years.

I would like to thank the past and present members of my lab as well as members of the EMCF. I will forever treasure the expertise, openness and support from everyone I met here. I have been truly inspired by these teams. I simply loved learning from the scientific discussions we had over the last years.

Thank you, Nicole Schieber, for introducing me to sample preparation and so many techniques. Thank you as well for the help during COVID times. Thank you, Rachel Templin, for showing me so many things in the lab, from mounting samples for X-ray to discussing vEM and sample preparation. Thank you Rosa Pipitone, for helpful discussions and introducing me to Amira which I used so often during my thesis. Thank you, Kimberly Meechan, for showing me how the automatized microtome works, introducing me to MOBIE and to the SSP Club to make music at EMBL. I want to thank Christan Tischer as well for helping out with MOBIE.

I want to thank Julian Hennies, for his support during his time in the lab as well as now in the IC. I learned not to fear getting into code from you, I'm very thankful for it.

I want to thank Anna Steyer. Your support during the expeditions was incredible, I loved teaming up with you. Thank you for the advice and support outside of expeditions as well.

I want to thank Hiral Shah, Daniel Yee and Chandni Bhickta, I really enjoyed our plankton discussions both in the lab and on the field.

Thank you, Hannah Fleckenstein and Marianne Beckwith, for our scientific and other discussions, I really enjoyed our short routine of small forest walks. Thank you, Nadezda Matzko, I won't forget our discussions in the lab and really enjoyed them.

I want to particularly thank Paolo Ronchi, who taught me about so many aspects of electron microscopy and vEM, and who guided me through the discovery of targeted CLEM. I want to thank Viola Oorschot as well, with whom I discovered the wonders of SEM and Tokuyasu, and so much more. I also want to thank Martin Schorb for all his help with the computational aspects, as well as for teaching me so much about the TEMs.

I want to thank Giulia Mizzon, for showing me so many software features and our discussions about science and art.

I want to thanks Rachel Mellwig for your advice every day in the lab and very nice discussions. Thank you Mandy Boermel, for helping me learn sectioning and showing me how to make formvar grids, these steps were crucial and I really enjoyed learning from you.

A huge thank you to Inés Romero Brey for the amazing support provided both scientifically and personally. Thank you for your contagious enthusiasm, high motivation and precious help.

I want to thank members of the ALMF and in particular Manuel Gunkel, Aliaksandr Halavatyi and Stefan Terjung for their precious help and advice.

I want to thank Johan Decelle, Charlotte le Kieffre, Fabien Chevalier for teaching me many aspects of environmental samplings, support during the expeditions and great discussions about planktonic life. Thank you, Benoit Gallet for teaching me about EM, I really enjoyed learning from you. Furthermore, I want to thank you again for sharing your protocols, they were very important for this thesis.

I would like to thank the marine stations and their teams that welcomed us when we came sampling, as well as the sampling teams and organizers involved in the four expeditions I participated in. Thanks as well to Nikolaus Leisch for great discussions and help.

I would like to thank Robert Kirmse and his colleges as well as the team of Nicole Dubilier for their help in bringing the HPFs to the sea.

I would also like to thank Martin Fritsch for introducing me to the many possibilities available when using the Leica Stellaris system.

I want to thank my PhD batch for being full of amazing people and scientists, that formed a community even when COVID times made it complicated. Particularly I want to thank Julia, Martin and Mukthi. I also want to thank Dewi.

I want to thank the teams of IT and SIMG for their support during these years at EMBL.

I want to thank my family for being supportive and incredible throughout these years abroad that are not always easy.

Thank you, Theo, for being an incredible partner.

Summary (EN)

As a consequence of human impact, our planet is experiencing an alarming decline in biodiversity. However, estimating the extent of this loss is complex as many environments are still understudied to this day. While marine systems have been studied for decades, due to their incredible diversity and heterogeneity, our knowledge concerning their biology is still limited.

Microplankton are widely distributed across the photic layer of the oceans and are responsible for an important fraction of CO2 absorption and O2 production on earth through photosynthesis (C. Field et al., 1998). Furthermore, these organisms play a crucial role in the equilibrium of the marine food web. They thus have a central ecological importance for climate and ecosystems regulation. Studying environmental microplanktonic cells populating our oceans is crucial to better assess the range in their biodiversity, as well as to investigate further their biology, physiology, and their response to changing environments. Additionally, thus far, it is only possible to preserve a small fraction of marine microorganisms in the laboratory, and setting large scale environmental investigations is difficult.

In my thesis project, I first focused on setting a workflow that would enable a detailed ultrastructural analysis of microplankton from the field. I collected microorganisms at sea in the early morning and afternoon, starting with an unsorted community of species taken from a 5 to 40 µm size fraction. From such bulk samples, I focused on a subset of eukaryotic phytoplanktonic organisms, dinoflagellates, and studied their subcellular morphologies using Electron Microscopy (EM).

Using unbiased 2D EM screens, I built an image atlas that gathers ultrastructural details of all species collected during our field expeditions across morning and afternoon conditions. From this Transmission Electron Microscopy (TEM) screen, I could annotate classes of subcellular structures which seemed to be associated to certain genera or trophic modes. Furthermore, this screen enabled me to observe variations, at the population level, in the occurrence of a subset of organelles.

I then contributed in developing a light microscopy guided targeting strategy to perform volume EM imaging of a subset of organisms of interest from a heterogeneous environmental sample. Combining 2D and 3D EM modalities, I could work towards determining group-specific subcellular characteristics, and better understanding morphological variations existing in a

mixed population, or in targeted organisms, across an ecological gradient (morning and afternoon).

My work has set the ground for some projects of the ongoing large scientific expedition called TREC and I am very excited to see how my results and also those from my colleagues in the lab will contribute to a better understanding of the marine ecosystems and their response to changing environments.

Zusammenfassung (DE)

Als eine Folge des menschlichen Einflusses erlebt unser Planet eine alarmierende Abnahme an Biodiversität. Jedoch das Ausmaß dieses Verlustes zu schätzen ist sehr komplex, da viele Lebensräume bis heute zu wenig untersucht sind.
Obwohl marine Systeme seit Jahrzehnten untersucht werden, ist auf Grund ihrer unglaublichen Diversität und Heterogenität, unser Wissen über deren Biologie immer noch sehr limitiert.

Mikroplankton ist großflächig über die lichtdurchfluteten Schichten des Ozeans verteilt und für einen wichtigen Teil der CO_2-Absorption und O_2-Produtktion auf der Erde durch Photosynthese verantwortlich (C. Field et al., 1998). Außerdem spielen diese Organismen eine kritische Rolle im Equilibrium des marinen Nahrungsnetzes. Daher haben sie eine zentrale ökologische Bedeutung für die Regulation des Klimas und des Ökosystems. Das Untersuchen von umweltbedingten microplanktonischen Zellen, die unsere Ozeane bevölkern, ist entscheidend um besser deren Spektrum in der Biodiversität zu verstehen, sowie vertiefend ihre Biologie, Physiologie und ihre Reaktion auf sich verändernde Umweltbedinungen zu erforschen. Zusätzlich ist es bisher nur möglich eine kleine Anzahl an marinen Mikroorganismen im Labor zu kultivieren und groß angelegte Umweltuntersuchungen sind schwierig umzusetzen.

In meiner Doktorarbeit habe ich mich zuerst daruaf fokussiert einen Arbeitsablauf zu etablieren, der es mir erlauben würde, detaillierte ultrastrukturelle Analysen von Mikroplankton aus der Feldforschung durchzuführen. Hierfür habe ich Mikrooragnismen im Meer am frühen Morgen und am Nachmittag gesammelt, beginnend mit unsortierten Gemeinschaften von Spezies, welche aus der 5 bis 40 µm Partikelgröße gewonnen wurden. Von dieser Gesamtprobe habe ich mich auf einen Teil der eukaryotischen, phytoplanktonischen Organismen, Dinoflagellaten, fokussiert, und deren subzelulläre Morphologie mittels Elektronenmikroskopie (EM) studiert.

Mit Hilfe unvoreingenommener 2D EM Voruntersuchungen habe ich einen Bildatlas, welcher ultrastrukturelle Details von allen Spezies die während der Exkursionen sowohl unter den Bedingungen vormittags als auch nachmittags gesammelt wurden, aufgebaut. Von dieser transmissionselektronenmikroskopischen (TEM) Analyse konnte ich Klassen von subzellulären Strukturen, die zu bestimmten Gattungen oder trophischen Modi gehören

schienen, annotieren. Desweiteren hat es mir diese Voruntersuchung erlaubt Variationen, auf dem Populationslevel, an dem Auftreten eines Teils der Organellen, zu beobachten.

Ich habe danach dazu beigetragen eine lichtmikroskopisch geführte Targeting-Strategie zu entwickeln, um Volumen-EM Bildaufnahmen an einem Teil der Organismen aus einer heterogenen Probe aus der Umwelt durchzuführen. Die Kombination aus 2D und 3D EM Modalitäten, half mir gruppenspezifische subzelluläre Charakteristika herauszuarbeiten und ein besseres Verständnis der morphologischen Variationen in einer gemischten Population oder in einem bestimmten Organismus über einen ökologischen Gradienten (vormittags und nachmittags) zu verstehen.

Meine Arbeit hat die Grundlage für weitere Projekte im Zuge der großen wissenschaftlichen, aktuell laufenden Expedition, genannt TREC, geschaffen. Ich bin sehr gespannt zu sehen wie meine Resultate und die meiner Kollegen im Labor dazu beitragen werden ein besseres Verständnis der marinen Ökosysteme und deren Antwort auf die sich verändernde Umwelt zu schaffen.

Content

List of figures

III- Figure 7: Starch granules quantification and comparison between morning (AM) and afternoon (PM) samplings of 2020 and 2021.

III- Figure 8: Plastoglobuli quantification and comparison between morning (AM) and afternoon (PM) samplings of 2020 and 2021.

III- Figure 9: Occurrence analysis of a subset of organelles in dinoflagellates bearing plastids (phototrophic or mixotrophic, in red) or not (heterotrophic, in white).

III- Figure 10: Subset of organelles identified as associated to specific genus or species.

IV- Figure 1: Description of the workflow for vEM targeting of an environmental dinoflagellate.

IV- Figure 2: Identification of diverse organisms within the resin block.

IV- Figure 3: Targeting of a plastid bearing dinoflagellate from a heterogeneous mix of organisms.

IV- Figure 4: Overlay of the endogenous fluorescence and subcellular morphology.

IV- Figure 5: Thecal shape and ornamentation, visualized from the reconstruction of the segmentation of the vEM data and compared to SEM analysis of the same species.

IV- Figure 6: Thecal pores and trichocysts localization.

IV- Figure 7: Morphometrics of a subset of organelles from the targeted dinoflagellate.

IV- Figure 8: Nucleolar and chromosomal organisation within the nucleus.

IV- Figure 9: Organisation of the flagellar apparatus and eyespot.

IV- Figure 10: Crystalline inclusions distribution.

IV- Figure 11: Raw images from the FIB-SEM dataset showing the subcellular details of different organelles.

V- Figure 1: Morphometric analysis of a subset organelles from morning sampled and afternoon sampled *Prorocentrum cf. gracile.*

V- Figure 2: Morphometric analysis of a subset organelles from morning sampled and afternoon sampled *Triadinium cf. sphaericum*.

V- Figure 3: Distribution of plastoglobuli in *Prorocentrum cf. gracile* and *Triadinium cf. sphaericum* collected in the morning and the afternoon.

V- Figure 4: Morphometric analysis of a subset organelles from morning sampled and afternoon sampled *Pseudalatosphaera cf. corsica*.

V- Figure 5: Autofluorescence profile of the electron dense striated compartment of *Pseudalatosphaera cf. corsica*,

List of Tables

List of abbreviations

AMST	Alignment to Median Smoothed Template
CLEM	Correlative Light and Electron Microscopy
Cryo-EM	Cryo - Electron Microscopy
Cryo-SEM	Cryo - Scanning Electron Microscopy
EM	Electron Microscopy
EtOH	Ethanol
FIB-SEM	Focused Ion Beam - Scanning Electron Microscopy
FOV	Field Of View
h	hour
HPF	High-Pressure Freezing
LB	Longitudinal basal body
LM	Light Microscopy
LMR	Longitudinal Microtubular Root
LN2	Liquid Nitrogen
min	minute
ml	millilitre
NA	Numerical Aperture
NI	Non identified
nm	nanometer
OsO4	Osmium tetroxide
PAS	Periodic Acid Shift
PHEM	PIPES, HEPES, EGTA, magnesium (buffer composition)
Pg	Picogram
ROI	Region Of Interest
SEM	Scanning Electron Microscopy
SESI	Secondary Electron Secondary Ions
TB	Transversal basal body
TEM	Transmitted Electron Microscopy
TMR	Transversal Microtubular Root
TSMR	Transverse striated root and associated microtubule
vEM	volume Electron Microscopy
UA	Uranyl Acetate
µl	microliter
µm	micrometer

Chapter I: Introduction

In the latest years we became more and more aware of how anthropogenic changes are affecting our environment. Indeed, multiple reports concerning biodiversity loss have recently emerged (Desquilbet et al., 2020; Jandt et al., 2022). As a response, multidisciplinary efforts have, and are being developed, in order to record existing biodiversity and build solutions to preserve it (Sigwart et al., 2018). While some groups, or specific species have been described extensively, the vast majority of organisms are to this day understudied (Mora et al., 2011), making it difficult to fully apprehend the full extent of the biodiversity decline. This is easily explained by the complexity of setting large, in-depth, investigations on a broader range of organisms. However, based on the latest technological developments and high-throughput methods, these types of studies are becoming more conceivable.

In the last century, temporal studies have been performed thoroughly at marine stations and in the last decades, global taxonomic and diversity analysis have been deployed such as expeditions from the TARA Oceans project. Nonetheless, organisms from marine systems have been classified as not “poorly known” in the report from the symposium “Measuring Biodiversity and Extinction: Present and Past” (Sigwart et al., 2018). As for many other systems, studies on marine organisms have been mainly focused on specimens that could be maintained in laboratories or reliably isolated from the environment. These types of studies and generally research on axonic cultures are highly valuable as they allow to tackle a wide range of biological questions. However, as they are focused on a subset of organisms that can be preserved in the laboratory, this leads to knowledge gaps. Therefore, it is also of high importance to perform environmental studies even though they present great challenges due to the high complexity in setting these investigations, the important heterogeneity of the samples as well as the numerous variables existing in native ecosystems. However, even though these studies are difficult to set up, they are crucial to investigate more exhaustively, and in physiological conditions, marine organisms populating our ecosystems.

Starting this thesis, the aim was to study small marine microorganism from an environmental heterogeneous community at the ultrastructural level using a combination of different modalities. During the first sampling session in Villefranche-sur-Mer in 2020, I got captivated by a subset of organisms belonging to the infraphylum of dinoflagellates. Indeed, as for many others before me, these protists presenting an important diversity and complexity in their morphology, trophy and cell cycles particularities caught my attention. Furthermore, as these organisms present a high ecological relevance and were representing an important fraction of

the collected samples, they appeared as microorganisms of choice for this ultrastructural study.

In this introduction, I will first guide you through the definition and high importance of this group of organisms. Then, I will discuss more in details the history of dinoflagellates research and the implication of electron microscopy. Finally, I will provide information on the various subcellular characteristics of these microorganisms. Indeed, as this thesis has a strong focus on subcellular ultrastructure of dinoflagellates, reviewing the diverse organelles previously described in the literature is key. Furthermore, as I will later be discussing the possible association from a subset of subcellular compartments to specific genus, information about taxonomically indicative organelles which were formerly described will be indicated here. I strongly believe that a thorough understanding of their sub-cellular organisation will contribute to a better understanding of the key cellular functions that are centrale to the dinoflagellates' life.

1- General:

Dinoflagellates are eukaryotic organisms populating marine and freshwater ecosystems in free living, parasitic or symbiotic forms. These microorganisms have been populating the globe ubiquitously for more than 100 MY (Jeong et al., 2010). There are approximately 2000 species described, presenting a wide variety of morphologies (Fig. 1), life cycle specificities and trophic modes (Gomez, 2012; Taylor, 1987a) . In fact, approximately half of these microorganisms have been described as heterotrophs (devoid of chloroplasts). The other half, possessing chloroplast, or acquiring them more temporarily, has been described as phototrophs. While heterotrophs need external sources of nutrients such as preys to survive, phototrophs can gain energy from performing photosynthesis. Dinoflagellates presenting chloroplast and who are able to feed on preys simultaneously are called mixotrophs (Gomez, 2012).

These protists are ecologically important as they are contributing to primary production (Field et al., 1998), to the ocean carbon cycle and are key organisms in the marine food web (Jeong et al., 2010). Furthermore, a subset of dinoflagellates can be at the origin of harmful algal blooms, which can be devastating for the local ecosystems with strong economical consequences (Anderson et al., 2008). Additionally, some dinoflagellates are forming mutualistic symbiosis necessary for the survival of larger organisms such as coral reefs (Glynn, 1993).

To this day, only a small fraction of dinoflagellates has been deeply studied. This is partially originating from the complexity to maintain most of these organisms in culture (Dixon and Syrett, 1988; Oliveira et al., 2020). Thus, developing techniques to analyse samples directly from their environment, in combination to culture systems when possible, would be very powerful to better understand the biology of these highly important organisms.

The aims of this thesis were the following. First, to start building an ultrastructural atlas of dinoflagellates diversity by developing a workflow to deploy in the field and subsequently investigate the sub-cellular organisation of small marine dinoflagellates from their native environment using 2D TEM. Additionally, the goal was to study subcellular morphological variations, at the population level, across a gradient (here based on two different period of the daily light cycle). From this screen, another aim was to annotate described or undescribed organelles and to investigate the potential associations between certain ultrastructural characteristics and taxonomical identity. As it became of interest, after the 2D analysis, to perform a volumetric characterization of a subset of species, an additional aim was to develop a targeting strategy for vEM imaging based on the endogenous fluorescence signal of these organisms. After validation of this vCLEM targeting method, the goal was to perform vEM on a subset of organisms and to both study their sub-cellular organization and perform morphometric analysis on a subset of organelles. Importantly, one final aim is to make these datasets publicly available.

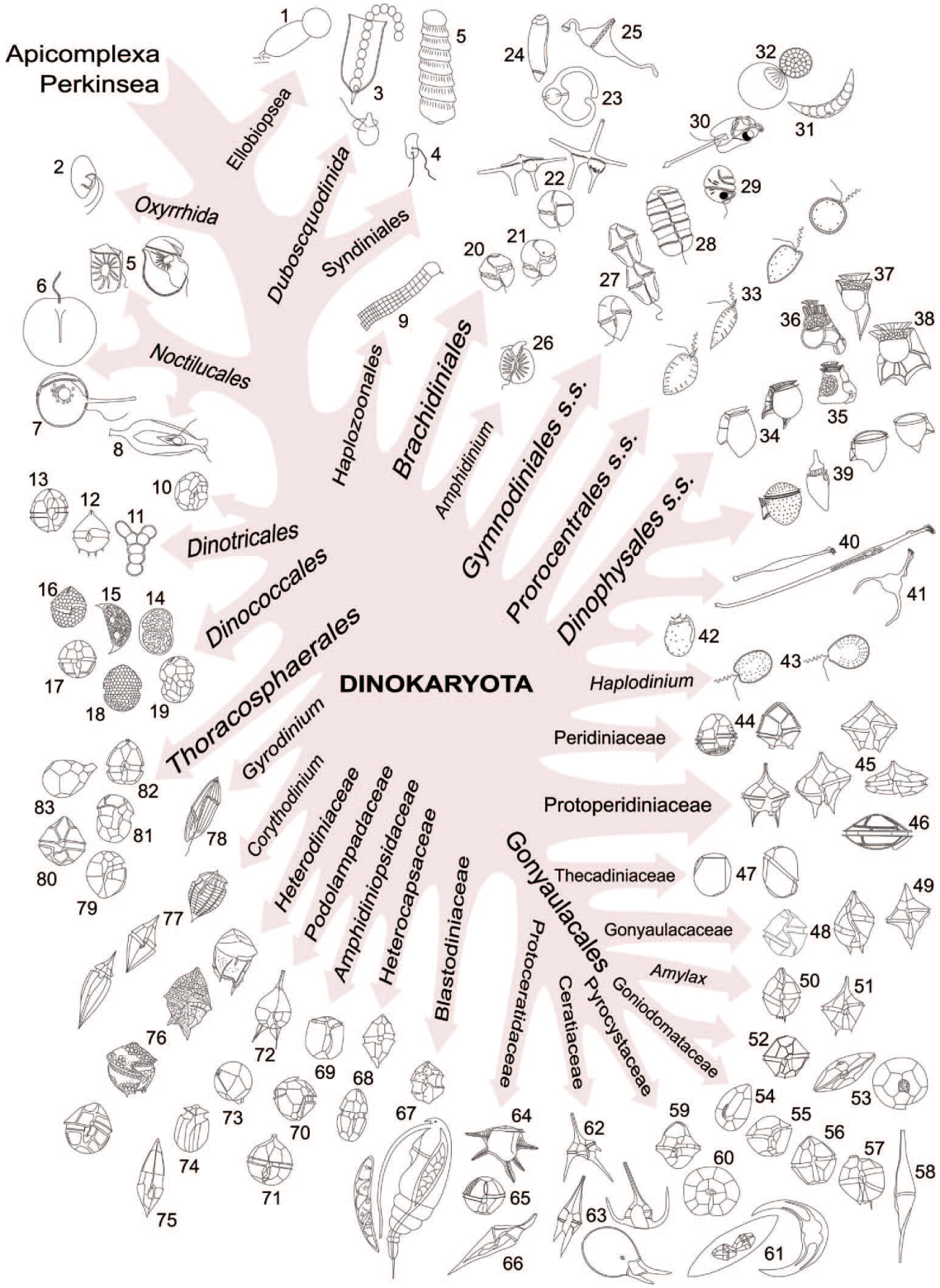

Figure 1: Principal lineages of dinoflagellates. 1) *Ellobiopsis*; 2) *Oxyrrhis*; 3) *Duboscquella*; 4) *Syndinium*; 5) *Kofoidinium*; 6) *Noctiluca*; 7) *Spatulodinium*; 8) *Scaphodinium*; 9) Haplozoon; 10)

Crypthecodinium; 11) *Dinothrix*; 12) *Peridinium quinquecorne*; 13) *Durinskia*; 14) *Phytodinium*; 15) *Cystodinium*; 16) *Borghiella*; 17) *Sphaerodinium*; 18) *Biecheleria*; 19) *Symbiodinium*; 20) *Takayama*; 21) *Karlodinium*; 22) *Brachidinium*; 23) *Pseliodinium*: 24) *Torodinium*; 25) *Gynogonadinium*; 26) *Amphidinium*; 27) *Gymnodinium*; 28) *Polykrikos*; 29) *Warnowia*; 30) *Erythropsidinium*; 31) *Dissodinium*; 32) *Chytriodinium*; 33) *Prorocentrum* s.s); 34) *Dinophysis*; 35) *Citharistes*; 36) *Histioneis*; 37) *Parahistioneis*; 38) *Ornithocercus*; 39) *Phalacroma*; 40) *Amphisolenia*; 41) *Triposolenia*; 42) *Sinophysis*; 43*) Exuviaella/Haplodinium*; 44) *Peridinium s.s.*; 45) *Protoperidinium s.s.;* 46) *Diplopsalis*; 47) *Thecadinium*; 48) *Gonyaulax*; 49) *Spiraulax*; 50) *Lingulodinium*; 51) *Amylax*; 52) *Goniodoma*; 53) *Gambierdiscus*; 54) *Ostreopsis*; 55) *Coolia*; 56) *Alexandrium*; 57) *Pyrodinium*; 58) *Centrodinium*; 59) *Fragilidium*; 60) *Pyrophacus*; 61) *Pyrocystis*; 62) *Ceratium*; 63) *Neoceratium*; 64) *Ceratocorys*; 65) *Protoceratium*; 66) *Schuettiella*; 67) *Blastodinium*; 68) *Heterocapsa*; 69) *Amphidiniopsis*; 70) *Herdmania*; 71) *Archaeperidinium*; 72) *Podolampas*; 73) *Blepharocysta*; 74) *Roscoffia*; 75) *Lessardia*; 76) *Heterodinium*; 77) *Corythodinium*; 78) *Gyrodinium*; 79) *Hemidinium*; 80) *Glenodinium*; 81) *Pfiesteria*; 82) *Scrippsiella*; 83) *Oodinium*. Figure from Gomez., 2012 and adapted from Taylor., 1987.

2- History

As they are ecologically highly relevant and possess atypical characteristics, dinoflagellates have been studied for close to two centuries. Indeed, their earliest description appeared in the 1750's by Baker, describing *Noctiluca*, a dinoflagellate known for its bioluminescence properties. From then on, multiple scientists started recording the occurrence of these protists. Among the numerous contributions made on dinoflagellates research, Christian Gottfried Ehrenberg, from 1828 and throughout his carrier, described an abundant number of common species and proposed multiple new genera, including the vast genus of *Peridinium*.

The study of dinoflagellates was soon accelerated by the developments of light microscopy in the 1880's. Across the world, multiple scientists started precise descriptions of these microorganisms, noting their morphological and life cycle specificities. The need for classification to synergize these studies soon appeared, and taxonomic groups based on morphological observation were created.

Some dinoflagellates present a theca, this cell wall shows a combination of thecal plates called tabulation. The tabulation has been historically used for taxonomical assignment of organisms to specific species. The first to consistently use thecal plates organisation as a taxonomic feature was Stein in 1883. From this tendency of using tabulation as taxonomical traits, different systems for classification based on the plate or amphiesmal vesicle arrangement

emerged. The Kofoid system (Kofoid, 1907; Kofoid, 1909) is one reference that became universally used for gonyaulacoids and peridinioids (Fig. 2C-D), and presents a nomenclature based on number and shapes of latitudinal series of plates.

The first EM studies on dinoflagellates were performed in the 1950's on the flagella (Pitelka and Schooley, 1955), theca (Braarud et al., 1958; Fott and Ludvik, 1956) and chromosomes (Grassé and Dragesco, 1957; Grell and Wohlfarth-Bottermann, 1957). The later, because of its unique structure, led to further studies of member of this group. As a consequence, culture systems got further developed leading to life cycle descriptions.

In parallel to TEM studies, Scanning Electron Microscopy (SEM) studies of dinoflagellates started to develop. Using SEM, it became evident that tabulation could be elucidated with very high precision (Taylor, 1971). This led to a broader use of SEM, and ultimately to its use as a tool of reference for species identification.

Since the 1960s, there have been many studies of dinoflagellates ultrastructure using EM. Over the past decades, TEM and SEM analysis, in combination with molecular studies, have been included quite systematically for the description of new species (Jang et al., 2019; Jeong et al., 2014; Kang et al., 2014). Recently, studies including volume EM datasets of dinoflagellates are also arising (Decelle et al., 2021; Decelle et al., 2022; Gavelis et al., 2017; Gavelis et al., 2019; Mocaer et al., 2023; Uwizeye et al., 2021). All of these ultrastructural analyses contributed to a better understanding of the biology of these microorganisms. You will find here descriptions of dinoflagellates' striking organelles, which were reviewed from the ultrastructural studies performed until now.

3- Specific morphological characteristics

3.1- Cell covering

As mentioned above, through time, classification of motile unicellular microorganisms has been based on their outer cell morphology. Dinoflagellates belong to the clade of alveolates, and one common feature of this clade is the presence of flattened vesicles under their cell membrane. In dinoflagellates, these vesicles are referred to as "amphiesmal vesicles" and their cellular membrane is called the "plasmalemma".

The amphiesmal vesicles may contain cellulose-like plates, forming the theca (Loeblich, 1970), or can be devoid of cellulosic material. The presence or absence of these plates is

used for taxonomical identification. Either cells are considered “naked”/”athecate” or “armoured”/”thecate” if they possess cellulosic material within their amphiesmal vesicles. Microtubule are usually visible under the amphiesmal vesicles. The role of these peripheral microtubules has been previously hypothesized to help in maintaining cell shape (Morrill and Loeblich, 1983) and to have a role in thecal development by allowing the migration of immature amphiesmal vesicles (Bricheux et al., 1992) or through potential interaction with the cellulose synthase complex (Kwok and Wong, 2003). More recently, Kwok et al., 2023 added that these microtubules could contribute to the mechanical sensitivity of the cell, as for instance to perceive directional flows (Maldonado and Latz, 2007). The theca provides mechanical protection to the cell (Kwok et al., 2023).

Six main tabulation types are now recognized (Fig. 2), namely:

- Gymnodinoid (Fig. 2A): tabulation for naked dinoflagellates where the amphiesmal vesicles are numerous, often hexagonal, located randomly or in latitudinal series >10. The alveolae series are clearly distinguishable only in the sulcus and cingulum area.
- Suessioid (Fig. 2B): the thecal plates are fine and arranged in 6 to 11 latitudinal series. The cingulum is well defined.
- Peridinoid and Gonyaulacoid (Fig. 2C-D): the thecal plates are arranged in 5 latitudinal series and present additional cingular and sulcal series. These cells usually show an apical pore complex. Differently to the gonyaulacoid, peridinoid cells usually have a symmetrical first apical plate and possess two antiapical plates.
- Dinophysioid (Fig. 2E): there are two main thecal plates, joining through a vertical suture. However, the cingulum and sulcus are present.
- Prorocentroid (Fig. 2-F): these cells don’t present a cingulum, nor a sulcus. There are mainly presenting two large thecal plates, linked by a sagittal suture. Additionally, there is a series of small plates around the pore where the flagella are apically inserted, called periflagellar platelets.

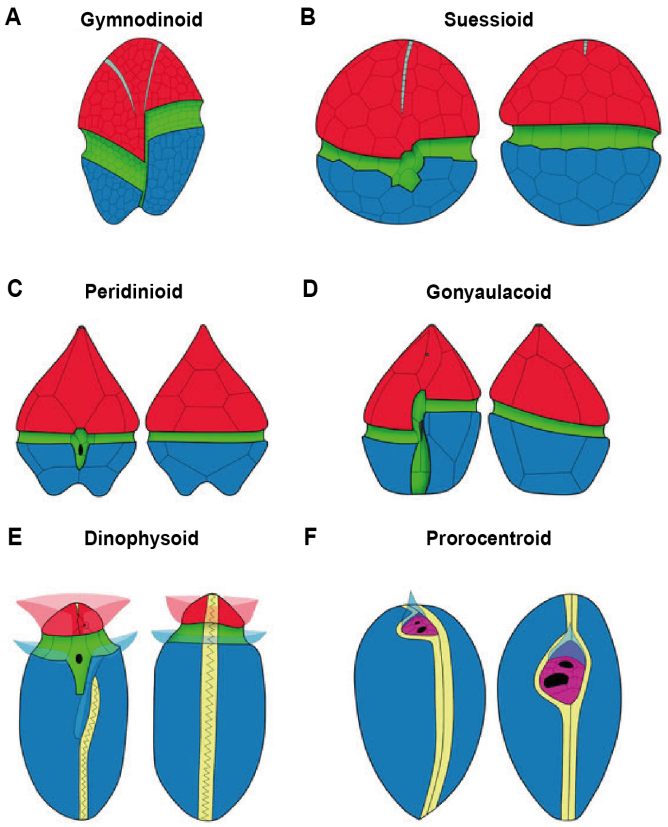

Figure 2: Tabulation types. A) Gymnodinoid, ventral view. B) Suessoid, ventral (left) and dorsal view (right). C) Peridinioid, ventral (left) and dorsal view (right). D) Gonyaulcoid, ventral (left) and dorsal view (right). E) Dinophysoid, ventral (left) and dorsal view (right). F) Prorocentroid, ventral (left) and apical view (right). A-F) The epicone/epitheca is shown in red and the hypocone/ hypotheca is shown in blue for respectively athecate and thecate dinoflagellates. A-E) In green are shown the sulcus and cingulum grooves. A) In light blue the apical suture complex is shown. B) In light blue the apical furrow apparatus of Suessioid taxa is shown, E-F) In yellow are shown the sagittal suture. F) In pink are shown the small thecal plates in the flagellar insertion region. Adapted from Hoppenrath., 2017 and the tabulation figure on dinophyta.org, from Mona Hoppenrath.

3.1.1 Thecate dinoflagellates

For the “armoured” dinoflagellates, the number, shape and organization of their thecal plates allows to distinguish species. These arrangements, called tabulation patterns permit further classification. Depending on the genus, the thecal plates can range in thickness drastically, acting as an additional indicator for classification. Interestingly, a correlation has been observed between the number of plates and their thickness. Indeed, the more numerous plates there are, the thinner they are and inversely (Dodge and Crawford, 1970a; Taylor, 1980). Furthermore, within a genus, the thecal pore distribution as well as the ornamentation will also constitute an extra indicator for species determination (Dodge and Crawford, 1970a), as shown for instance in species from the genus *Prorocentrum* (Hoppenrath et al., 2013, Fig. 3). Interestingly, maturational changes of the theca have been observed, and newly produced

theca often lack ornamentation (Taylor, 1987a). The pores on the other hand, have been shown to be present from the initial theca formation (Taylor, 1973).

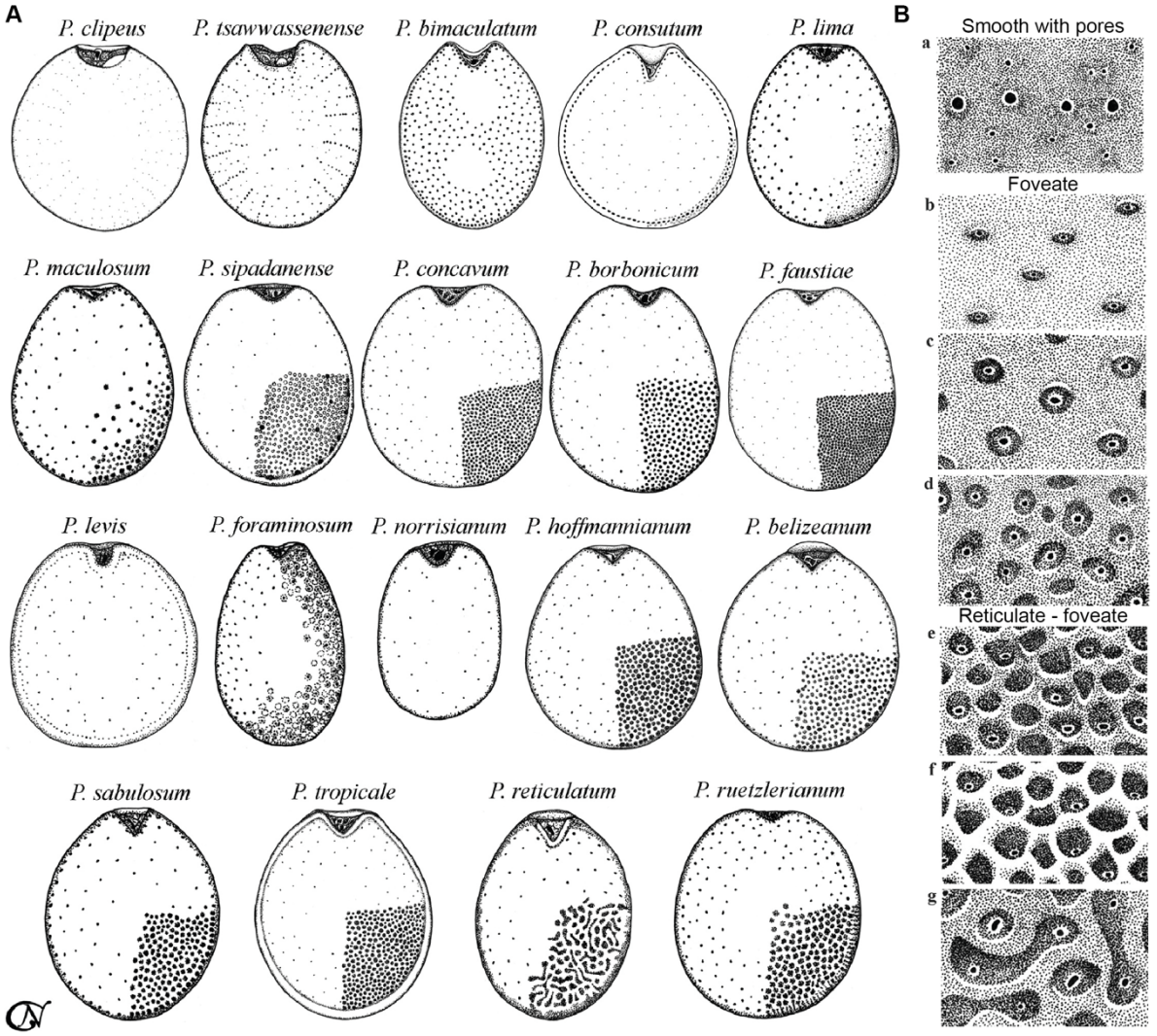

Figure 2: Overview of various morphological specificities among the genus *Prorocentrum.* A) Right lateral view of the theca of diverse *Prorocentrum* species showing the thecal global shape, pore distribution, ornamentation and shape of the periflagellar region. B) Different thecal ornamentation existing in the genus *Prorocentrum*. a) Smooth theca with pores, b-d) Different degrees of foveate ornamentation of the theca, e-f) Various shapes of ornamentation combining reticulate and foveate forms. Figure adapted from Hoppenrath et al., 2013.

3.1.2 Athecate dinoflagellates

Dinoflagellates that present very thin of no material within their amphiesmal vesicles are called “athecate”.

3.1.3 Other type of cell covering: pellicle and cyst wall

Dinoflagellates are known to present two main life stages, which are the motile phase and the resting phase. During the motile phase, for armoured cells, the cell wall is usually the theca.

Under stress conditions and/or upon formation of a cyst, certain cells can shed their theca and their outer amphiesmal layer along with their flagella. This phenomenon is called “Ecdysis” (Kofoid, 1908) and results in a non-motile cell surrounded by a membrane and a thin wall called “the pellicle” (Loeblich, 1970). The pellicle is constituted of an amorphous layer, continuously covering the cell surface (Loeblich, 1970).

Certain dinoflagellates are known to produce cyst forms. There are different types of cysts, which include temporary resting cysts, dormant zygotes (resting cysts) and coccoid cysts and fossilized cysts. These cysts can present a variety of cyst walls, with different compositions and that show highly diverse shapes. The cyst wall can range from a simple gelatinous layer in some athecate genera to more substantial cell walls. In the latter, the wall can be composed of 1 to 4 layers, one of each usually including a resistant material such as chitin in *Peridinium cinctum*, crystallin calcium carbonate in *Scrippsiella trochoidea* (Dürr, 1979; Wall et al., 1970).

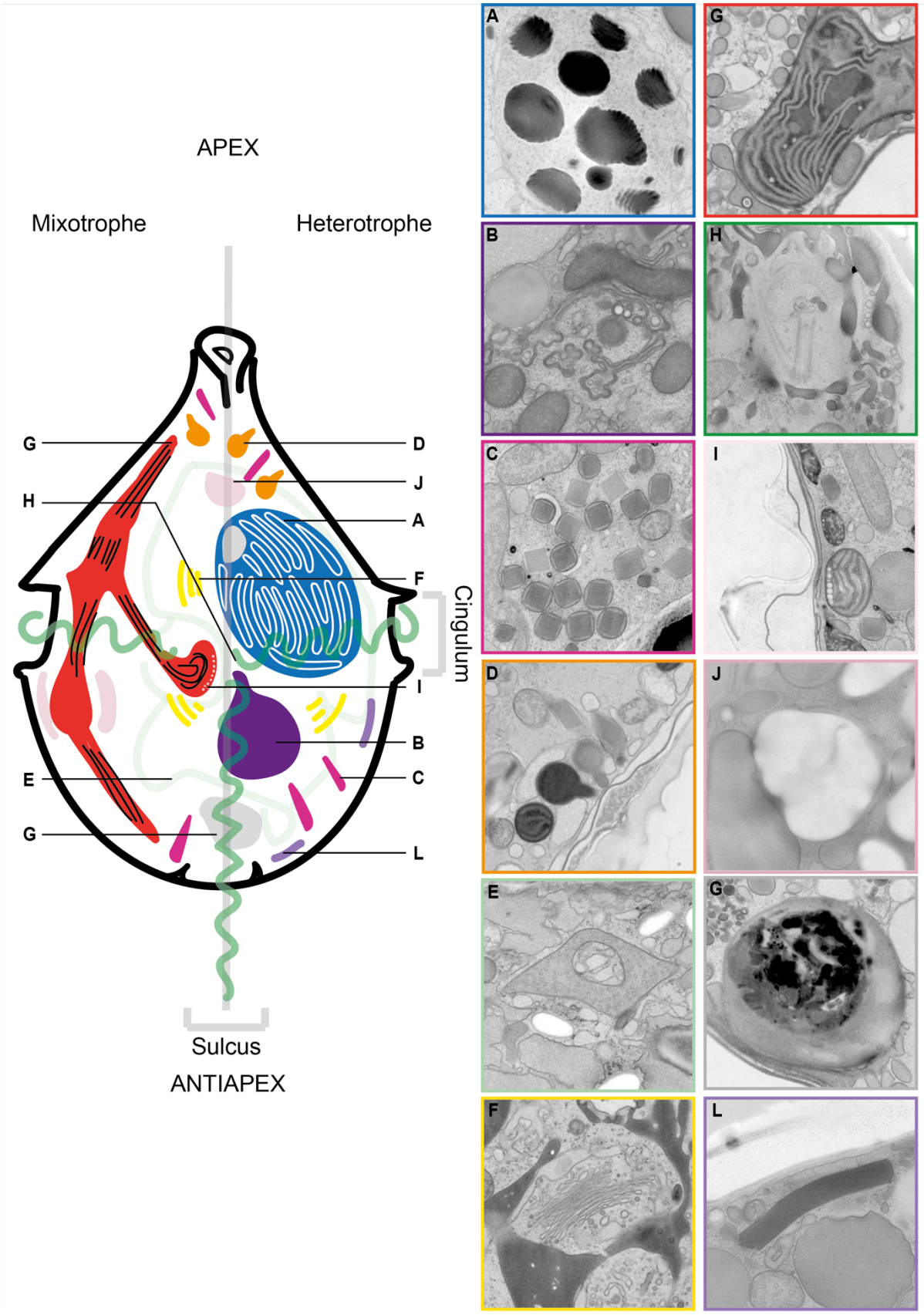

Figure 4: Overview of the general ultrastructure of mixotrophic and heterotrophic dinoflagellates. Phototroph microorganisms would fit in the mixotrophic part of the scheme (left) without the food vacuole (G, in grey). A) Nucleus, B) Pusule, C) Trychocyst, D) Mucocysts,

E) Mitochondrion, F) Golgi Apparatus, G) Chloroplast, H) Basal body / Flagellar insertion, I) Eyespot (Type 1A), J) Starch, K) Food vacuole, L) Electron dense rods

3.2- Nucleus

Dinoflagellates have a very peculiar nucleus called “dinokaryon” (Fig. 4A) that can contain large amounts of DNA ranging from 2.2-200 picogram (pg) depending on the species (Rizzo and Noodén, 1973). In comparison, a human endothelial cell contains around 5 pg of DNA (Gillooly et al., 2015). Their genome is packed in a large amount of chromosomes, indeed Bhaud et al., 2000 report the occurrence of 4 to 200 chromosomes in certain cells. These microorganisms generally possess chromosomes that remain condensed throughout the cell cycle, with the exception of some species as *Noctiluca scintillans* (Fukuda and Endoh, 2006) and *Blastodinium sp* (Skovgaard et al., 2012; Soyer, 1971). Furthermore, the chromosomes present liquid crystalline structure (Gautier et al., 1986; Livolant and Bouligand, 1978). Dinoflagellates can present one or multiple nucleolus. Note that the nucleolus is/are present throughout the cell division.

As the nuclear envelope remains intact during cell division, with the exception of *Oxyrrhis marina* presenting an internal spindle (Triemer, 1982), the chromosomes are segregated by an extranuclear spindle to the two daughter nuclei. Dinoflagellates chromosomes appear mostly devoid of typical histones and don’t present nucleosomes (Herzog and Soyer, 1981; Rizzo and Noodén, 1972), explaining their condensed structure. Interestingly, they present an important quantity of hydroxymethyluracil (Rae, 1976) in comparison to other eukaryotes.

Dinoflagellates have been shown to present nuclear pores, measuring around 100 nm in diameter (Spector, 1984). The size of this structure is close to observations made in human nuclear pore where there were reported to measure 1,200 Å (Kosinski et al., 2016; Lin et al., 2017). Interestingly, in some species of dinoflagellates nuclear pores are present in a higher density in regions close the nucleolus (Kalvelage et al., 2023).

3.3- Pusule

The pusule (Fig. 4B) is an organelle only found in dinoflagellates. It consists in a complex arrangement of tubules or chambers opening at the flagellar base or in the vicinity of the basal bodies. It is formed by an invagination of the plasma membrane and presents 1 or 2 additional characteristic membranes (Dodge, 1972). The function of this organelle is still being debated and has been proposed to be the localization for absorption of nutrient (Kofoid, 1909), for excretion (Chatton, 1970; Schütt, 1895), as an osmoregulatory organelle (Dodge, 1972; Klut

et al., 1986) or for flotation and diurnal vertical migration (Klut et al., 1986; Norris, 1966). Interestingly, morphological diurnal changes have been observed in different species (Biecheler, 1952). Klut et al., 1986 also showed morphological changes when varying the culture temperature or salinity. A comparative study between 40 freshwater and marine dinoflagellates from Dodge., 1972 allowed to identify 7 potential types of pusules that are mainly divided in two categories: (1) Pusule connected with the flagellar canal, collecting chamber or pustular tubes, (2) Pusule made of tubules or sac only. Abe, 1981 mentioned that a given group, section or subgenus is correlated with the different pusule morphologies.

3.4- Extrusomes

Extrusomes are defined as organelles that can excrete material outside of the cell. Dinoflagellates generally present two types of extrusomes namely “trichocysts” and “mucocysts”, which are described below. Additionally, a subset of species can present nematocysts, which are harpoon-like organelles.

3.4.1 Trichocysts

Trichocysts are rod like structures first described in ciliates (Allman, 1855) but also found in other groups of alveolates as dinoflagellates (Fig. 4C). These structures have been deeply studied in Paramecium, where their function as a local defensive mechanism has been demonstrated (Harumo and Miyake., 1991, Miyake et al., 1989). However, their function is to this day unknown in dinoflagellates. Nonetheless, these structures have been shown to be extruded from multiple species (Bouk et al., 1965, Messer., 1971, Westerman., 2015, Rhiel., 2018). Furthermore, these organelles have been hypothesised to be involved in protection, adhesion or predation mechanisms.

In their mature undischarged state, they are composed of two different regions, “the neck” linked to the thecal membrane as well as the core surrounded by a membrane (Fig. 5A). The neck presents a set of twisted fibres surrounding the beginning of the core and linking it to the thecal membrane. The main body has a square shape when cut orthogonally, and is composed of a proteinous structure that is packed in a paracrystalline array (Fig. 5A). The potential synthesis and “crystallisation” localisation are described by Bouk and Sweeney in 1965. Indeed, from 2D TEM studies they established that these organelles are originating from the Golgi apparatus (Fig. 5B).

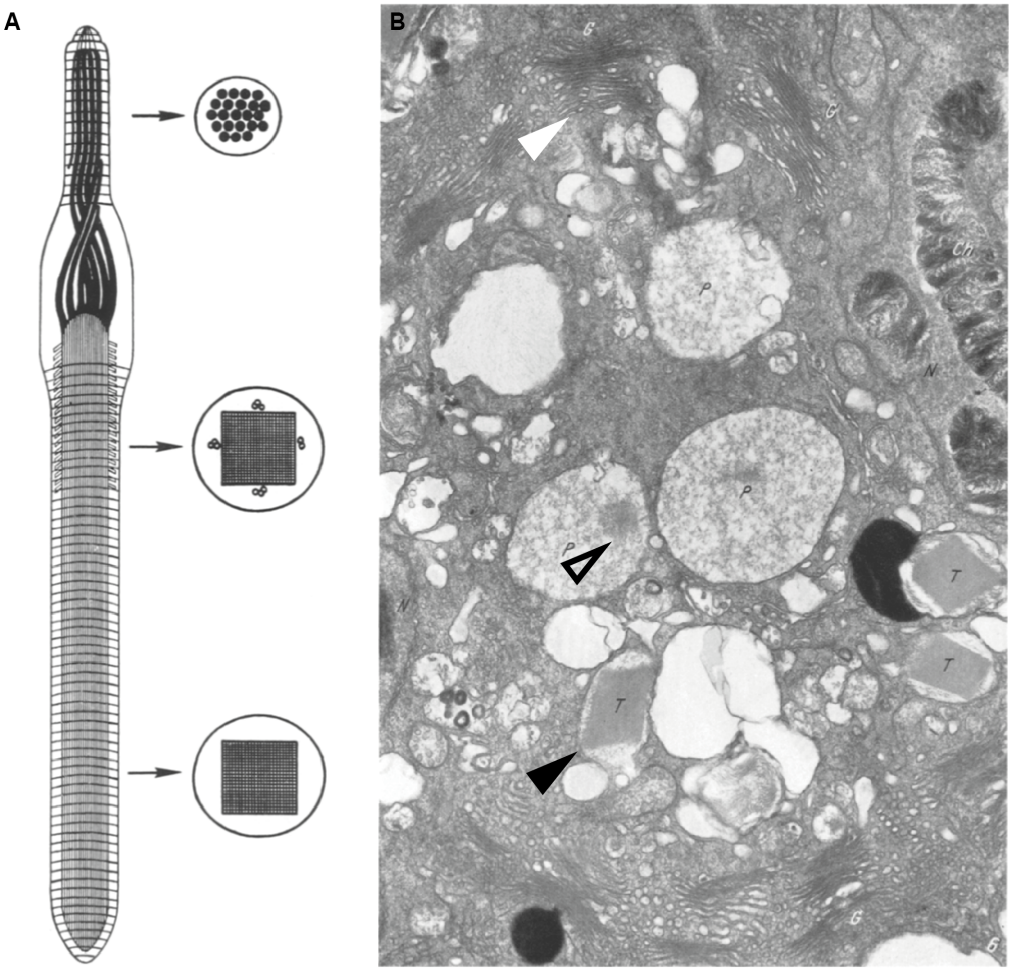

Figure 5: Mature undischarged trichocyst organisation and hypothetical site of formation. A) Scheme of the organisation of a mature trichocyst. On its upper part, the neck is shown and under it the core of this organelle. Multiple cross sections of different areas of the trichocyst are shown on the right side. B) Micrograph of the potential site of formation of trichocysts in *Lingulodinium polyedra* (= Formerly *Gonyaulax polyedra*). These structures are described to be formed in the Golgi region. The white arrow points at a Golgi Apparatus, the empty black arrow points at a trichocyst in formation and the full black arrow at a mature trichocyst. This figure was adapted from Bouck and Sweeney, 1966.

3.4.2 Mucocysts

Mucocysts are found in a number of protists including dinoflagellates (Fig. 4D, Fig. 6). They have been initially visualized using light microscopy, however a deeper characterization of these organelles was only possible with the development of electron microscopy.

In dinoflagellates, they are present most of the time within the cytoplasm or under the cellular envelope. These organelles are delimited by a single membrane, can present a polarity and are thought to excrete mucilaginous material (Cachon et al., 1975). These structures would origin from the Golgi apparatus or specific regions of the endoplasmic reticulum before

migrating to the cell cortex (Cachon et al., 1975). When they are present under the cell cortex, their material can be discharged when subjected to various stimuli (Haussmann, 1978). These organelles then get in contact with the plasma membrane upon secretion.

Mucocysts are described to possess diverse functions as for prey capture as in *Noctiluca scintillans* (=Formerly *Noctiluca miliaris*, Soyer, 1969; Soyer, 1970a; Soyer, 1970b), adhesion, or cohesion between cells in colonies (Cachon et al., 1975).

The mucocysts lumen can present a variety of structures (granular (Fig. 6A), fibrillar, fibrillo-granular (Fig. 6C,D) and paracrystalline (Fig. 6G) and multiple types of mucocysts can be present within one species (Cachon et al., 1975).

The mature granular mucocysts are described to present a pyriform shape and a size around 1 µm (Fig. 6A).

The fibrillo-granular mucocysts usually possess an amphora shape. In the neck of the mucocyst, some granular material has been observed (Fig. 6C,D). And, from this region, fibrillar components emerge and show an entangled pattern (Cachon et al., 1975; Dragesco and Hollande, 1965; Schütt, 1895).

The mucocyst presenting a paracrystalline partial or complete structure, observed in various species of peridinian can have a polyhedric structure (Fig. 6G) or be more circular. The paracrystalline structure is formed seemingly by dense filaments regularly organized in a staggered arrangement when cut orthogonally to the filament axis (Cachon et al., 1975). Vesicles measure around 20 µm in diameter containing paracrystalline structure of this type have also been described by Lee in 1977 in *Gyrodinium lebouriae*. Cachon et al., 1975, performed PATAG treatment on these types of structures to investigate their potential polysaccharidic nature. However, these structures were not stained using this technique leading them to hypothesize the proteinic nature of these paracrystalline structures.

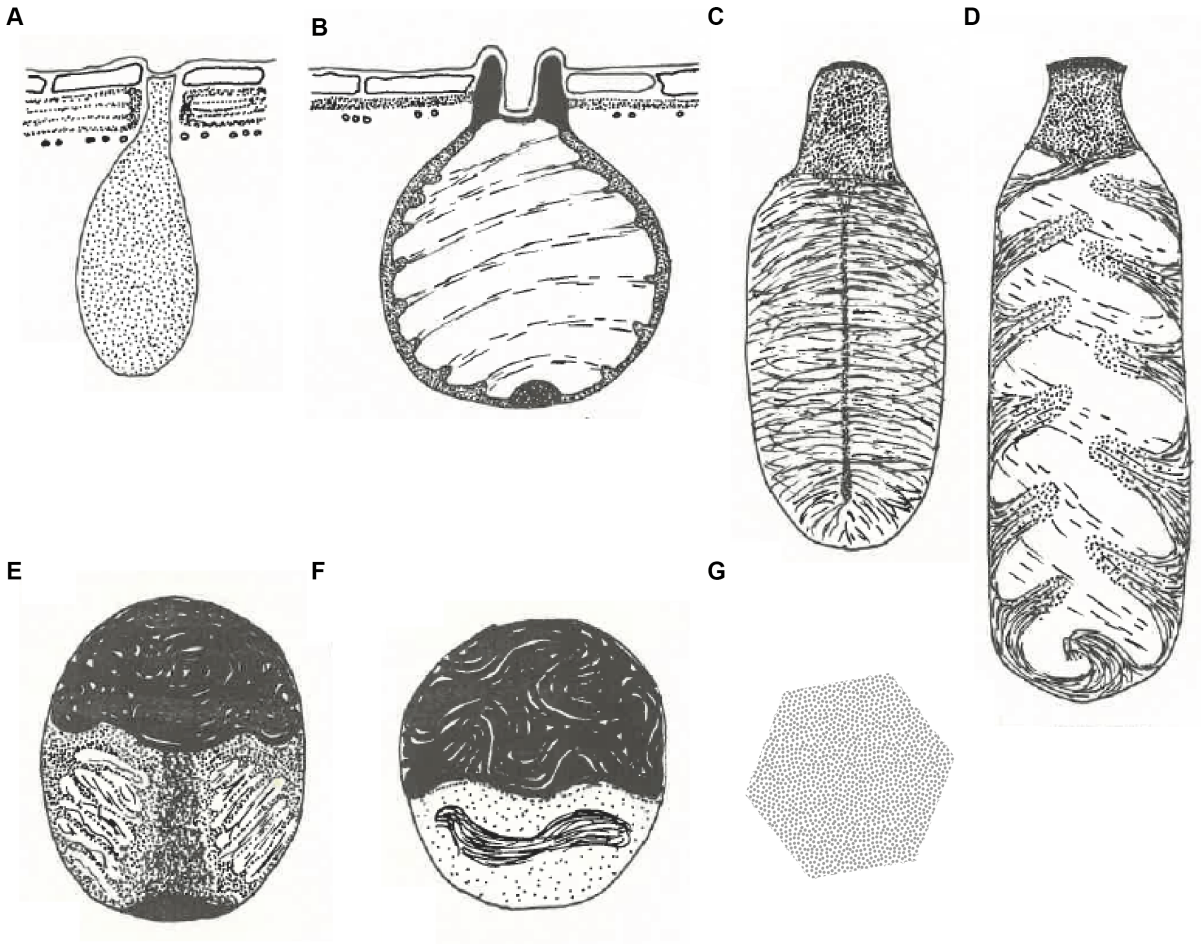

Figure 6: Schemes of different types of fibrillar, fibrillo-granular and paracrystalline organelles. A) Mucocyst from Peridinian dinoflagellate, B) Mucocyst from *Kofoidinium*, C) Organelle from *Kofoidinium,* D) Organelle from *Erythropsidinium*, E, F) Organelle observed in *Pyrocystis lunula,* G) Paracrystalline organelle from *Peridinium antarticum*. Figure adapted from Cachon et al., 1975.

3.5 Mitochondria

Mitochondria can present a large variety of shapes in dinoflagellates (Fig. 4E), however they generally bear tubular cristae (Dodge, 1973). Recent papers, including vEM data segmentations show that certain cells can present a unique mitochondrion spanning throughout the cell volume (Decelle et al., 2022; Mocaer et al., 2023).

3.6 Golgi apparatus

The Golgi Apparatus is usually positioned as a hemisphere close to the nucleus (Fig. 4F).

3.7- Chloroplasts

Half of the described species of dinoflagellates are known to present chloroplasts (Schnepf and Elbrächter, 1999). Chloroplast number and organization can vary between species. Photosynthetic dinoflagellates either acquired these plastid(s) through various events of endosymbiosis during evolution, or some species do acquire them more transiently during their life through symbiosis or kleptoplastidy. Different independent endosymbiotic events probably lead to the variation in pigment pattern in various dinoflagellate genus.

Kleptoplastidy is the uptake of chloroplasts from another organism, later retained for various amounts of time, depending of the species, for their photosynthetic potential. A few genus are known to have species performing kleptoplastidy such as *Dinophysis* (Myung et al., 2006) *Durkinsa* (Yamada et al., 2019) and *Shimiella* (Ok et al., 2021; Park et al., 2021).

It has been shown that the position of the chloroplast can vary depending on the light intensity (Sweeney, 1984). Furthermore, Zinssmeister et al., 2013, report that during the resting life stage of dinoflagellates, their number is decreased.

3.7.1 Peridinin containing chloroplast

These classical chloroplasts (Fig. 4G) generally contain the following pigments: chlorophyll a, chlorophyll ß and c_2, ß-carotene, peridinin, dinoxanthin and diadinoxanthin (Dodge, 1975; Jeffrey and Vesk, 1997; Loeblich, 1976; Whatley, 1993). Of which peridinin is specific to dinoflagellates, represents the main light harvesting pigment and is closely associated to chlorophyll a (Schnepf and Elbrächter, 1999). They are delimited by three membranes and presents thylakoid composed of an average of 3 lamellae following the longitudinal axis of the plastid (Dodge, 1975; Keeling, 2004; Schnepf and Elbrächter, 1999).

3.7.2 Other type of chloroplast

A portion of dinoflagellates such as small gymnodinoid cells present fucoxanthin or its derivates instead of peridinin as main pigment (Johansen et al., 1974; Mandelli, 1968; Riley and Wilson, 1967). Additionally, some photosynthetic species from the genus *Dinophysis* can present phycobilin as main pigment (Hewes et al., 1998), giving them a characteristic orange autofluorescence.

3.7.3 The pyrenoid

The pyrenoid is an important intracellular metabolic compartment. Indeed, in algal cells it is known to contain the enzyme Rubisco, which is essential for carbon fixation reactions. Pyrenoid(s) can be present or absent depending on the cells and their associated cycle. This structure is located within the chloroplast and show a wide variety of structures. One common feature is that they are composed of proteinaceous material. The presence of pyrenoids and their position has been shown to vary in some dinoflagellate species following a diurnal rhythm (Seo and Fritz, 2002). In some species the pyrenoid has a crystalline substructure as for instance in *Prorocentrum micans* (Kowallik, 1969).

Dodge and Crawford, 1971 describe 5 main types of pyrenoids, associated to groups of dinoflagellates. This classification is based on the pyrenoid arrangement in relation to the rest of the plastid structure (Fig. 7A). Furthermore, as the pyrenoid can be surrounded by starch (type “S”) or not (type “0”), Schnepf and Elbrächter, 1999 also mention that the pyrenoid and their association with a starch sheet can be used as an additional taxonomical criterion (Fig. 7B).

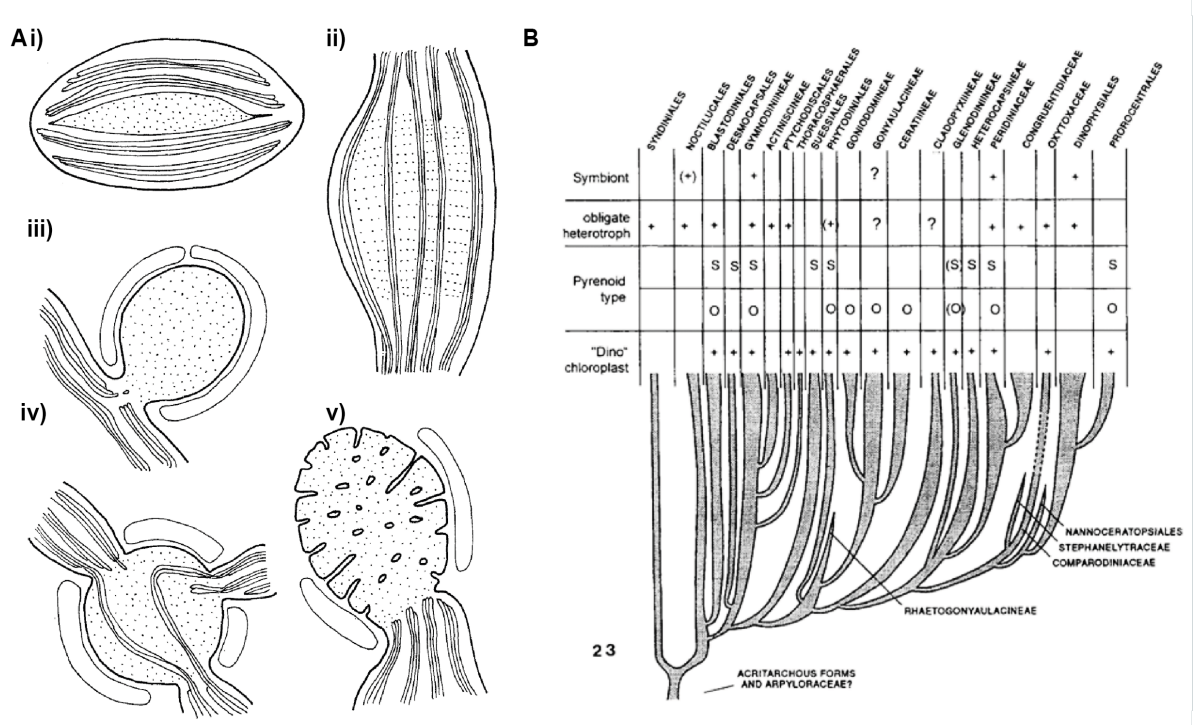

Figure 7: Classification based on pyrenoid arrangement and potential association to starch. A-i) Fusiform pyrenoid located centrally between the thylakoid stacks, A-ii) Pyrenoid situated in between thylakoid stacks, A-iii) Pyrenoid lobe located on one plastid branch, A-iv) Pyrenoid lobe originating from multiple plastid branches, A-v) Pyrenoid lobe presenting membrane invaginations,

located on one plastid branch. A-iii – A-v, present a starch sheet associated to the pyrenoid. A) Adapted from Dodge and Crawford., 1971. B) Adapted from Schnepf and Elbrächter., 1999.

3.7.4 Plastoglobuli

In photosynthetic algae or plants, the chloroplast often contains small lipoprotein structures linked to the thylakoid membranes called plastoglobuli (Austin et al., 2006). These structures present a lipid monolayer coat and a hydrophobic core (Austin et al., 2006). Historically, plastoblobuli were thought to be storage compartments. However, recent proteomic studies of plastoglobuli in plants (Ytterberg et al., 2006) have shown that they possess an active metabolic role. Some of their lipidic components come from the remodelling of the photosynthetic apparatus. Another part is synthetised in the lipoprotein structure and present a role in the electron transport chain as well as a protective role under stress conditions. In non-stress conditions, they generally possess an average diameter of 100-200 nm (Arzac et al., 2022). In stress response such as temperature and salinity variations or high light, the number or volume of plastoglobuli is generally increasing in plants (Venzhik et al., 2019). Furthermore, it has been shown that plastoglobuli can reach an very important size in senescent cells in plants (Kaup et al., 2002).

In their review, Dodge and Crawford., 1970 mention that dinoflagellate's chloroplast can present lipid globules, or plastoglobuli, however they specify that these structures are not very common in dinoflagellates. However, structures have been described in various genera such as in *Amilax* (Koike and Takishita, 2008), *Cystodinium* (Timpano and Pfiester, 1985) *Glenodinium* (Dodge and Crawford, 1971), *Thecadinium* (Hoppenrath et al., 2004), *Prorocentrum* (Prévôt and Soyer-gobillard, 1985, Fig. 8) and the kleptoplastidic genus *Durinskia* (Yamada et al., 2019). Interestingly, Prévot and Soyer-Gobillard in 1985 report a significant increase of plastoglobuli's number in *Prorocentrum micans* when in contact with the insecticide "malathion".

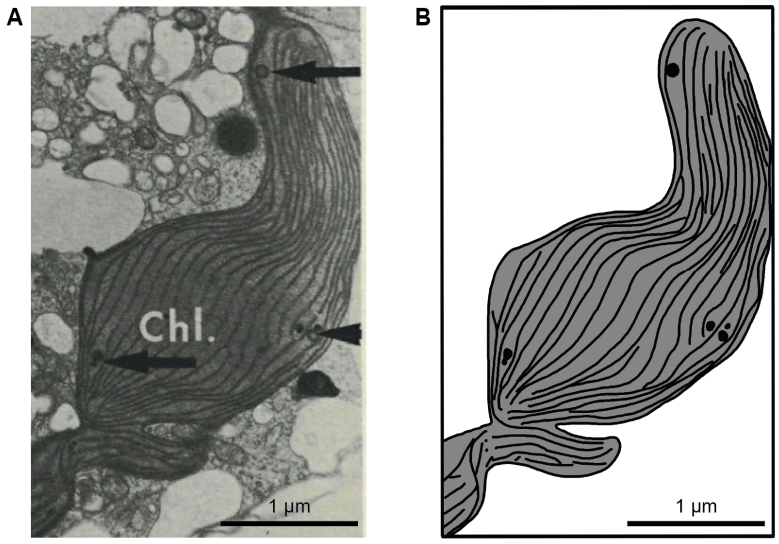

Figure 8: Example of plastoglobuli within the chloroplast of *Prorocentrum micans*. A) Micrograph of a chloroplast of *P. micans*. The plastobuli are designated by arrows. B) Simplified scheme of the same chloroplast underlining the positioning of the plastoglobuli close to thylakoids. Adapted from Prévot and Soyer-Gobillard., 1985.

3.8- Flagellar apparatus and eyespot

3.8.1 Flagellar apparatus

One main characteristic of dinoflagellates, as their name indicates, is the presence of flagella in their motile phase. There are two types of flagellations in dinoflagellates, respectively desmokont (Fig. 2A-E) and dinokont (Fig. 2F). Desmokont cells, which represent a major part of dinoflagellate genera, present two grooves (“cingulum” and “sulcus”), where the transversal and longitudinal flagella are positioned. These flagellar insertions give rise to the characteristic spiralling swimming pattern. In dinokont cells, belonging to the prorocentroid, the grooves are absent and thus the flagellation is independent of these areas (Fig. 2F).

A large number of various components can constitute the flagellar apparatus in different dinoflagellates species. Nonetheless, a few components are commonly found. For instance, these microorganisms ubiquitously possess two basal bodies (called longitudinal basal body, LB, and transversal basal body, TB, Fig. 4H). In most dinoflagellates, microtubular roots are also found. These structures are composed of a variable number of microtubules. They are respectively named longitudinal microtubular root (LMR), transverse microtubular root (TMR) and transverse striated root and associated microtubule (TSRM, Calado, 2010). The LMR and TMR are in close proximity to their respective basal body.

3.8.2 Eyespot (=Stigma)

With a few exceptions, most motile algal cells present an arrangement of tightly packed lipid globules constituting an eyespot or stigma (Solymosi, 2012). This structure can be present within a chloroplast or in the cytoplasm. However, independently of the intracellular compartmentation, this organelle is generally localised close to the basal body area and in proximity to the plasma membrane (Solymosi, 2012). In algae, the eyespot potentially has a role in light response, as for positive and negative phototaxis (moving towards or away from the light), photophobia (abrupt change in the cell's direction due to a rapid change in light intensity) and gliding in algal cells. However, the function and underlying mechanisms responsible for this role have not yet been determined.

In dinoflagellates, the eyespot is generally composed of lipid globules containing carotenoid pigments (Dodge and Crawford., 1971). These microorganisms show a wide diversity of eyespot structures in comparison to other protists, and the organization of the eyespot has been determined as a reliable morphological feature used for taxonomical classification. They are generally located close to the intersection between the cingulum and the sulcus and can be present within the chloroplast in some cases (Fig. 4I). There are 8 types of eyespots reviewed in Hoppenrath et al., 2017 (Fig. 9). Furthermore, some dinoflagellates don't seem to present an eyespots as for instance in some heterotrophic species of peridinoids or *Heterocapsa pygmaea* (Bullman and Roberts, 1986; Calado, 2010; Wedemayer and Wilcox, 1984).

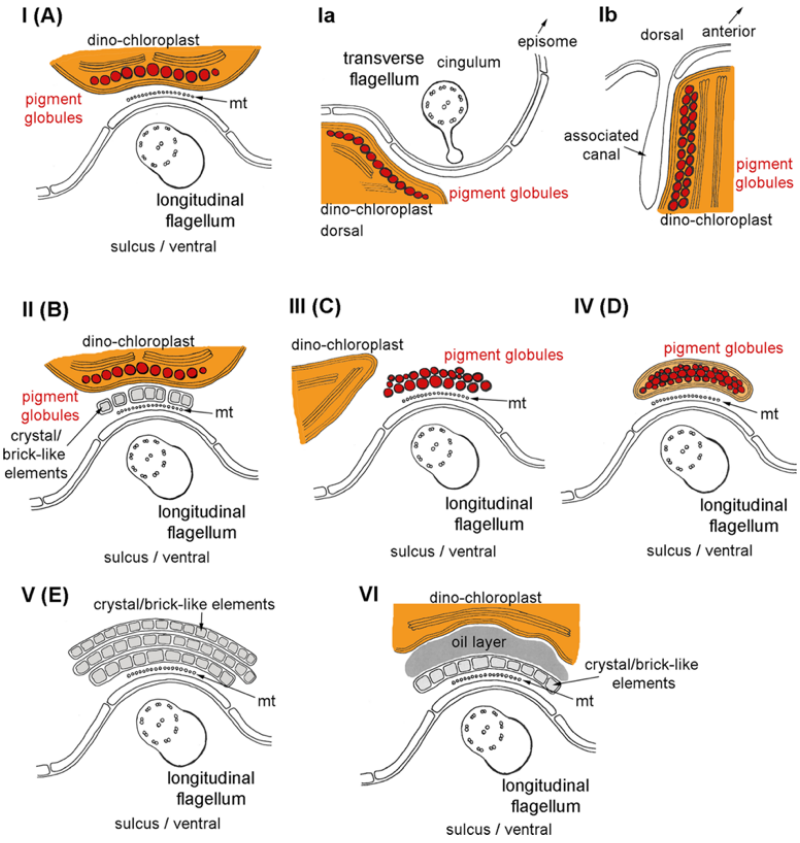

Figure 9: Schematic representation of the eight types of eyespots described in dinoflagellates. Except for type Ia and Ib, the section depicted is taken from the same orientation. Type I-IV present pigment globules, included or not (Type III) in a plastidic structure. Type V and VI, on the other hand, present characteristic crystal or brick like elements in combination to other structures. Figure from M. Hoppenrath (2017).

3.9- Structures associated with feeding strategy

Dinoflagellates can present three main heterotrophic feeding strategies (Fig. 10) namely: (1) phagotrophy, where the prey is engulfed, (2) “peduncle feeding” where the prey’s cytoplasm is ingested through a cytoplasmic extension named “peduncle”, and (3) “pallium feeding” where the prey is digested externally in a pseudopod structure called “pallium”.

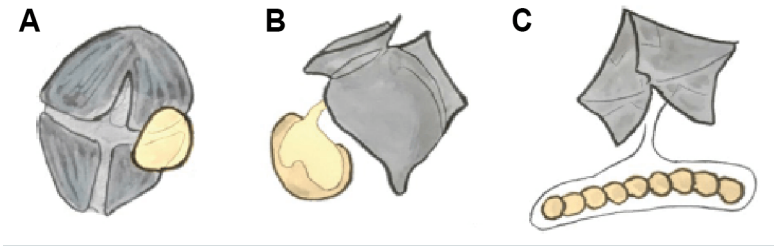

Figure 10: Scheme of the three main different heterotrophic feeding mechanisms (Prey in yellow). (A) phagocytosis of an entire prey through the sulcus/cingulum area, (B) Peduncle feeding,

where the cytoplasm of the prey is ingested through a pseudopod called peduncle and (C) Pallium feeding, where the prey is surrounded by a veil, called pallium, and digested externally. Figure adapted from O. García and K. Wirtz (2022).

A structure called microtubular basket is usually described as being related to the peduncle and pallium structures. The microtubular basket consists in a varying number of imbricated microtubules that are several micrometres long (Dodge, 1971). They were described in *Crypthecodinium cohnii* (Kubai and Ris, 1969) and *Aduncodinium glandula* (=Formerly *Katodinium glandulum*, Dodge and Crawford, unpublished).

3.9.1 Cytostome

Members of Noctilucales and Warnowiacea can possess a cytostome. This structure is alike a cell mouth, where preys are directed by their flagellum or prehensible tentacle, before being enclosed in food vacuoles and digested (Gross, 1934; Lucas, 1982; Soyer, 1968).

3.9.2 Peduncle

Some heterotrophic, or mixotrophic dinoflagellates, have a specific feeding structures called the peduncle (Schnepf and Elbrächter, 1992; Taylor, 1987b). This structure, described to be retractable, is composed of a column of cytoplasm, densely filled with microtubules. These microtubules are thought to be an extension of the microtubular basket localized internally (Lee, 1977). This extension may also present vesicles with amorphous or fibrillar content and rod-shaped bodies. This organelle can extend both internally and externally from the flagellar insertion area (Lee, 1977; Spero, 1982; Wedemayer and Wilcox, 1984). It can have a diameter from around 0.5 to 3.3 µm (Spector, 1984). Internally, this appendage can measure around 6 µm within the cell. Externally, this appendage protrudes from the sulcal/cingular vicinity and can measure up to 12 µm long (Spero, 1982). This structure has been described to be used for adherence to substrates (Lee, 1977) or food uptake (Spero, 1982). The uptake of the prey's cytoplasm using a peduncle has been described to be relatively quick and would only last for 20-30 seconds (Spero, 1982). A recent study showed that prey capture for peduncle feeding can be facilitated by the cyclic production of a large mucosphere in *Prorocentrum. cf. balticum* (Larsson et al., 2022).

3.9.3 Pallium

Some heterotrophic thecate dinoflagellates (from the genera *Protoperidinium*, *Oblea* and *Zygabikodinium*) can engulf preys such as diatoms using a structure called pallium. As the

peduncle, this structure is originating from the sulcus/cingulum area. This organelle internally originates from a microtubular basket and externally consists in a complex set of membranous vesicles deployed within a membranous sac, which can include microtubular ribbons (Jacobson, 1991). It presents a very high plasticity as it can surround a whole diatom colony. After engulfment, the preys are digested and transported through the pallium for up to two hours (Jacobson, 1991).

3.10 Energy storage

Dinoflagellates are known to be able to store energy primarily in the form of polysaccharides (mostly starch) and/or lipids. These storages compartments are located within the cytoplasm (Taylor, 1987b). When both products are present, lipids have been visible often to be localized anteriorly while starch was usually present posteriorly (Taylor, 1987b). The ratio of these two components has been described to fluctuate depending on the life cycle of the cells (Kelley and Pfiester, 1991). Other types of inclusions, potentially associated to life cycle stages, have also been thought to be nutrient storage bodies.

3.10.1 Starch

Starch has been described as the most abundant cellular carbohydrate in certain photosynthetic dinoflagellate species, as *Heterocapsa niei* (Loeblich, 1977). In this particular species, it can represent up to 27% of the dry weight (Zobell and Hittle, 1969). The starch granules can be of various size and shapes, and are known to form in the cytoplasm (Fig. 4J), generally in proximity to the pyrenoids. Contrary to other algae, starch granules have been shown to never form within the chloroplast (Schnepf and Elbrächter, 1999). Starch content has been shown to fluctuate during the day in marine dinoflagellates (Loeblich, 1977; Seo and Fritz, 2002). In their article, Seo and Fritz (2002) established that cells had large and rounded cytosolic granules during the light period whereas they were absent in the dark period. Loeblich (1977) reports a similar pattern in *Heterocapsa niei* where cells present starch grains at the end of the light period. From these observations, they hypothesized that cells degrade their starch reserves at night.

During the resting stage, dinoflagellates have been shown to possess an increase in storage products as starch grains and lipid bodies (Zinssmeister et al., 2013). Dinoflagellate starch has been reported to possess a similar structure than in higher plants.

3.10.2 Lipids

A large proportion of dinoflagellates store fat in the form of droplets within their cytoplasm (Dodge and Crawford, 1971). Fatty acids have been described to represent 1.5% of the dry weight in some marine photosynthetic dinoflagellates (Harrington et al., 1970). Dinoflagellate, along with other phytoplankton have been suggested to present a diurnal pattern in TAG concentration (Becker et al., 2018). Indeed, Becker et al., 2018 estimated diverse phytoplankton, including dinoflagellates, could contain up to 40% more calories in the late evening comparing to early morning because of TAG being produced during the day. In addition to fatty acids, there are reports of numerous sterols in dinoflagellates. Interestingly, cholesterol was found ubiquitously in the diverse dinoflagellates species in the different studies (Spector, 1984).

3.10.3 Food vacuole & PAS bodies (Periodic Acid Shift reaction positive bodies)

Food vacuole and PAS bodies are temporary structures commonly found in dinoflagellates which enclose respectively ingested food, or potentially autophagic material or stored metabolites (Fig. 4K). PAS bodies are membrane bound organelles that present acid phosphatase activity, leading to their putative “digestive” role (Schmitter, 1971; Schmitter and Jurkiewicz, 1981). Both are here described in parallel as they have many similarities and their distinction in EM from 2D sections is complex. These organelles are bound by a single membrane bilayer and can contain a variable combination of residual organelles from ingested preys (chloroplast, trichocyst or chromosomes for instance), amorphous material which has potentially been digested in case of phagocytosis and / or membranous vesicles, electron dense material and fibrillar material in case of autophagy (Dodge and Crawford, 1970b; Lee, 1977; Schmitter, 1971; Schmitter and Jurkiewicz, 1981). Of note, PAS bodies were described to be present both in light and dark conditions, suggesting that their occurrence is probably linked to the cell’s life cycle or growth condition (Schmitter, 1971). In the literature, there are also mentions of “accumulation bodies”, that would have waste storage and elimination function, but would appear more homogeneous in their content compared to food vacuoles and PAS bodies.

3.10.4 Crystalline inclusions

Crystalline inclusions have been reported in a number of dinoflagellate genera as *Gymnodiniales*, *Prorocentrales*, *Peridiniales*, *Noctilucales* and *Thoracosphaeraceae* (DeSa and Hastings, 1968; Jantschke et al., 2019; Pokorny and Gold, 1973). These crystals are often in membrane delimited vacuoles. In *Lingulodinium polyedra* (= Formerly Gonyaulax polyedra),

the crystals isolated were of guanine nature (DeSa and Hastings, 1968). As guanine has been shown to function as nitrogen storage in yeast, the authors hypothesized these crystals to possess a similar function (Roush et al., 1959). Other putative functions were their use as light reflectors, however due to their random orientation this hypothesis was first qualified unlikely (Schmitter, 1971). Jantschke et al., 2019 performed a multimodal study (combining Cryo-FIB-SEM, Cryo-SEM, Raman spectroscopic imaging) on these guanine crystal in a photosynthetic dinoflagellate (*Calciodinellum operosum aff,* Fig. 11). Based on their results and the close proximity of these structures to chloroplasts, they suggested that these structures acted as light scatterers to enhance the light exploitation by the chloroplasts or protect organelles such as the nucleus from UV radiations (Jantschke et al., 2019). Based on the presence of guanine crystals only during the motile stage, and absence during the resting stage, Jantschke et al., 2019 deduced that they are less likely to possess storage functions. Nonetheless, it has been recently reported that in the dinoflagellate *Amphidinium carterae*, the nitrogen storage through guanine crystals could be sufficient to provide nitrogen reserves for multiple new generations (Mojzeš et al., 2020). These guanine crystals have been shown to dissolve in water (Kimura et al., 2020), possibly leading to holes in 2D TEM sections when collected on water or during post staining as observed by Schmitter., 1971.

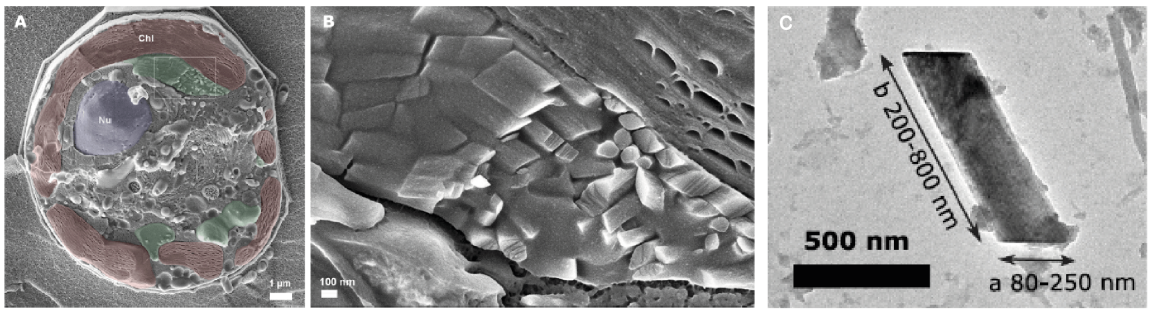

Figure 11: Crystal localisation and ultrastructure in *Calciodinellum operosum aff*. A-B) Cryo-SEM micrograph, the vacuole containing the crystal is in green, nucleus in blue and chloroplast in red. B is a close up of the area marked by a white square in A. C) Guanine crystal extracted from *Calciodinellum operosum aff* in TEM with indication of their size. Figure adapted from Jantschke et al., 2019.

3.11 Crystalline rods / Membrane like lamellae (=lamellar bodies)

In some species of heterotrophic dinoflagellates, vesicles described as “containing crystalline rods structures” or “membrane like lamellae” (MLL) have been observed (Calado and Moestrup, 1997; Jacobson and Anderson, 1992; Jeong et al., 2014; Kang et al., 2011; Wedemayer and Wilcox, 1984). These structures are usually localised parallel to the cell surface and in its proximity (Fig. 4L, Fig. 12). Their function or the nature of their content is currently unknown (Jeong et al., 2014; Wedemayer and Wilcox, 1984).

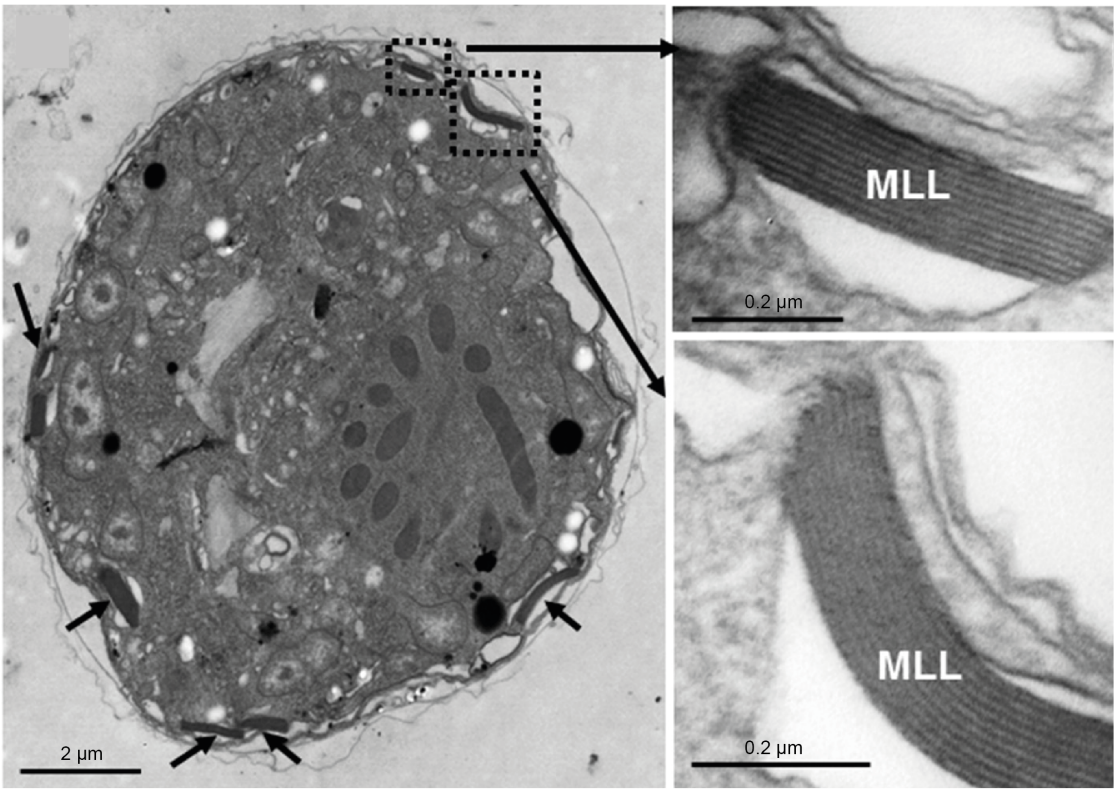

Figure 12: Position of MLL in *Stoeckeria algicida* SAMS07 and close up on their organisation. On the right, the positioning of MLL at the cell periphery, parallel to the cell cortex is visible. On the left are two close ups (from the dashed rectangles on the right panel) allowing to visualize the striated arrangement within these organelles. Figure adapted from Jeong et al., 2014.

4- Morphological parameters for cellular identification

Historically, a subset of organelles and their ultrastructural characteristics have been used for taxonomical identification. The main one is of course the tabulation from the theca or amphiesmal vesicles. However, the specific morphology of a subset of intracellular structures also seems to be associated to genus or species. This is the case for organelles such as the pusule, the chloroplast, the pyrenoid and the eyespot (when present), which have been described to be indicators of certain order, genus or species (Dodge, 1972; Dodge and Crawford, 1971; Hoppenrath, 2017; Moestrup and Daugbjerg, 2007; Schnepf and Elbrächter, 1992). In the next Chapters, I will describe structures which are potentially associated to certain genera or trophic modes using 2D and 3D electron microscopy. I hope that this type of subcellular analysis, at an environmental population scale, can bring some additional information towards taxonomical identification.

5- References

Abe, T. H. (1981). Studies on the Family Peridinidae an Unfinished Monograph on the Armoured Dinoflagellata. *Publ. Seto Mar. Biol. Lab. Spec. Publ. Ser.* **6**, 1–409.

Anderson, D. M., Burkholder, J. M., Cochlan, W. P., Glibert, P. M., Gobler, C. J., Heil, C. A., Kudela, R. M., Parsons, M. L., Rensel, J. E. J., Townsend, D. W., et al. (2008). Harmful algal blooms and eutrophication: Examining linkages from selected coastal regions of the United States. *Harmful Algae* **8**, 39–53.

Arzac, M. I., Fernández-Marín, B. and García-Plazaola, J. I. (2022). More than just lipid balls: quantitative analysis of plastoglobule attributes and their stress-related responses. *Planta* **255**, 1–14.

Austin, J. R., Frost, E., Vidi, P. A., Kessler, F. and Staehelin, L. A. (2006). Plastoglobules are lipoprotein subcompartments of the chloroplast that are permanently coupled to thylakoid membranes and contain biosynthetic enzymes. *Plant Cell* **18**, 1693–1703.

Becker, K. W., Collins, J. R., Durham, B. P., Groussman, R. D., White, A. E., Fredricks, H. F., Ossolinski, J. E., Repeta, D. J., Carini, P., Armbrust, E. V., et al. (2018). Daily changes in phytoplankton lipidomes reveal mechanisms of energy storage in the open ocean. *Nat. Commun.* **9**, 5179.

Bhaud, Y., Guillebault, D., Lennon, J. F., Defacque, H., Soyer-Gobillard, M. O. and Moreau, H. (2000). Morphology and behaviour of dinoflagellate chromosomes during the cell cycle and mitosis. *J. Cell Sci.* **113**, 1231–1239.

Biecheler, B. (1952). *Recherche sur les Péridiniens*. Laboratoire d`Evolution des Etres Organises.

Bouck, G. B. and Sweeney, B. M. (1966). The fine structure and ontogeny of trichocysts in marine dinoflagellates. *Protoplasma* **61**, 205–223.

Braarud, T., Foeyn, B. and Hasle, G. R. (1958). *The marine and fresh-water phytoplankton of the Dramsfjord and the adjacent part of the Oslofjord,March-December 1951.*

Bricheux, G., Mahoney, D. G. and Gibbs, S. P. (1992). Development of the pellicle and thecal plates following ecdysis in the dinoflagellate *Glenodinium foliaceum*. *Protoplasma* **168**, 159–171.

Bullman, V. and Roberts, K. R. (1986). Structure of the flagellar apparatus in *Heterocapsa pygmaea* (Pyrrophyta). *Phycologia* **25**, 558–571.

Cachon, J., Cachon, M. and Greuet, C. (1975). *Les "mucocystes"des Péridiniens. Constitution, évolution des structures et comparison avec celles des trichocystes.*

Calado, S. C. F. C. (2010). Ultrastructure and phylogeny of peridinioid dinoflagellates.

Calado, A. J. and Moestrup, Ø. (1997). Feeding in *Peridiniopsis berolinensis* (Dinophyceae): new observations on tube feeding by an omnivorous, heterotrophic dinoflagellate. *Phycologia*, 47-59.

Chatton, E. (1970). Le systeme pusulaire de quelques peridiniens libres ou parasites.

Protistologica **6**, 467–476.

Decelle, J., Veronesi, G., LeKieffre, C., Gallet, B., Chevalier, F., Stryhanyuk, H., Marro, S., Ravanel, S., Tucoulou, R., Schieber, N., et al. (2021). Subcellular architecture and metabolic connection in the planktonic photosymbiosis between Collodaria (radiolarians) and their microalgae. *Environ. Microbiol.* **23**, 6569–6586.

Decelle, J., Kayal, E., Bigeard, E., Gallet, B., Bougoure, J., Clode, P., Schieber, N., Templin, R., Hehenberger, E., Prensier, G., et al. (2022). Intracellular development and impact of a marine eukaryotic parasite on its zombified microalgal host. *ISME J.* **16**, 2348–2359.

DeSa, R. and Hastings, J. W. (1968). Bioluminescent particles from the marine dinoflagellate, *Gonyaulax polyedra*. *J. Gen. Physiol.* **51**, 105–122.

Desquilbet, M., Gaume, L., Grippa, M., Céréghino, R., Humbert, J. F., Bonmatin, J. M., Cornillon, P. A., Maes, D., Dyck, H. Van and Goulson, D. (2020). Comment on "meta-analysis reveals declines in terrestrial but increases in freshwater insect abundances. *Science (80-.).* **370**, 417–420.

Dixon, G. K. and Syrett, P. J. (1988). The growth of dinoflagellates in laboratory cultures. *New Phytol.* **109**, 297–302.

Dodge, J. D. (1971). Fine Structure of the Pyrrophyta. *Bot. Rev.* **37**, 481–508.

Dodge, J. D. (1972). The ultrastructure of the dinoflagellate pusule: A unique osmo-regulatory organelle. *Protoplasma* **75**, 285–302.

Dodge, J. . (1973). *The fine structure of Algal Cells*. Academic Press.

Dodge, J. D. (1975). A survey of chloroplast ultrastructure in the Dinophyceae. *Phycologia* **14**, 253–263.

Dodge, J. D. and Crawford, R. M. (1970a). A survey of thecal fine structure in the Dinophyceae. *Bot. J. Linn. Soc.* **63**, 53–67.

Dodge, J. D. and Crawford, R. M. (1970b). The morphology and fine structure of *Ceratium Hirundinella* (Dinophyceae). *J. Phycol.* **6**, 137–149.

Dodge, J. . and Crawford, R. . (1971). A fine-structural survey of dinoflagellate pyrenoids and food reserves. *Bot. J. Linn. Soc.* **64**, 105–115.

Dragesco, J. and Hollande, A. (1965). Sur la présence de trichocystes fibreux chez les péridiniens; leur homologie avec les trichocystes fusiformes des ciliés. *C. r. hebd. Séanc. Acad. Sci.* 2073–276.

Dürr, G. (1979). Elektronenmikroskopische untersuchungen am panzer von dinoflagellaten: II. Peridinium cinctum. *Arch. für Protistenkd.* **122**, 88–120.

Field, C. B., Behrenfeld, M. J., Randerson, J. T. and Falkowski, P. (1998). Primary production of the biosphere: Integrating terrestrial and oceanic components. *Science (80-.).* **281**, 237–240.

Fott, B. and Ludvik, J. (1956). Uber den submikroskopischen Bau des Panzers Ceratium hirundinel. *Preslia* **28**, 278–280.

Fukuda, Y. and Endoh, H. (2006). New details from the complete life cycle of the red-tide dinoflagellate *Noctiluca scintillans* (Ehrenberg) McCartney. *Eur. J. Protistol.* **42**, 209–219.

Gautier, A., Michel-Salamin, L., Tosi-Couture, E., McDowall, A. W. and Dubochet, J. (1986). Electron microscopy of the chromosomes of dinoflagellates in situ: confirmation of Bouligand's liquid crystal hypothesis. *J. Ultrastruct. Res. Mol. Struct. Res.* **97**, 10–30.

Gavelis, G. S., Wakeman, K. C., Tillmann, U., Ripken, C., Mitarai, S., Herranz, M., Özbek, S., Holstein, T., Keeling, P. J. and Leander, B. S. (2017). Microbial arms race: Ballistic "nematocysts" in dinoflagellates represent a new extreme in organelle complexity. *Sci. Adv.* **3**, 36.

Gavelis, G. S., Herranz, M., Wakeman, K. C., Ripken, C., Mitarai, S., Gile, G. H., Keeling, P. J. and Leander, B. S. (2019). Dinoflagellate nucleus contains an extensive endomembrane network, the nuclear net. *Sci. Rep.* **9**, 1–9.

Gillooly, J. F., Hein, A. and Damiani, R. (2015). Nuclear DNA content varies with cell size across human cell types. *Cold Spring Harb. Perspect. Biol.* **7**, 1–27.

Glynn, P. W. (1993). Coral reef bleaching: ecological perspectives. *Coral Reefs* **12**, 1–17.

Gomez, F. (2012). A quantitative review of the lifestyle, habitat and trophic diversity of dinoflagellates (Dinoflagellata, Alveolata). *Syst. Biodivers.* **10**, 267–275.

Grassé, P. P. and Dragesco, J. (1957). Ultrastructure of the chromosome of the peridinians and its genetic consequences. *C. R. Hebd. Seances Acad. Sci.* **245**, 2447–2452.

Grell, K. G. and Wohlfarth-Bottermann, K. E. (1957). Licht- und elektronenmikroskopische Untersuchungen an dem Dinoflagellaten *Amphidinium elegans n.* sp. *Zeitschrift für Zellforsch. und Mikroskopische Anat.* **47**, 7–17.

Gross, F. (1934). Zur Biologie und Entwicklungsgeschichte von *Noctulica miliaris*. *Arch. Protistenk.* **83**, 178—196.

Harrington, G. W., Beach, D. H., Dunham, J. E. and Holz, G. G. (1970). The Polyunsaturated fatty acids of Marine Dinoflagellates. *J. Protozool.* **17**, 213–219.

Haussmann, K. (1978). Extrusive organelles protists.**52,**197-276.

Herzog, M. and Soyer, M. O. (1981). Distinctive features of dinoflagellate chromatin. Absence of nucleosomes in a primitive species Prorocentrum micans E. *Eur. J. Cell Biol.* **23**, 295–302.

Hewes, C. D., Mitchell, B. G., Moisan, T. A., Vernet, M. and Reid, F. M. H. (1998). The phycobilin signature of chloroplasts from three dinoflagellate species: A microanalytic study of D*inophysis caudata, D. fortii,* and *D. acuminata* (Dinophysiales, Dinophyceae). *J. Phycol.* **34**, 945–951.

Hoppenrath, M. (2017). Dinoflagellate taxonomy — a review and proposal of a revised

classification. *Mar. Biodivers.* **47**, 381–403.

Hoppenrath, M., Saldarriaga, J. F., Schweikert, M., Elbrächter, M. and Taylor, F. J. R. (2004). Description of *Thecadinium mucosum* sp. nov. (dinophyceae), a new sand-dwelling marine dinoflagellate, and an emended description of *Thecadinium inclinatum* balech. *J. Phycol.* **40**, 946–961.

Jacobson, M. (1991). The ecology and feeding biology of thecate heterotrophic dinoflagellates. *J. Protozool.*

Jacobson, M. and Anderson, D. M. (1992). Ultrastructure of the feeding apparatus and myonemal system of the heterotrophic dinoflagellate *Protoperidinium spinulosum*. *J. Phycol.* **8**, 5–24.

Jandt, U., Bruelheide, H., Jansen, F., Bonn, A., Grescho, V., Klenke, R. A., Sabatini, F. M., Bernhardt-Römermann, M., Blüml, V., Dengler, J., et al. (2022). More losses than gains during one century of plant biodiversity change in Germany. *Nature* **611**, 512–518.

Jang, S. H., Jeong, H. J., Lee, M. J., Kim, J. H. and You, J. H. (2019). *Gyrodinium jinhaense* n. sp., a New Heterotrophic Unarmored Dinoflagellate from the Coastal Waters of Korea. *J. Eukaryot. Microbiol.* **66**, 821–835.

Jantschke, A., Pinkas, I., Hirsch, A., Elad, N., Schertel, A., Addadi, L. and Weiner, S. (2019). Anhydrous β-guanine crystals in a marine dinoflagellate: Structure and suggested function. *J. Struct. Biol.* **207**, 12–20.

Jeffrey, S. W. and Vesk, M. (1997). Introduction to marine phytoplankton and their pigment signatures.

Jeong, H. J., du Yoo, Y., Kim, J. S., Seong, K. A., Kang, N. S. and Kim, T. H. (2010). Growth, feeding and ecological roles of the mixotrophic and heterotrophic dinoflagellates in marine planktonic food webs. *Ocean Sci. J.* **45**, 65–91.

Jeong, H. J., Jang, S. H., Moestrup, Ø., Kang, N. S., Lee, S. Y., Potvin, É. and Noh, J. H. (2014). *Ansanella granifera gen. et sp. nov*. (Dinophyceae), a new dinoflagellate from the coastal waters of Korea. *Algae* **29**, 75–99.

Johansen, J. E., Svec, W. a, Liaaenje.S and Haxo, F. T. (1974). Carotenoids of Dinophyceae. *Phytochemistry* **13**, 2261–2271.

Kalvelage, J., Wöhlbrand, L., Schoon, R., Zink, F., Correll, C., Senkler, J., Hoppenrath, M., Rhiel, E., Braun, H., Winklhofer, M., et al. (2023). The enigmatic nucleus of the marine dinofmagellate *Prorocentrum cordatum*. *Am. Soc. Microbiol.* **8**,.

Kang, N. S., Jeong, H. J., Moestrup, Ø. and Park, T. G. (2011). *Gyrodiniellum shiwhaense* n. gen., n. sp., a new planktonic heterotrophic dinoflagellate from the coastal waters of western Korea: Morphology and ribosomal DNA gene sequence. *J. Eukaryot. Microbiol.* **58**, 284–309.

Kang, N. S., Jeong, H. J., Moestrup, Ø., Lee, S. Y., Lim, A. S., Jang, T. Y., Lee, K. H., Lee,

M. J., Jang, S. H., Potvin, E., et al. (2014). *Gymnodinium smaydae* n. sp., a new planktonic phototrophic dinoflagellate from the coastal waters of western Korea: Morphology and molecular characterization. *J. Eukaryot. Microbiol.* **61**, 182–203.

Kaup, M. T., Froese, C. D. and Thompson, J. E. (2002). A role for diacylglycerol acyltransferase during leaf senescence. *Plant Physiol.* **129**, 1616–1626.

Keeling, P. J. (2004). Diversity and evolutionary history of plastids and their hosts. *Am. J. Bot.* **91**, 1481–1493.

Kelley, I. and Pfiester, L. A. (1991). Ultrastructure of *Glenodinium montanum* (Dinophyceae). *J. Phycol.* **27**, 414–423.

Kimura, T., Takasaki, M., Hatai, R., Nagai, Y., Uematsu, K., Oaki, Y., Osada, M., Tsuda, H., Ishigure, T., Toyofuku, T., et al. (2020). Guanine crystals regulated by chitin-based honeycomb frameworks for tunable structural colors of sapphirinid copepod, *Sapphirina nigromaculata. Sci. Rep.* **10**, 4–5.

Klut, M. E., Bisalputra, T. and Antia, N. J. (1987). Some observations on the structure and function of the dinoflagellate pusule. *Can. J. Bot.* **65**, 736–744.

Kofoid, C. A. (1907). Dinoflagellata of the San Diego region, III. Description of new species. *Univ. Calif. Publ.* **3**, 299–340.

Kofoid, C. . (1908). *Exuviation, Autotomy and Regeneration in Ceratium*. Berkeley, The University Press.

Kofoid, C. A. (1909). n Peridinium steini Jörgensen, with a note on the nomenclature of the skeleton of the Peridinidae. *Arch. für Protistenkd.*

Koike, K. and Takishita, K. (2008). Anucleated cryptophyte vestiges in the gonyaulacalean dinoflagellates *Amylax buxus* and *Amylax triacantha* (Dinophyceae). *Phycol. Res.* **56**, 301–311.

Kosinski, J., Mosalaganti, S., Appen, A. Von, Teimer, R., Diguilio, A. L., Wan, W., Bui, K. H., Hagen, W. J. H., Briggs, J. a G., Glavy, J. S., et al. (2016). Molecular architecture of the inner ring scaffold of the human nuclear pore complex. *Science (80-.).* **352**, 363–365.

Kowallik, K. (1969). The crystal lattice of the pyrenoid matrix of prorocentrum micans. **269**, 251–269.

Kubai, D. F. and Ris, H. (1969). Division in the dinoflagellate *Gyrodinium cohnii* (Schiller). A new type of nuclear reproduction. *J. Cell Biol.* **40**, 508–528.

Kwok, A. C. M. and Wong, J. T. Y. (2003). Cellulose synthesis is coupled to cell cycle progression at G1 in the dinoflagellate *Crypthecodinium cohnii. Plant Physiol.* **131**, 1681–1691.

Kwok, A. C. M., Chan, W. S. and Wong, J. T. Y. (2023). Dinoflagellate Amphiesmal Dynamics: Cell Wall Deposition with Ecdysis and Cellular Growth. *Mar. Drugs* **21**, 70.

Larsson, M. E., Bramucci, A. R., Collins, S., Hallegraeff, G., Kahlke, T., Raina, J. B., Seymour, J. R. and Doblin, M. A. (2022). Mucospheres produced by a mixotrophic protist impact ocean carbon cycling. *Nat. Commun.* **13**, 1–16.

Lee, R. E. (1977). Saprophytic and phagocytic isolates of the colourless heterotrophic dinoflagellate *Gyrodinium lebouriae* Herdman. *J. Mar. Biol. Assoc. United Kingdom* **57**, 305–315.

Lin, D. H., Stuwe, T., Schilbach, S., Rundlet, E. J., Perriches, T., Mobbs, G., Fan, Y., Thierbach, K., Huber, F. M., Collins, L. N., et al. (2017). Architecture of the nuclear pore complex symmetric core Daniel. *Science (80-.).* **46**, 1247–1262.

Livolant, F. and Bouligand, Y. (1978). New observations on the twisted arrangement of Dinoflagellate chromosomes. *Chromosoma* **68**, 21–44.

Loeblich, A. R. (1970). The amphiesma or dinoflagellate cell covering. In *In Proceedings of the North American Paleontology Convention, Chicago, IL, USA, 5–7 September 1969*, p. Allen Press.

Loeblich, A. R. (1976). Dinoflagellate Evolution: Speculation and Evidencece. **23**, 13–28.

Loeblich, A. R. (1977). Studies on synchronously dividing populations of Cachonianiei, a marine dinoflagellate. *Bull. Japanese Soc. Phycol.* **25**, 118–128.

Lucas, I. A. N. (1982). Observations on *Noctiluca scintillans* Macartney (Ehrenb.) (Dinophyceae) with notes on an intracellular bacterium. *J. Plankton Res.* **4**, 401–409.

Maldonado, E. . and Latz, M. . (2007). Shear-stress dependance of dinoflagellate bioluminescence. *Mar. Biol. Lab.* **8**, 620–630.

Mandelli, E. F. (1968). Carotenoid pigments of the dinoflagellate *Glenodinium foliceum* (Stein). *J. Phycol.* **4**, 347–348.

Mocaer, K., Mizzon, G., Gunkel, M., Halavatyi, A., Steyer, A., Oorschot, V., Schorb, M., Kieffre, C. Le, Yee, D. P., Chevalier, F., et al. (2023). Targeted volume Correlative Light and Electron Microscopy of an environmental marine microorganism. *J. Cell Sci.* **c**, 2023.01.27.525698.

Moestrup, Ø. and Daugbjerg, N. (2007). On dinoflagellate phylogeny and classification. 215–230.

Mojzeš, P., Gao, L., Ismagulova, T., Pilátová, J., Moudříková, Š., Gorelova, O., Solovchenko, A., Nedbal, L. and Salih, A. (2020). Guanine, a high-capacity and rapid-turnover nitrogen reserve in microalgal cells. *Proc. Natl. Acad. Sci. U. S. A.* **117**, 32722–32730.

Mora, C., Tittensor, D. P., Adl, S., Simpson, A. G. B. and Worm, B. (2011). How many species are there on earth and in the ocean? *PLoS Biol.* **9**, 1–8.

Morrill, L. C. and Loeblich, A. R. (1983). Ultrastructure of the Dinoflagellate Amphiesma. *Int. Rev. Cytol.* **82**, 151–180.

Myung, G. P., Kim, S., Hyung, S. K., Myung, G., Yi, G. K. and Yih, W. (2006). First successful culture of the marine dinoflagellate *Dinophysis acuminata. Aquat. Microb. Ecol.* **45**, 101–106.

Norris, R. E. (1966). Unarmoured marine dinoflagellates. *Endeavour* **25**, 124–128.

Ok, J. H., Jeong, H. J., Lee, S. Y., Park, S. A. and Noh, J. H. (2021). *Shimiella gen. nov.* and Shimiella gracilenta sp. nov. (Dinophyceae, Kareniaceae), a Kleptoplastidic Dinoflagellate from Korean Waters and its Survival under Starvation. *J. Phycol.* **57**, 70–91.

Oliveira, C. Y. B., Oliveira, C. D. L., Müller, M. N., Santos, E. P., Dantas, D. M. M. and Gálvez, A. O. (2020). A Scientometric Overview of Global Dinoflagellate Research. *Publications* **8**, 50.

Park, S. A., Jeong, H. J., Ok, J. H., Kang, H. C., You, J. H., Eom, S. H. and Park, E. C. (2021). Interactions Between the Kleptoplastidic Dinoflagellate *Shimiella gracilenta* and Several Common Heterotrophic Protists. *Front. Mar. Sci.* **8**, 1–12.

Pitelka, D. R. and Schooley, C. N. (1955). *Comparative Morphology of Some Protistan Flagella*. University of California Press.

Pokorny, K. . and Gold, K. (1973). Two morphological types of particulate inclusions in marine dinoflagellates. *J. Phycol.* **9**, 218–224.

Prévôt, P. and Soyer-gobillard, M. (1985). Effets du Malathion, insecticide organosphoré, sur le dinoflagellé marin *Prorocentrum micans. Vie Milieu* **35**, 15–21.

Rae, P. M. M. (1976). Hydroxymethyluracil in eukaryote DNA: A natural feature of the pyrrophyta (Dinoflagellates). *Science (80-.).* **194**, 1062–1064.

Riley, J. P. and Wilson, T. R. S. (1967). The pigments of some marine phytoplankton species. *J. Mar. Biol. Assoc. United Kingdom* **47**, 351–362.

Rizzo, P. J. and Noodén, L. D. (1972). Chromosomal proteins in the dinoflagellate alga Gyrodinium cohnii. *Science (80-.).* **176**, 796–797.

Rizzo, P. J. and Noodén, L. D. (1973). Isolation and Chemical Composition of Dinoflagellate Nuclei. *J. Protozool.* **20**, 666–672.

Roush, A. H., Questiaux, L. M. and Domnas, A. J. (1959). The active transport and metabolism of purines in the yeast, *Candida utilis. J. Cell. Comp. Physiol.* **54**, 275–286.

Schmitter, R. E. (1971). The fine structure of *Gonyaulax polyedra,* a bioluminescent marine dinoflagellate. *J. Cell Sci.* **9**, 147–173.

Schmitter, R. E. and Jurkiewicz, A. J. (1981). Acid phosphatase localization in PAS-bodies of *Gonyaulax. J. Cell Sci.* **Vol. 51**, 15–23.

Schnepf, E. and Elbrächter, M. (1992). Nutritional strategies in dinoflagellates: A review with emphasis on cell biological aspects. *Eur. J. Protistol.* **28**, 3–24.

Schnepf, E. and Elbrächter, M. (1999). Dinophyte chloroplasts and phylogeny - A review.

Grana **38**, 81–97.

Schütt, F. (1889). *Die Peridineen der Plankton-Expedition*.

Schütt, F. (1895). *Die Peridineen der Plankton-Expedition*.

Seo, K. S. and Fritz, L. (2002). Diel changes in pyrenoid and starch reserves in dinoflagellates. *Phycologia* **41**, 22–28.

Sigwart, J. D., Bennett, K. D., Edie, S. M., Mander, L., Okamura, B., Padian, K., Wheeler, Q., Winston, J. E. and Yeung, N. W. (2018). Measuring Biodiversity and Extinction-Present and Past. *Integr. Comp. Biol.* **58**, 1111–1117.

Skovgaard, A., Karpov, S. A. and Guillou, L. (2012). The parasitic dinoflagellates *Blastodinium spp*. Inhabiting the gut of marine, Planktonic copepods: Morphology, ecology, and unrecognized species diversity. *Front. Microbiol.* **3**, 1–22.

Solymosi, K. (2012). Plastid Structure, Diversification and Interconversions I. Algae. *Curr. Chem. Biol.* **6**, 167–186.

Soyer, M. (1968). Présence de formations fibrillaires complexes chez *Noctulica miliaris S*. et discussions de leur rôle dans la motiliité de ce dinoflagellé. *Zeitschrift für Zellforsch. und Mikroskopische Anat.* **104**, 29–55.

Soyer, M. (1969). Étude cytologique ultrastructurale d'un dinoflagellé libre, *Noctiluca miliari*s Suriray: trichocystes et inclusions paracristallines.

Soyer, M. O. (1970a). Les ultrastructures liées aux fonctions de relation chez *Noctiluca miliaris* S. (Dinoflagellata). *Zeitschrift für Zellforsch. und Mikroskopische Anat.* **104**, 29–55.

Soyer, M. O. (1970b). Etude ultrastructurale de l'endoplasme et des vacuoles chez deux types de Dinoflagellés appartenant aux genres *Noctiluca* (Suriray) et *Blastodinium* (Chatton). *Zeitschrift für Zellforsch. und Mikroskopische Anat.* **105**, 350–388.

Soyer, M.-O. (1971). Structure du noyau des *Blastodinium* (Dinoflagellates parasites). *Chromosoma* **33**, 70–114.

Spector, D. L. (1984). *Dinoflagellates*.

Spero, H. J. (1982). Phagotrophy in *Gymnodinium fungiforme* (Pyrrhophyta): the peduncle as an organelle of ingestopn. *J. Phycol.* **18**, 356–360.

Sweeney, B. M. (1984). 10 - Circadian Rhythmicity in Dinoflagellates. In *Cell Biology* (ed. Spector, D. L. B. T.-D.), pp. 343–364. San Diego: Academic Press.

Taylor, F. J. R. (1971). Scanning Electron Microscopy of the thecae of the dinoflagellate genus *Ornithocerus*. *J. Phycol.* 5–24.

Taylor, F. J. R. (1973). Topography of cell division in the structurally complex dinoflagellate genus *Ornithocercus*. *J. Phycol.* **3**, 10–27.

Taylor, F. J. R. (1980). On dinoflagellate evolution. *BioSystems* **13**, 65–108.

Taylor, F. J. R. (1987a). *The biology of dinoflagellates*.

Taylor, F. J. R. (1987b). *The biology of dinoflagellates*. Oxford, Boston.

Tim*pano, P. and Pfiester, L. .* *(1985). Fine structure of the immobile dinococcalean Cystodinium bataviense* (Dinophyceae). *J. Phycol.* 5–24.

Triemer, R. E. (1982). A unique mitotic variation in the marine dinoflagellate Oxyrrhis marina (Pyrrophyta). 1–23.

Uwizeye, C., Decelle, J., Jouneau, P.-H., Flori, S., Gallet, B., Keck, J.-B., Bo, D. D., Moriscot, C., Seydoux, C., Chevalier, F., et al. (2021). Morphological bases of phytoplankton energy management and physiological responses unveiled by 3D subcellular imaging. *Nat. Commun.* **12**, 1049.

Venzhik, Y. V., Shchyogolev, S. Y. and Dykman, L. A. (2019). Ultrastructural Reorganization of Chloroplasts during Plant Adaptation to Abiotic Stress Factors. *Russ. J. Plant Physiol.* **66**, 850–863.

Wall, D., Guillard, R. R. L., Dale, B., Swift, E. and Watabe, N. (1970). Calcitic resting cysts in *Peridinium trochoideum* (Stein) Lemmermann, an autotrophic marine dinoflagellate. *Phycologia* **9**, 151–156.

Wedemayer, G. J. and Wilcox, L. W. (1984). The Ultrastructure of the Freshwater, Colorless Dinoflagellate *Peridiniopsis berolinense* (Lemm.) Bourrelly (Mastigophora, Dinoflagellida). *J. Protozool.* **31**, 444–453.

Whatley, J. M. (1993). The Endosymbiotic Origin of Chloroplasts. In (ed. Jeon, K. W.) and Jarvik, J. B. T.-I. R. of C.), pp. 259–299. Academic Press.

Yamada, N., Bolton, J. J., Trobajo, R., Mann, D. G., Dąbek, P., Witkowski, A., Onuma, R., Horiguchi, T. and Kroth, P. G. (2019). Discovery of a kleptoplastic 'dinotom' dinoflagellate and the unique nuclear dynamics of converting kleptoplastids to permanent plastids. *Sci. Rep.* **9**, 1–13.

Ytterberg, A. J., Peltier, J. B. and Van Wijk, K. J. (2006). Protein profiling of plastoglobules in chloroplasts and chromoplasts. A surprising site for differential accumulation of metabolic enzymes. *Plant Physiol.* **140**, 984–997.

Zinssmeister, C., Keupp, H., Tischendorf, G., Kaulbars, F. and Gottschling, M. (2013). Ultrastructure of Calcareous Dinophytes (Thoracosphaeraceae, Peridiniales) with a Focus on Vacuolar Crystal-Like Particles. *PLoS One* **8**,.

Zinssmeister, C., Wilke, T. and Hoppenrath, M. (2017). Species diversity of dinophysoid dinoflagellates in the Clarion–Clipperton Fracture Zone, eastern Pacific. *Mar. Biodivers.* **47**, 271–287.

Zobell, C. E. and Hittle, L. L. (1969). Deep-Sea Hydrolysis Pressure Effects on Starch by marine Bacteria .*Journal of the Oceaographical Society of Japan* . **25**, 36–47.

Chapter II: Setting up the sampling expeditions

1- Introduction

As human, we tend to enjoy or feel the need to make detailed records of our surroundings, whether geographically through maps or describing the fauna and flora through scientific reports and atlases. Interestingly, both maps and environmental descriptions are intricately linked, as the presence of an ecosystems is relying on specific localizations, their associated climate, topography and so on.

The first long expeditions at sea had the objective to discover new grounds, which in combination to in land exploration, led to the progressive creation of detailed geographical maps. Through time, the world boundaries and knowledge of our planet were then slowly extended, until reaching the maps as we know of today.

Additionally, on top of these maps, annotations of the occurrence of macroscopic to microscopic organisms were progressively added. Indeed, while humans pushed the limits of their geographical knowledge, they also started to include dedicated people in their expeditions to produce descriptions of land and water plants and animals.

A very well-known example are the descriptions made by Charles Darwin, published in 1939, after he had embarked on the Beagles (1831-1836) as the naturalist of the expedition. This extensive work, as we know today, not only led to descriptions of a wide range landscapes as well as organisms and their distribution across the globe, but also to be his spark for the theory of evolution. Interestingly, during the expedition, Darwin who investigated lands as well as shallow seas, had the idea to collect small organisms from the steamer in 1832 and observed what would later be named “plankton” by Victor Hensen in 1887. Furthermore, the mysteries of deep seas were later investigated during the expedition of the Challenger from 1872-1876.

Many expeditions and time series were performed at marine stations over the last centuries, leading to growing knowledge on marine life. Among oceanic life, the plankton word has always been source of fascination. Of course, one could not omit the fantastic descriptions of Ernst Haeckel of various phyla published from 1899 to 1904. Or more recently, the collection of images published by Christian Sardet, as well as the informational videos (plankton chronical) on these beautiful microorganisms, sensibilizing a wider population to the life in our oceans.

Lately, scientific projects engaging the public as the TARA ocean project, and the newly TREC expedition, have been focusing on developing a more comprehensive understanding of the microorganisms populating our rivers, seas and coastal areas. From the first expeditions to missions performed nowadays, it is interesting to think about scales. Indeed, when in the past one naturalist was joining a five-year travel, nowadays a team of tens of scientists can participate to month long expeditions. Furthermore, the technological aspect also developed drastically, allowing to extensively deepen our analysis. One component that has not change is the curiosity of the actors involved, which does not seem to have faded over centuries of observations and scientific reports.

Expeditions are usually thrilling in our eyes; indeed, they make our imagination wander. Early on, as children, we often read books counting discoveries of unknown territories. This excitement of the unknown led us daydreaming about what it could be like to go and explore (sometimes somewhere as easy as in the neighbouring pond, which led already to mind-blowing observations). Thus, having the opportunity to work on a PhD project that would include field work was incredible. In this chapter, I will describe the setting up of the procedures now used in the context of the TREC expedition and its mobile laboratory in order to investigate the ultrastructure of marine microorganisms across gradients.

2- Contributors

I had the chance to participate in 4 missions that were aimed to pilot the workflows and some of the projects currently running in the ongoing TREC expedition, namely in Ischia (Italy) at the Stazione Zoologica Anton Dohrn in 2019, in Villefranche-sur-Mer (France) at the Institut de la Mer in 2020 and 2021 and in 2022 in Iceland at the Marine and Freshwater Research Institute in Hafnafjordur. For each of these missions, a wide number of scientists and organizers were involved. Their name and contributions will be underlined here.

For the expedition of Ischia, I had the great help from Rachel Templin (former member of the Schwab team, now at Monash University), Yannick Schwab and Rick Webb (formerly at Queensland University) both for setting up the material needed for the expedition as well as for the methodology during sampling and processing of the plankton cells. I also had the support of the group of Detlev Arendt (EMBL Heidelberg), who were already quite experienced in the field and particularly from Emily Savage, Leslie Pan and Phil Oel. From the Marine station site, I had support from Domenico D'Alelio and many team members of the institute.

For the expeditions in Villefranche-sur-Mer in 2020 and 2021, I had support from my supervisor, Yannick Schwab, the group of Detlev Arendt (Emily Savage, Leslie Pan) as well as from the group of Johan Decelle (CEA Grenoble) and Rainer Pepperkok (Hugo Berthelot and Joanna Zukowska, EMBL Heidelberg). Indeed, I learned how to collect microplankton thanks to Johan Decelle, Charlotte Le Kieffre and Fabien Chevalier. This sampling would also not have been possible without the contribution of the drivers of the boat from the marine station. Moreover, I had great help from team from the Marine station in Villefranche and particularly Raffaela Cattano from EMBRC and Paola Bertucci from EMBL, who made it easy to set up our investigations on site. I had the great support from Anna Steyer (Mattei Group, EMBL Heidelberg) for both the organization of the mission in 2021 and on site for the preparation of the samples on site. During this expedition, I also got the support from Daniel. P. Yee (Johan Decelle Group, CEA Grenoble) for experiments including light microscopy and staining of the samples on site as well as Benoit Gallet (IBS Grenoble) for the cryopreservation set up on site. Leica Microsystems also highly contributed in the success of sample preparation for EM as they provided an HPF EM ICE for both these expeditions.

For the expedition in Iceland, I had once again the support from my supervisor, Yannick Schwab, as well as from the Group of Johan Decelle (CEA Grenoble), Rainer Pepperkok (EMBL Heidelberg), Ben Engels (Biozentrum, Basel), Gautam Dey (EMBL Heidelberg) as well as Omaya Dudin (EPFL Lausane). Once again, I got the great help of Anna Steyer (Mattei Group). I had help from the TREC / Mobile laboratory Teams and particularly Paola Bertucci as main coordinator of the expedition, Cristian Tambley for logistics and Nikolaus Leisch for help on site as well as with the HPF. On site, I had help from many people from the institute and particularly from Valerie Maier and Christophe Pampoulie. The boat drivers, who had great knowledge of the sampling areas, also highly contributed to the sampling. For this expedition, we greatly benefited from the generous loan of a HPF machine from the group of Nicole Dubilier (MPI Bremen).

3- Results

One general aim of this thesis was to develop a workflow to investigate, by electron microscopy (in parallel to LM and metabarcoding), the subcellular structures of microplankton from the environment. For each marine station, the goal was then to bring every consumable, chemical product as well as pieces of equipment needed.

3.1- Setting of an EM laboratory at a marine station

The first step of this thesis was to research and optimize as much as possible the strategies and potential protocols that would be used on site.

Sample preparation for electron microscopy generally requires special care in how cells are handled. Thus, reading on how to be as gentle as possible with this type of sample during sampling, filtration and their concentration was crucial (Sournia, 1978). Following previous reports in the literature of HPF yielding better ultrastructural preservation than chemical fixation, I was interested in performing HPF on these microorganisms. Additionally, as an HPF is not a common piece of equipment in marine stations, I was interested in comparing the ultrastructure resulting from cryopreserved samples versus chemically fixed ones.

In both the cases of chemical fixation or HPF, particular reagents and machinery are required. For chemical fixation, either a microwave protocol or chemical fixation at 4°C was performed (see Material and Methods). Note that both of these procedures required a chemical hood. For HPF, we used the EM ICE (Leica microsystems) and liquid nitrogen for cooling of the machine and sample storage. Thus, when planning for experiments outside of the comfort zone of a typical specialized EM laboratory, a lot of variables have to be taken into consideration. Indeed, it was very important to collaborate with the different marine stations in order to have a precise idea of where we would set up the different work stations to allow both optimal sample preparation as well as safety.

Furthermore, each year during the preparation of the TREC expedition, the number of groups collaborating together and joining the pilots progressively rose, along with the expertise present on site (Fig. 1). Correlated to larger teams, the amount and variety of equipment brought to marine stations also increased, requiring a more extensive planning and organization. Indeed, on the expeditions of 2021 in VSM as well as 2022 in Iceland, plunge freezers were added to the equipment specific to EM sample preparation. Plunge freezing is pivotal to prepare samples for cryo-EM studies, as well as for expansion microscopy.

After the elaboration of the sample preparation protocols that would be performed on site in Villefranche (Chapter II, 3.1, 3.2), I tried conceiving exhaustive lists of material (which would also allow to adapt to the unpredictability of environmental sampling). This was followed by verifying legislation and safety measures on chemicals and the equipment that would be transported to the sampling site. The next steps consist in packing and either driving to the site of interest, or organizing shipment for things to arrive at the right time and place.

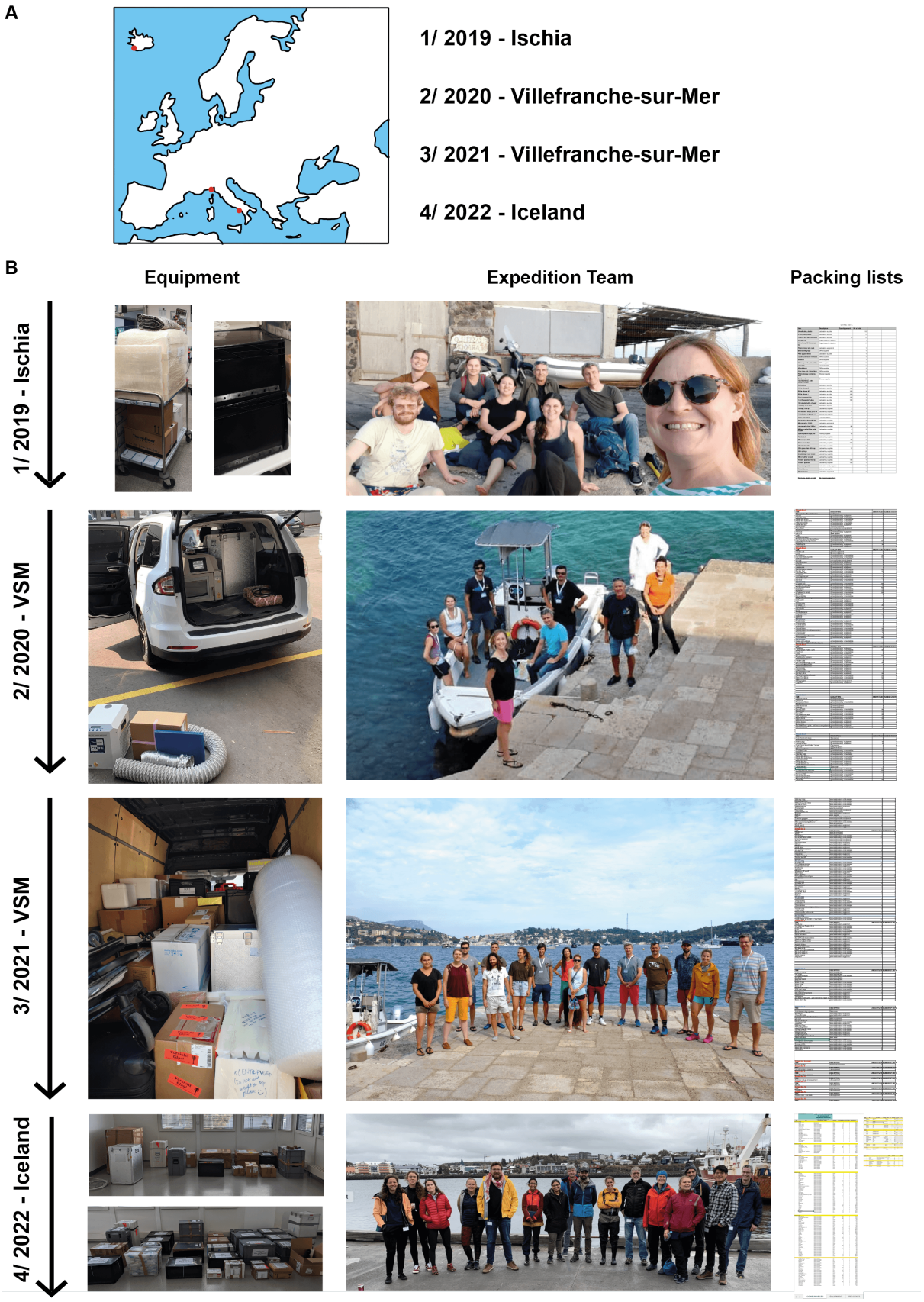

Figure 1: Overview of the four samplings sites (Ischia, Villefranche-sur-Mer (VSM) and Iceland) along with the growing team and amount of material.

3.1.1- Sample collection

For collection, as microphytoplankton density in the Bay of Villefranche-sur-Mer is known to be low even during maxima periods in spring and autumn (Gómez and Gorsky, 2003), after discussing with the experienced Group of Johan Decelle, net tows appeared as the method of choice (in opposition to the use of Niskin bottles for example). The mesh selected were measuring 5-7 µm and 10 µm for both nets and cod ends, as they would allow to collect the small size fraction that I was interested in (Fig. 2). The net presenting a 10 µm mesh size was preferably coupled with a cod end presenting a mesh of 5 µm for this study. Indeed, this combination allowed to collect more biomass than the combination of a 5 µm meshed net with a 5 µm meshed cod end. This is potentially due to lower sea water reflux when towing the net presenting a wider mesh in comparison to a finer mesh size.

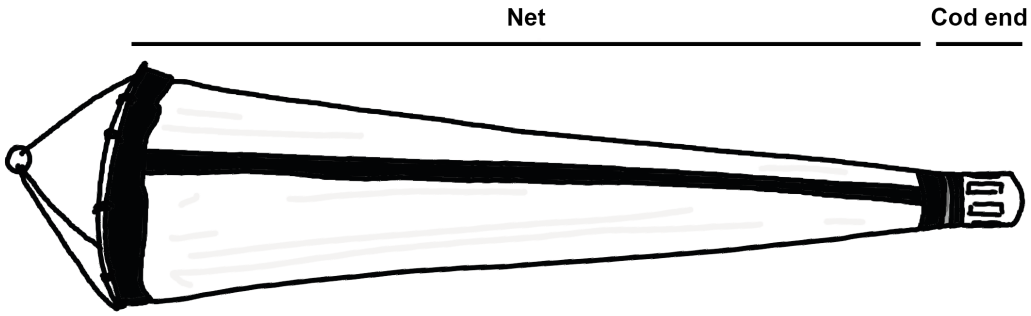

Figure 2: Scheme of a net and its cod end for sample collection.

Furthermore, one advantage of using nets is that the duration of the tow could be adapted depending on the cell density present for this size fraction and what I needed for my analysis. The optimal tow duration for each site was estimated by towing nets for different times as trials on the first sampling day, and looking at the cell density after concentration. Based on this, the tow time that led to the greater biomass without damaging cells or impacting the overall viability of the sample was selected for the rest of each expedition for consistency. One drawback of using nets is the potential distortion in species composition of the collected mix. Indeed, cells from the smaller fraction have more chances to pass through the mesh in comparison to bigger cells or colonies of cells. To avoid damaging delicate cells, sampling with a net was performed at very low cruising speed.

Note that other methods exist for collection, such as the use of water pumping systems on board or Niskin bottles. The water pumping systems require a particular set up (which are not accessible on every vessel) that has the advantage of allowing sampling for the entire size spectrum, and being quantitative as the volume collected can be measured precisely.

However, it was described as potentially harmful for delicate cells, and is limited to collecting cells at the depth of the tubing position (Sournia, 1978).

Niskin bottles, inspired from the invention of Fridtjof Nansen, are bottles which allow to sample at precise depth. However, the volume of water collected is here depending on the bottle(s) capacity, which can be a limiting feature in case of low biomass. As a net, filtering a large amount of water, yielded a quite low final biomass, using Niskin bottles would not have been optimal for the biomass required for EM processing in my case in Villefranche-sur-Mer.

Additionally, after a net tow, as our cod end could contain 750 ml of sample, this volume was easier to further concentrate, in comparison multiple litters obtained from towing Niskin bottles.

3.1.2- Use of serial sieves to collect the smaller fraction

Subsequently, on board, the organisms from the smaller size fraction were selected by passing the sample through a series of sieves (of 500, 100 and 40 µm mesh size), eliminating cells from the larger size fraction. The collected small size fractions were placed in plastic bottles, and kept in a cooler containing sea water to preserve them as close as possible to their initial living condition. Furthermore, the samples collected before daylight were kept away from light by closing the cooler.

3.1.3- Cell concentration

Back at the marine station, the samples were concentrated on a 1.2 µm mesh membrane made of mixed cellulose ester (MCE, Merk). I was interested in using these membrane filters as they allow a gentle and quite large solution flow (270 mL/min-cm^2 water flow rate, https://www.sigmaaldrich.com/DE/en/product/mm/rawp04700) compared to other materials as polycarbonate (175 mL/min x cm²,https://www.merckmillipore.com/DE/en/product/Isopore-Membrane-Filter,MM_NF-RTTP04700), allowing to avoid rapid clogging and putting too much pressure on the cells which could be detrimental for their ultrastructure. Furthermore, the MCE filters were described to be used for establishing cultures, which is encouraging concerning the preservation of the optimal viability of the sample.

In order to be as gentle as possible, a manual pump (Mityvac) was used over an electric pump, as it allowed for a slow and controlled concentration of the sample. When the sample volume filtered on the MCE membrane was reaching approximately 2-4 ml, cells were gently resuspended on the filter using a Pasteur pipette, and placed in low binding 1.5ml tubes

(Eppendorf). Indeed, as small planktonic cells easily bind to plastic or glass, low binding tubes were used to avoid cell loss.

As the cell density was very low in samples from the south of France, an extra step of centrifugation at 1000G was performed (the centrifuge temperature was adapted to sea water temperature). During the first day of the expedition in 2020, I tried multiple speeds and various amount of centrifugation times. After observation of the cells using light microscopy, 1000G for 5' was selected as it allowed for enough concentration of the cells for EM processing, without creating apparent damage to their global structure. Note that the use of a centrifuge with swinging bucket is preferable in order to have a pellet forming at the bottom of the tube simplifying downstream processing.

In Iceland the cell density was much higher in the sea than in the France, thus the nets were towed for only 1 minute. Furthermore, after concentrating on the MCE filters (Merk), collected samples were left to sediment for 15 minutes (at sea temperature) yielding a dense cell pellet used for subsequent analysis.

3.2- Sample processing for EM, LM and metabarcoding

These concentrated samples were each then rapidly processed in parallel for EM analysis, LM analysis and metabarcoding. The aim was to have a maximum of 2 hours between sample collection and final processing of the sample, as these cells are fragile and have been reported to decay rapidly (Sournia, 1978). Indeed, ultrastructural analysis requires healthiest cells as possible in order obtain the best ultrastructure.

3.2.1- Sample preparation for EM

EM processing for TEM or vEM analysis was done either by using chemical fixation or High-Pressure Freezing. The chemically fixed samples were kept at 4°C and brought back to EMBL, while the HPF samples were kept at cryogenic temperatures and brought back to EMBL. After comparing the chemically fixed or high-pressure frozen samples from Villefranche-sur-Mer in 2020, the strategy of performing HPF over chemical fixation was chosen as it was essential to preserve at best the microorganisms ultrastructure.

Indeed, chemical fixation introduced numerous artifacts in comparison to cryopreservation (Fig. 3). For instance, there was much more extraction in general (Fig. 3, asterisks). Furthermore, the chemically fixed samples often presented membrane showing discontinuity

and appearing detached from their initial position (Fig. 3C, empty black arrow). Additionally, in general the chemically fixed samples appeared as if they suffered from osmolarity issues as they seem to show shrinkage, associated to “empty” areas (Fig. 3A, full black arrow), and present structures that appear less rounded. Note that some structures seem to be less affected, as the trichocysts. Overall, our observations were consistent with previous studies where HPF was shown to allow better subcellular preservation of the samples over chemical fixation (Dahl and Staehelin, 1989; McDonald et al., 2010; Steinbrecht and Müller, 1987).

Note that these artifacts are probably not only coming from the fixation (due to chemicals and/or use of the microwave), but could also have been introduced during the sample preparation for EM. Indeed, to be able to process the chemically fixed samples without losing cells (that would resuspend at each solution exchange, and which are additionally not directly visible to the human eye), I embedded them in low melting agarose using centrifugation (1000 G). This step, and other following steps of the sample preparation could also have had an effect on the cells’ ultrastructure.

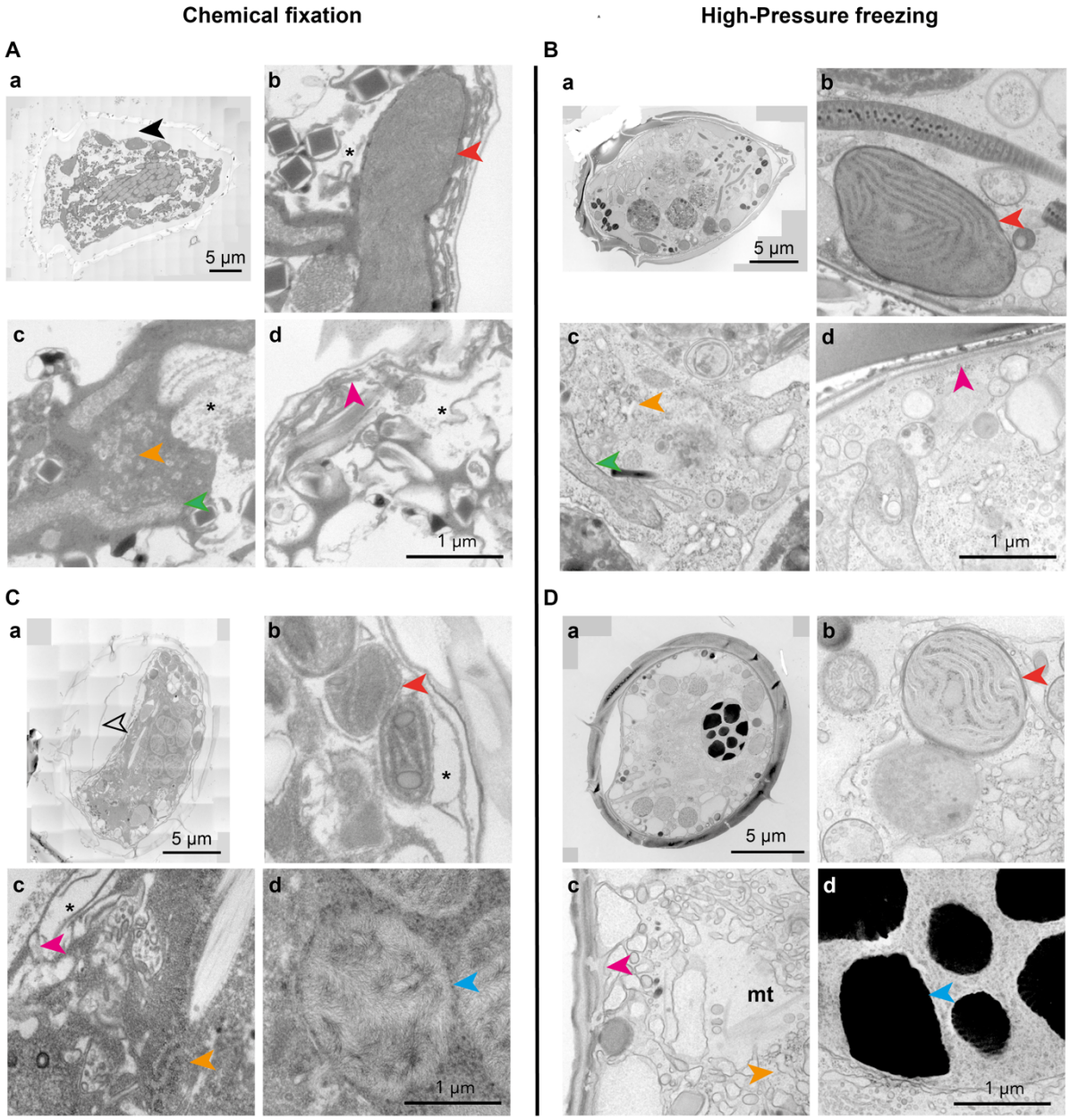

Figure 3: Electron microscopy micrographs representative of samples collected in Villefranche-sur-Mer (2020) that were chemically fixed or High-Pressure Frozen. A,C) Dinoflagellate that were chemically fixed and processed for EM. B,D) Dinoflagellate that were High-Pressure Frozen and processed for EM analysis (See Material and Method and Chapter III). a) Overview of the cell, b) Close ups from a region containing a chloroplast (red arrow), c) Close up of a region containing ER (orange arrow), d) Close up to the cortical region (pink arrow) for A-B and nuclear region containing chromosomes (blue arrow) for C-D. The full black arrow shows potential chemical fixation induced shrinkage of the cell, the empty black arrow shows detachment of membrane and the asterisk show regions that show extraction. The mitochondria is pointed out by a green arrow. In HPF samples, microtubules (mt) can often be observed, an example is shown in D-c).

3.2.2- Sample preparation for LM

A short light microscopy screen of each sampling session was performed on site on living cells. This allowed to check for sample quality especially by assessing the quantity of healthy cells that usually displayed a richer cytoplasm (Fig. 4B-K) or of damaged cells showing altered morphology (Fig. 4M). Furthermore, during this screen, I was verifying if cells were moving and whether there were debris or sediments within the sample (Fig. 4L). Additionally, this allowed to make a first general assessment of the cell community composition after collection. For instance, it was possible to evaluate whether there are a majority of diatoms or dinoflagellates, as well as which genus are predominant (Fig. 4). Aside from observation of living samples, a fraction of cells was fixed for later LM analysis performed at EMBL.

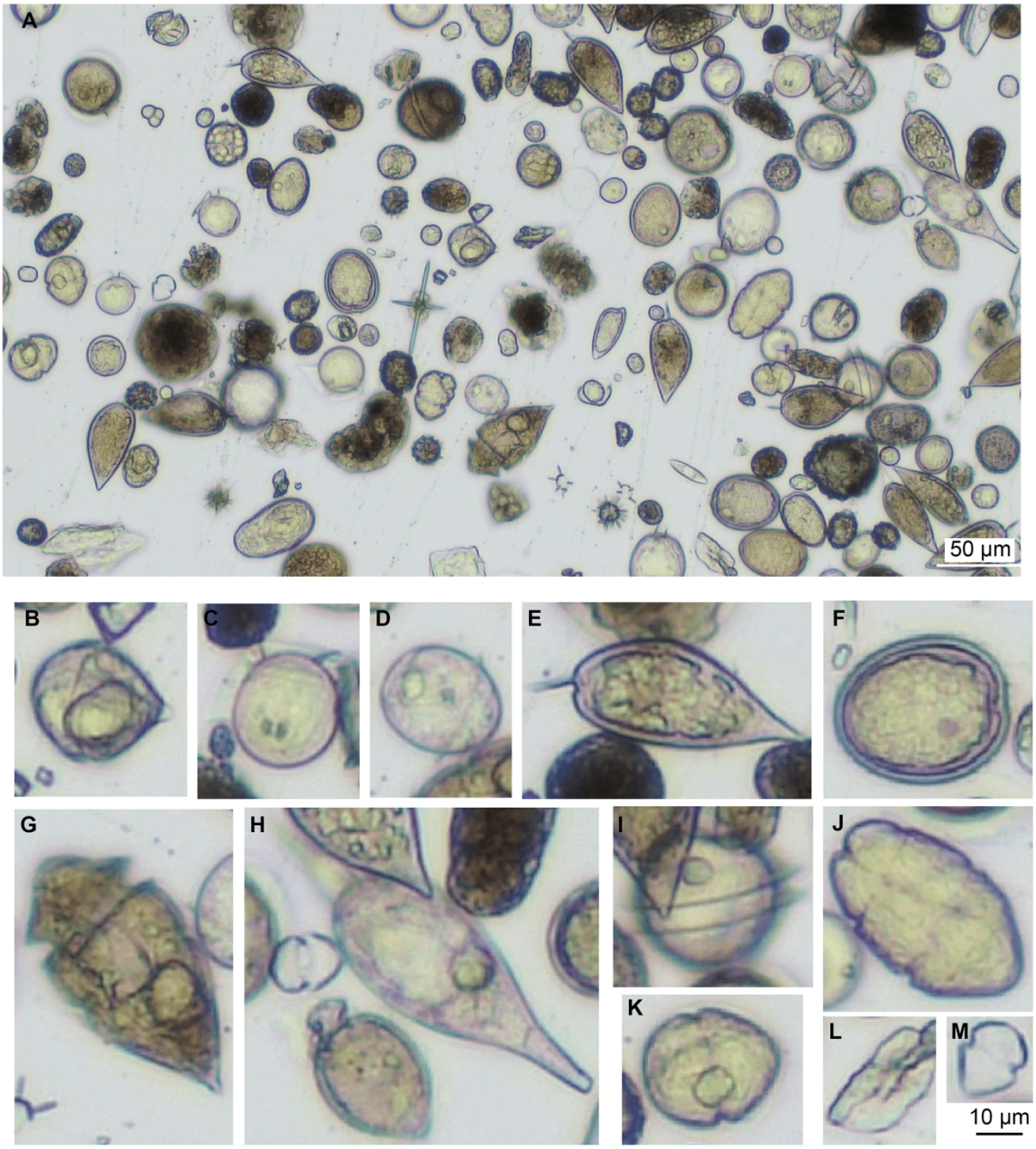

Figure 4: Light microscopy micrograph representative of a sample collected in Villefranche-sur-Mer (2020) after cell concentration. General quality assessment is done by verifying whether the cells seem full of material, and do not show breakage, as well as examining whether they are still swimming within the sample. Furthermore, this approach allows to have an idea of the principal genera that will be imaged in the TEM screen and whether a lot of debris or other material are present. B) *Protoperidinium sp,* C) *Dinophysis sp,* D) *Paleophalacroma sp,* E) *Prorocentrum cf. gracile,* F) *Prorocentrum sp*, G) *Oxytoxum sp,* H) *Podolampas sp,* I) *Triadinium sp,* J) *Polykrikos sp*, K) Non identified, L) Example of debris or other type of material in the sample, M) Example of an empty theca.

3.2.3- Sample preparation for 18S analysis

Processing of the sample for metabarcoding consisted in snap freezing part of the concentrated sample (divided in 3 for EM, LM and metabarcoding downstream processing) or

snap freezing of the concentrated sample on a 1.2 PC membrane (Merk) and bringing them back at EMBL Heidelberg at cryogenic temperatures before further processing with the help of Joanna Zukowska and Hugo Berthelot.

4- Material and Methods

4.1 Chemical fixation and sample preparation for TEM

During the expedition of VSM 2020, part of the concentrated cells was primarily fixed using 2.5% Glutaraldehyde (EMS) and 4% Formaldehyde (EMS) in 0.15M marPHEM (Montanaro et al., 2016) using the biowave (Pelco, Table 1). After fixation, the samples were pelleted using centrifugation (5-10 minutes at 1000G), the supernatant was removed and replaced by 2% Formaldehyde in 0.15 PHEM buffer. The samples were then kept at 4°C and transported back to EMBL.

At EMBL, one sample from the morning sampling and one from the afternoon sampling of the 20/09/16 were processed for EM analysis. Note that during this procedure, low binding tubes were used in order to avoid loosing cells as much as possible. The samples were first washed three times using 0.15 M PHEM at 4°C before embedding the pellet in 2% low melting agarose according to Dittrich et al., 2022. After the agarose solidification on ice, the pellet was cut off the tube and transferred to 0.15M PHEM buffer. After two washes in 0.15 M PHEM, 2 washes in H_2O were performed. Then, osmification was done in the microwave (Table 2, step 1-7) using 1% OsO_4 (Serva) in H_2O. The samples underwent 1 rinse with H_2O on the bench and 2 rinses with H_2O in the microwave (Table 2, step 8-9). The next step was done using 1% UA (Agar Scientific) on ice in the microwave (Table 2, step 10-16). The samples underwent 1 rinse with H_2O on the bench and 2 rinses with H_2O in the microwave (Table 2, step 17-18). The samples were then progressively dehydrated using an acetone/H_2O (vol/vol) series of 30%, 50%, 75% of acetone (EMS). For each step of the series of dehydration, one exchange was done on the bench and one in the microwave (Table 2, step 19-21). For the 100% acetone step, two exchanges were done on the bench and two in the microwave (Table 2, step 22-23). The samples were then progressively infiltrated in liquid resin using an acetone/resin (vol/vol) series of 30%, 50%, 75% acetone. For each step, one exchange was done on the bench and one in the microwave (Table 2, step 24-28). For the 100% resin step, two exchanges were done on the bench and three in the microwave (Table 2, step 29-31). The samples were then placed for 1h at room temperature in 100% fresh resin, before embedding in moulds in 100% fresh resin. The samples were then polymerized for 48h at 60°C.

Step	Description	User prompt	Time	Power (Watts)	Temp (°C)/ Load cooler	Vacuum	Steady temp pump (on/off)	Steady temp (°C)
1	GA/FA 0.15M mPHEM	Off	2’	100	50 / Off	On	On	20
2	GA/FA 0.15M mPHEM	Off	2’	0	50 / Off	On	On	20
3	GA/FA 0.15M mPHEM	Off	2’	100	50 / Off	On	On	20
4	GA/FA 0.15M mPHEM	Off	2’	0	50 / Off	On	On	20
5	GA/FA 0.15M mPHEM	Off	2’	100	50 / Off	On	On	20
6	GA/FA 0.15M mPHEM	Off	2’	0	50 / Off	On	On	20
7	GA/FA 0.15M mPHEM	Off	2’	100	50 / Off	On	On	20
8	0.15M PHEM	On	40’’	250	50 / Off	Off	On	20
9	0.15M PHEM	On	40’’	250	50 / Off	Off	On	20

Table 1: Description of the microwave protocol used to chemically fixe samples from VSM 2020.

Step	Description	User prompt	Time	Power (Watts)	Temp (°C)/ Load cooler	Vacuum	Steady temp pump (on/off)	Steady temp (°C)
1	OsO_4	On	2’	100	50 / Off	Vacuum cycle	On	23
2	OsO_4	Off	2’	0	50 / Off	Vacuum on	On	23
3	OsO_4	Off	2’	100	50 / Off	Vacuum on	On	23

4	OsO_4	Off	2’	0	50 / Off	Vacuum on	On	23
5	OsO_4	Off	2’	100	50 / Off	Vacuum on	On	23
6	OsO_4	Off	2’	0	50 / Off	Vacuum on	On	23
7	OsO_4	Off	2’	100	50 / Off	Vacuum cycle	On	23
Bench rinse (in the hood)								
8	H_2O	On	40’’	250	50 / Off	Off	On	23
9	H_2O	On	40’’	250	50 / Off	Off	On	23
10	UA on ice	On	1’	150	50 / Off	Vacuum cycle	On	23
11	UA on ice	Off	1’	0	50 / Off	Vacuum on	On	23
12	UA on ice	Off	1’	150	50 / Off	Vacuum on	On	23
13	UA on ice	Off	1’	0	50 / Off	Vacuum on	On	23
14	UA on ice	Off	1’	150	50 / Off	Vacuum on	On	23
15	UA on ice	Off	1’	0	50 / Off	Vacuum on	On	23
16	UA on ice	Off	1’	150	50 / Off	Vacuum cycle	On	23
Bench rinse (in the hood)								
17	H_2O	On	40’’	250	50 / Off	Off	On	23
18	H_2O	On	40’’	250	50 / Off	Off	On	23
On the bench - 30% Acetone								
19	30% Acetone	On	40’’	250	50 / Off	Off	On	23
On the bench - 50% Acetone								
20	50% Acetone	On	40’’	250	50 / Off	Off	On	23
On the bench - 75% Acetone								
21	75% Acetone	On	40’’	250	50 / Off	Off	On	23
On the bench - 100% Acetone (x 2)								
22	100% Acetone	On	40’’	250	50 / Off	Off	On	23
23	100% Acetone	On	40’’	250	50 / Off	Off	On	23
On the bench - 25% Resin								
24	25% Resin	On	3’	250	50 / Off	Vacuum cycle	On	23
On the bench - 50% Resin								
25	50% Resin	On	3’	250	50 / Off	Vacuum cycle	On	23
On the bench - 50% Resin								
26	50% Resin	On	3’	250	50 / Off	Vacuum cycle	On	23
On the bench - 75% Resin								
27	75% Resin	On	3’	250	50 / Off	Vacuum cycle	On	23

On the bench - 75% Resin								
28	75% Resin	On	3’	250	50 / Off	Vacuum cycle	On	23
On the bench - 100% Resin (x2)								
29	100% Resin	On	3’	250	50 / Off	Vacuum cycle	On	23
30	100% Resin	On	3’	250	50 / Off	Vacuum cycle	On	23
31	100% Resin	On	3’	250	50 / Off	Vacuum cycle	On	23
On the bench – fresh 100% Resin for 60’								
Embedding in moulds in fresh 100% resin – 48h oven at 60°C								

Table 2: Details of the microwave protocol used for EM processing of the chemically fixed samples from VSM 2020.

Note that during the other expedition in Villefranche-sur-Mer and in Iceland, chemical fixation was performed by using a primary fixation at 4°C during 4 hours with 2% formaldehyde (EMS) and 0.5% glutaraldehyde (EMS) in 0.1 marPHEM buffer. During these 4h, the cells sedimented and the primary fixative was removed and replaced by 1% formaldehyde in 0.1M PHEM. The protocol for fixation was adapted after trying two fixative concentrations in combination to HPF, in collaboration with the Group of Johan Decelle and Benoit Gallet. From our observations, mixed cultures of phytoplankton that were chemically fixed with lower amounts of formaldehyde and glutaraldehyde, in combination with HPF after primary fixation, showed better preservation of subcellular compartments. Thus, as a safety measure in case shipment of HPF samples fails or in order to perform later LM experiments or SEM processing at EMBL, samples from VSM 2021 and Iceland 2022 were chemically fixed as described in this paragraph.

4.2 HPF and sample preparation

See material and methods in Chapter III.

5- Discussion

During my thesis, I contributed in setting up the expeditions and worked on developing workflows to investigate by electron microscopy, in combination with LM and metabarcoding, the small size fraction of marine microplankton (5/10 to 40 µm). As these workflows were established initially to collect samples from south of France, they were designed particularly to sample in condition of low biomass. However, based on the Icelandic expedition these workflows could be easily adapted for investigations of denser waters.

HPF machines are usually not common at marine stations. Thus, having the opportunity to investigate the ultrastructure of environmental field samples using this technique, allowed to realize the potential in subcellular studies for these microorganisms offered by this approach. These technologies are now further used in the context of the TREC expedition. Indeed, among other advanced technologies, an HPF is present within the EMBL's Advanced Mobile Laboratory that has been designed for TREC and that is traveling across the European coastline to study ecosystems across environmental gradients.

However, even though HPF yielded great results concerning ultrastructure preservation, during our TEM screen analysis on VSM 20 and VSM 21 samples (Chapter III), it seemed that the flagella of many dinoflagellates were lost, or located within the theca. This observation raised the question on when these cells could have shredded, lost or internalised their flagella. As of now, I am still unsure about the step at which this might be occurring. Indeed, as many cells were still swimming when observed by LM on site, my first assumption was that this phenomenon might happen during High-Pressure Freezing or later sample preparation for electron microscopy. However, I also have been wondering whether this could be linked to the step of centrifugation, leading me to choose sedimentation over centrifugation in Iceland. In the future, it might be interesting to optimize further for the gentlest concentration possible for cells to be High-Pressure Frozen.

Environmental samples are highly complex, being influenced by numerous parameters independent of one's control (stream forces, weather condition etc…) that could modify their physiology and morphologies. Thus, in order to work towards a more comprehensive understanding of the studied system, it important to capture further metadata in parallel to the sampling. This can be performed for instance by using dedicated instruments such a CTD, to acquire information on the water's conductivity, temperature and depth, and to derive parameters such as the water salinity. Furthermore, using added sensors could reveal information on the pH, oxygen levels, fluorescence pics, nitrogen concentration etc. Altogether, these measurements would permit better understanding of the chemistry, physics and biology of the area where samples were collected. Measuring the concentration of chlorophyl at different depth also enables to establish which layer is enriched in phytoplankton, paramount to target these organisms in stratified environments.

A major challenge then is to deal with the large biodiversity sampled in natural ecosystems. Net tows do not discriminate the species present in the water, and even when performing size fractionation as I have been doing during the expeditions, the concentrated samples present

an important taxonomic diversity. In the following chapters, I will show haw we have tried to address these challenges by either performing systematic observation of all cells present in a 2D section at the TEM, or by adapting a correlative light and electron microscopy technique to target cells of interest. Another, solution, that I have not used during my thesis work, would have been to utilize semi-automatic pipelines in order to screen and sort the samples, back at the marine station, via gentle cell sorting. Indeed, this could allow to give more time and flexibility to the experimenter to perform the parallel processing of the samples for each modality. Furthermore, if such a pipeline would include some Artificial Intelligence (AI) assisted processing of the images, this would allow to have an estimate of the species present within the sample and their approximate relative concentration, and eventually to purify them from the community. One future direction for this type of workflows done on the field would thus be to add a step of cell sorting. This will allow to enrich in a certain cell type opening the door to complementary integrated analyses such as metabolomics, transcriptomic or proteomics, performed in parallel to ultrastructural studies.

6- References

Dahl, R. and Staehelin, L. A. (1989). High pressure freezing for the preservation of biological structure: Theory and practice. *J. Electron Microsc. Tech.* **13**, 165–174.

Gómez, F. and Gorsky, G. (2003). Annual microplankton cycles in Villefranche Bay, Ligurian Sea, NW Mediterranean. *J. Plankton Res.* **25**, 323–339.

McDonald, K., Schwarz, H., Müller-Reichert, T., Webb, R., Buser, C. and Morphew, M. (2010). *"Tips and tricks" for high-pressure freezing of model systems*. Elsevier Inc.

Sournia, A. (1978). *Phytoplankton manual*.

Steinbrecht, R. . and Müller, M. (1987). *Freeze-substitution and Freeze-Drying*.

Chapter III: Transmission Electron Microscopy screen of environmental microorganisms

1- Introduction

In the previous chapter, I walked you through how the laboratory was set up at marine stations, as well as how strategies were developed to preserve at best the ultrastructure of environmental samples for electron microscopy analysis. In this chapter, I will now describe how the 2D ultrastructural analysis was carried out, as well as the results it yielded.

One aim of this thesis was to execute an unbiased subcellular analysis of microorganisms from their native habitat. The samples were collected in surface waters of the Villefranche-sur-Mer Bay for two consecutive years, in September 2020 and 2021. Furthermore, for each year, sampling was performed both in the early morning (before sunrise) or in the afternoon.

With this analysis, one goal was to construct an ultrastructural atlas of marine dinoflagellates of the surface waters of Villefranche-sur-mer. Furthermore, another aim of this project was to investigate whether we could identify, at the population level, morphological variations between the two sampling conditions (early morning and early afternoon). Lastly, as previously hypothesized that certain ultrastructural features correlate with taxonomical identification, one objective was to investigate whether we could identify subcellular characteristics that could be indicative of certain genus or species.

In order to answer these questions, samples from 3 mornings and 3 afternoons of the years 2020 and 2021 were prepared for electron microscopy and subsequently sectioned and acquired using TEM. All cells present in single sections were systematically imaged and micrographs were then carefully analysed to build a complete annotation of a number of organelles and other subcellular structures.

Whilst deeper analyses will be necessary to thoroughly compare the ultrastructure of cells across this diurnal gradient, we could already observe a higher number of starch granules in dinoflagellates collected in the afternoon, compared to the ones collected in the morning. Furthermore, in plastid bearing dinoflagellates, we could observe a more important number of plastoglobuli in cells collected later during the day, than before sunrise.

I will also describe in this chapter a subset of organelles that seem to be associated to certain genera. Furthermore, after analysis, a few organelles appeared to be present particularly in heterotrophic dinoflagellates. The combination of an optimal sample preparation with the utilisation of high-throughput TEM image acquisition thus bears the potential to utilize organelles to characterise plankton species within a highly heterogeneous community.

2- Contributors

Sample collection for this work was done in collaboration with the team of Johan Decelle at Grenoble CEA (Johan Decelle, Charlotte LeKieffre, Daniel. P. Yee, Fabien Chevalier) and Anna Steyer (Mattei Group, EMBL Heidelberg). The conceptualization for this work was done with Yannick Schwab. Benoit Gallet, Martin Schorb, Viola Oorschot, Anna Steyer, Ines Romero Brey contributed to the methodology. Ines Romero Brey, contributed in the trimming, sectioning and imaging of cells for this screen. Martin Schorb contributed in software and visualization development for this project. Nadezda Matzko helped with the identification of certain structures and Paolo Ronchi with scientific discussions. Furthermore, contributors for the organisation of this mission are listed in Chapter II.

Mona Hoppenrath, Raffaele Siano, Nicolas Chomerat, Kenneth Mertens and Hugo Berthelot helped with taxonomical identification from SEM images.

The metadata was obtained thanks to a public data base associated to the marine station of Villefranche-sur-Mer. “This project was/is funded by CNRS-INSU, the Observatoire de Villefranche and the OSU STAMAR. It has benefited from the support of the SOMLIT (www.somlit.fr) and the French Research Infrastructure for Coastal Ocean Observations ILICO (www.ir-ilico.fr).We'd like to thank all of the people helping us to obtain the data set through time, as well as the crew members of the different boat of the stations for their help at sea”.

3- Material and methods

3.1- Sample collection

Sampling of marine planktonic cells was done by towing a net (5 or 10 µm mesh size) for 10 minutes at around 2 knots in surface waters of the Villefranche-sur-Mer bay (France). Sampling sessions were performed in the early mornings and afternoons of the consecutive

years 2020 and 2021, in the same area, on the 16-17-18th of September, 2020 and 9-10-13-14th of September, 2021. After collection, the samples were then filtered through serial sieves (Retsch) onboard to collect cells measuring less than 40 µm in size. At the marine station, this size fraction was concentrated by filtration using manual pumping on a 1.2 mixed cellulose ester membrane (Merck). The samples were then resuspended in a final volume of about 4 ml, and further centrifuged for 5 minutes at 1000g to obtain a pellet. The supernatant was carefully removed and approximately 1.2 µl of the pellet was loaded in a gold copper type A carrier (Leica; 200 µm deep and 3 mm wide) precoated with hexadecane (Merk). The sample was subsequently covered by the flat side of an aluminium type B carrier (Leica microsystems), also precoated with hexadecane (Merk), and high-pressure frozen using the Leica EM ICE (Leica microsystems).

3.2- Sampling metadata

The nets were towed approximately between -10 and -30 m in 2020, and preferably around -30 m in 2021 using weights and an appropriate length of rope. This corresponds to where the biomass was higher according to the CTD fluorescent profiles from point B (ref, Fig. 1A,B). The oxygen profiles were similar between 2020 and 2021 and ranged from 3.5 and 5.5 ml/L (Fig. 1A,B). According to metadata extracted from the point B coastal hydrology CTD casts dataset, the sea water temperature from 0 to -30 meters was ranging between 24.5°C and 15.0°C in September, 2020 (Fig. 1A). The sea water temperature from 0 to -30 meters was ranging between 24.5°C and 17.0° C in September, 2021 (Fig. 1B). The salinity across these same depths was ranging from 37.70 to 38.15 in 2020 (Fig. 1A) and from 38.00 to 38.35 in 2021 (Fig. 1B).

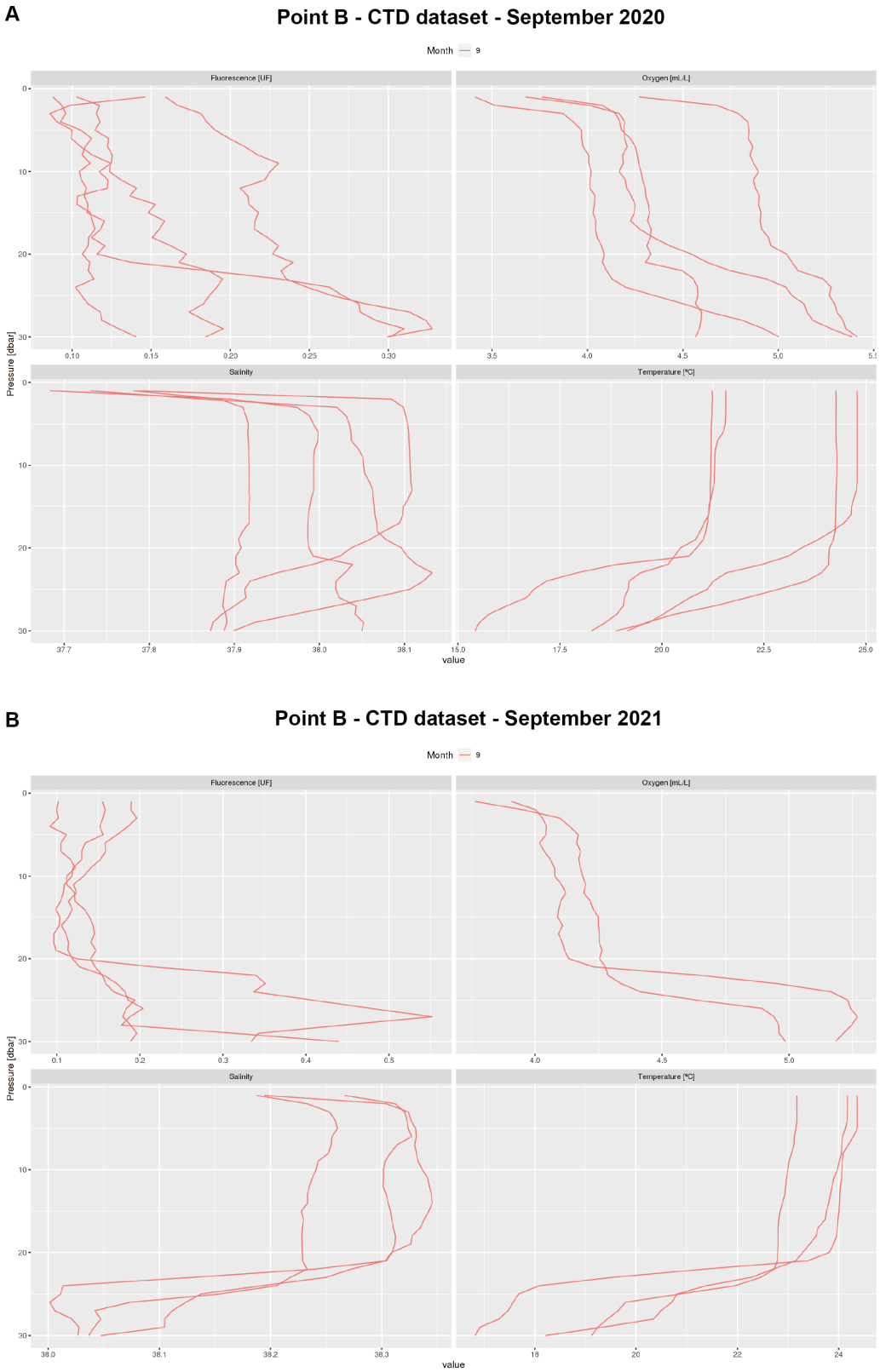

Figure 1: CTD fluorescence (UF), oxygen (ml/L), salinity and temperature (C°) vertical profiles from Point B for September 2020 and 2021. A) Profiles for September 2020, B) Profiles for September 2021. A,B) the upper left panels show the fluorescence profiles (UF), the upper right

panels show the oxygen levels (ml/L), the lower left panels show the salinity profiles and the lower right panels show the temperature (°C) profiles.

3.3- High Pressure Freezing and Freeze Substitution

HPF samples were transported back to EMBL Heidelberg at cryogenic temperatures. Following arrival, the cryoimmobilized samples underwent freeze-substitution (EM-AFS2, Leica microsystems) using the following program and solutions: 60h at -90°C in 2% osmium tetroxide (Serva) in dry acetone (EMS), heating rate of 2°C/h for 15h to -60°C, 10h at -60°C, heating rate of 2°C/h for 15h to -30°C, 10h at -30°C, maximum heating rate to 0°C in 1 minute, 1h at 0°C, maximum cooling rate to -30°C in 1 minute, 5 washes at -30°C using dry acetone (EMS).

The samples were then gradually infiltrated with EPON hard. The resin (without accelerator)/acetone (v/v) series were the following: 25% for 2h starting at -30°C and raising to -10°C, 50% for 2h starting at -10°C and raising to +10°C with a heating rate of 10°C/h and 75% for 2h starting at +10°C and raising to +20°C with a heating rate of 5°C/h. Samples were then infiltrated in 100% resin without accelerator, successively for 12 hours and 48 hours.

Infiltration with 100% resin containing accelerator was then performed for 2 to 3 times for 3 hours and one time for 12 hours before polymerization at 60°C for 48 hours. 70nm thin sections were cut using an ultramicrotome (Leica EM-UC7, Leica microsystems) with an ultra-diamond knife (Diatome). The thin sections obtained were then post stained using successively 1% uranyl acetate (Agar Scientific) in water for 20 minutes and lead citrate (made in house with solutions from Sigma and Merck) for 3 to 5 minutes.

3.4- Imaging and annotation

Tile montages of each imaged sections were acquired using Serial EM, at low magnification (200x and 400x at 120 Kv, pixel size: 64.34 nm and 41.25 nm respectively on the Jeol 2100Plus and Jeol 1400Flash) on respectively the JEOL JEM 2100plus and the JEOL-JEM 1400 Flash system to determine the position of the cells. For each section, either every cell on the section was acquired, or if the number of cells was much greater than 100, around 100 cells were acquired (in a random manner to not introduce a selection bias). For each cell, higher magnification tile montages (8000X or 10000x at 120V, pixel size: 1.667 nm and 1.766 nm respectively on the Jeol 2100Plus and Jeol 1400Flash) were acquired through SerialEM on respectively the JEOL JEM 2100plus and the JEOL-JEM 1400 Flash systems. Montages

were processed using Imod and Fiji. High pressure frozen samples were processed in the Electron Core Microscopy Facility (EMCF) at EMBL Heidelberg.

3.5- Annotation and analysis

For each cell acquired, 18 categories of organelles were annotated. For most organelle, their presence was indicated as 1 and absence as 0. For a subset of organelles, the number of occurrences of that said organelle was annotated per cell. For instance, in dinoflagellates presenting chloroplasts, the presence of plastoglobuli as indicated as follows: 0 = none, 1 = occurrence of 1 to 5 plastoglobuli, 2 = occurrence of 6 to 10 plastoglobuli and 3 = occurrence of more than 11 plastoglobuli. Another case where this was used was for starch, in that case: 0 = none, 1 = occurrence of 1 to 5 starch granules, 2 = occurrence of 6 to 20 starch granules and 3 = occurrence of more than 21 starch granules. The category 18 corresponds to unknown organelles, which are putatively secretory, and were annotated with letters from a to v. When comparing the average occurrence of an organelle (per sample/per year) based on the morning or afternoon condition or between phototrophic/mixotrophic organisms and heterotrophic organisms, the multiple unpaired t-test was used for statistical analysis.

3.4- Data accessibility and visualization using MOBIE

The micrographs for each sampling session imaged were progressively added in a MOBIE project, along with the annotations. Both will be publicly available upon publication of my work.

3.6- Chemical fixation and SEM[1]

[1]The content of this paragraph has been copied with minor adaptations from my first author publication (Mocaer et al., 2023).

Part of the sample collected as described above was fixed with 2% formaldehyde (EMS) and 0.5% glutaraldehyde (EMS) in 0.1M marPHEM (Montanaro et al., 2016) for 6h at 4°C. The sample was then transferred to 0.1M PHEM containing 1% formaldehyde and preserved at 4°C until further processing. The sample was then rinsed once using 0.1M PHEM at 4°C and dehydrated at 4°C using the following (v/v) acetone/water series: 30%, 50%, 70%, 80%, 90%, followed by two pure acetone steps. Samples were left to sediment for a duration of 3 to 12h before each exchange to avoid loss of material. The sample was then critically point dried (CPD300, Leica microsystems) in small containers (1-1.6 µm pore size, Vitrapore ROBU, Hattert, Germany). In the CPD program, 30 slow exchange steps were used. CPD dried

plankton were then distributed onto carbon tape placed on an SEM stub (Agar scientific) before further gold sputtering (Quorum Q150RS). SEM imaging was performed using a Zeiss Crossbeam 540 with an acceleration voltage of 1.5 kV and a current of 700 pA and a Secondary Electron Secondary Ion (SESI) detector.

4- Results

4.1- TEM screen, annotation of organelles and genera identification

In total, over the year of 2020 and 2021, 773 micrographs were acquired and analysed. More precisely, a total of 398 micrographs were acquired for the year 2020, 187 for the morning condition (dark sampling, 3 sampling sessions) and 211 for the afternoon conditions (light sampling, 3 sampling sessions). Furthermore, a total of 375 micrographs were acquired for the year 2021, 203 for the morning conditions (dark sampling, 3 sampling sessions) and 172 for the afternoon conditions (light sampling, 3 sampling sessions). Precisions on the number of cells acquired per replicates and AM or PM condition per year are listed in table 1.

Sample ID (date)	Micrographs acquired 2020	Micrographs acquired 2021
AM_1 (20/09/16 & 21/09/09)	112	62
AM_2 (20/09/17 & 21/09/10)	25	86
AM_3 (20/09/18 & 21/09/14)	50	55
PM_1 (20/09/16 & 21/09/09)	77	43
PM_2 (20/09/17 & 21/09/10)	84	68
PM_3 (20/09/18 & 21/09/13)	50	55

Table 1: Summary of the acquired micrographs per morning and afternoon condition and per year.

For each condition, I imaged all or most of the cells present on the section. The rare cells that appeared dead or too damaged on the section were not considered for analysis. The largest proportion of cells present in my samples were dinoflagellates. Indeed, they represented overall 94% of the acquired micrographs in 2020 and 93% in 2021 (Fig. 2A). Nonetheless, the presence of coccolithophores, diatoms, flagellates, ciliates and sclerocytes were also recorded. These other microorganisms represented together 6% of the sample in 2020, and 7% in 2021 (Fig. 2A).

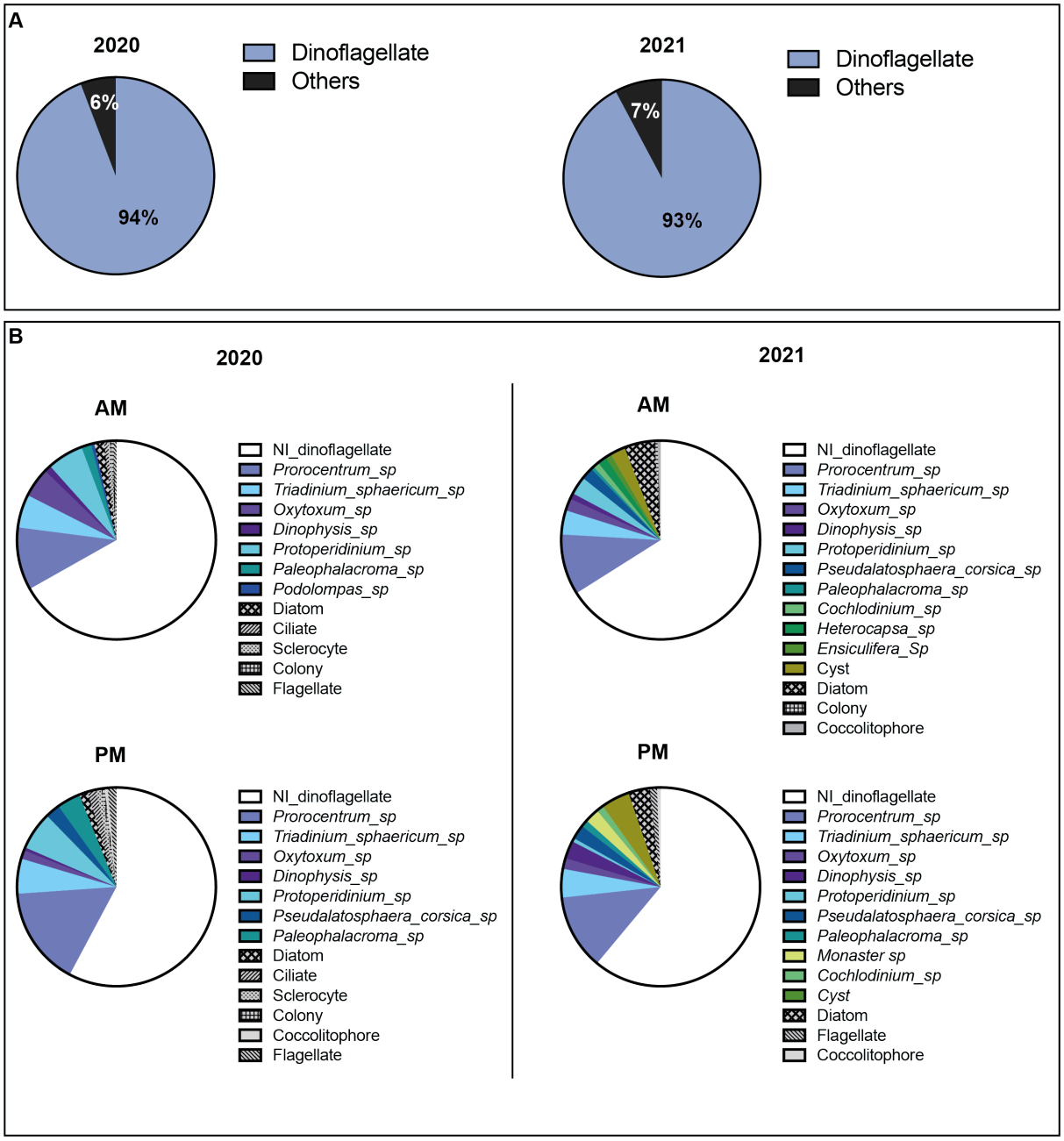

Figure 2: Distribution of the identified and non-identified cells from the TEM screen. A) Proportion of micrographs where cells were identified as dinoflagellates or others for the year 2020 and 2021. B) Putative distribution of cells from morning and afternoon samples of 2020 and 2021 identified based on specific ultrastructural characteristic from 2D sections.

Using the TEM screen analysis, and thanks to the LM images (Chapter II, Fig. 4) taken on site as well as the SEM micrographs performed at EMBL (Fig. 3), I could identify cell types occurring more often in the samples. The taxonomical identification of cells from the SEM screen was performed thanks to the help from Prof. Dr. Mona Hoppenrath, Dr. Raffaele Siano, Dr. Nicolas Chomerat, Dr. Kenneth Mertens and Dr. Hugo Berthelot. Even though the samples

presented a high diversity of genera, from combining the LM (Chapter II, Fig. 4)) and SEM (Fig. 3) and TEM modalities, I could progressively attribute subcellular 2D profiles to certain orders or genera. The proportion of cells with a presumed identification annotated from the TEM screen are shown in figure 2B. Note that after analysis of the three modalities, the samples consistently presented a high diversity of dinoflagellate genera. However, the following genera seemed to be more abundant: *Prorocentrum* (Fig. 2B, 3A-B, Chapter II Fig. 2E-F), *Triadinium* (Fig. 2B, 3C, Chapter II Fig. 2I)*, Paleophalacroma* (Fig. 2B, 3D, Chapter II Fig. 2D)*, Protoperidium* (Fig. 2B, 3E, Chapter II Fig. 2D), *Oxytoxum* (Fig. 2B, 3G-H, Chapter II Fig. 2G-H), *Podolompas* (Fig. 2B, 3I, Chapter II Fig. 2H), *Pseudalatospherae* (Fig. 2B, 3J) and *Dinophysis* (Fig. 2B, 3K-L, Chapter II Fig. 2C).

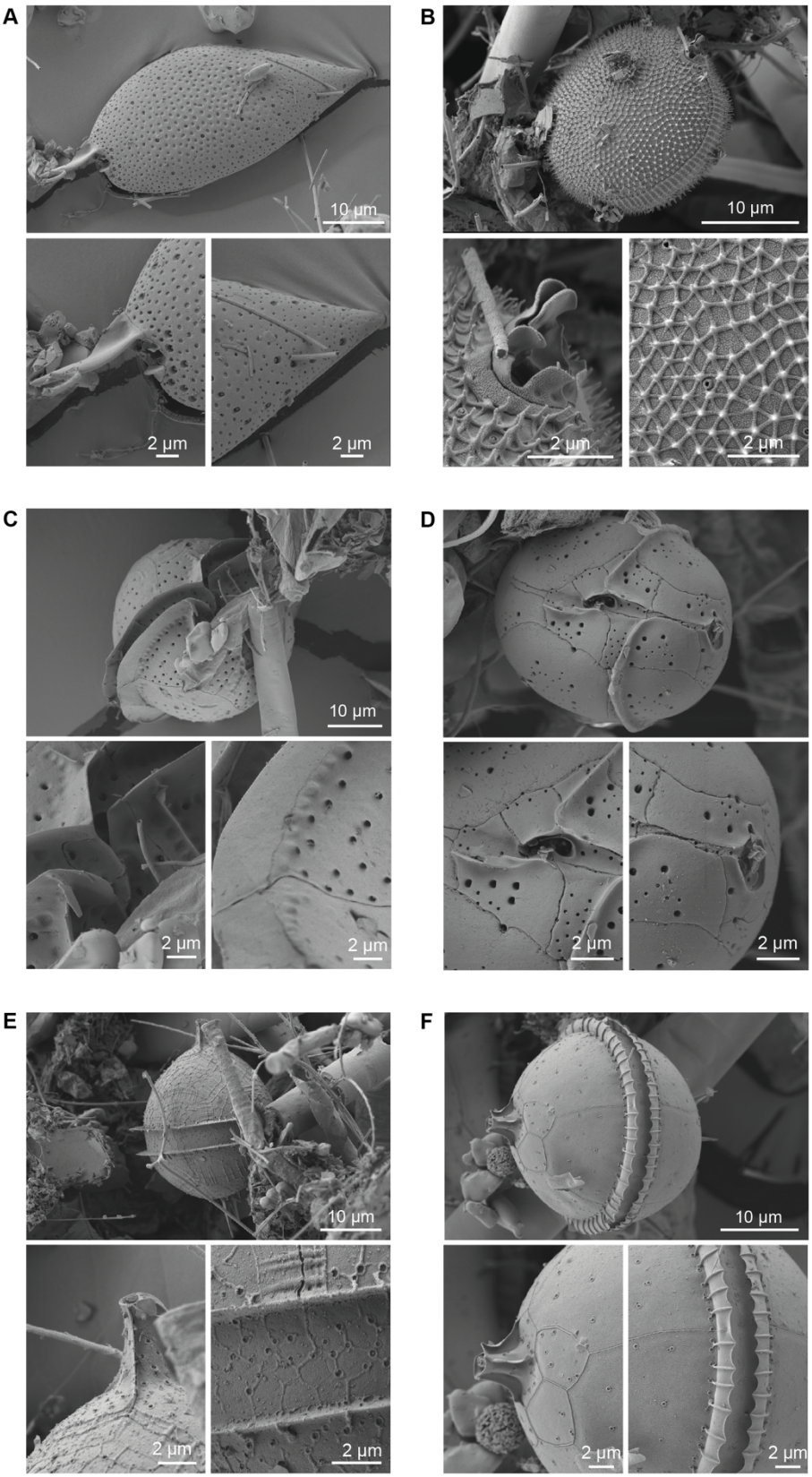
A
10 µm
2 µm
2 µm
B
10 µm
2 µm
2 µm
C
10 µm
2 µm
2 µm
D
2 µm
2 µm
E
10 µm
2 µm
2 µm
F
10 µm
2 µm
2 µm

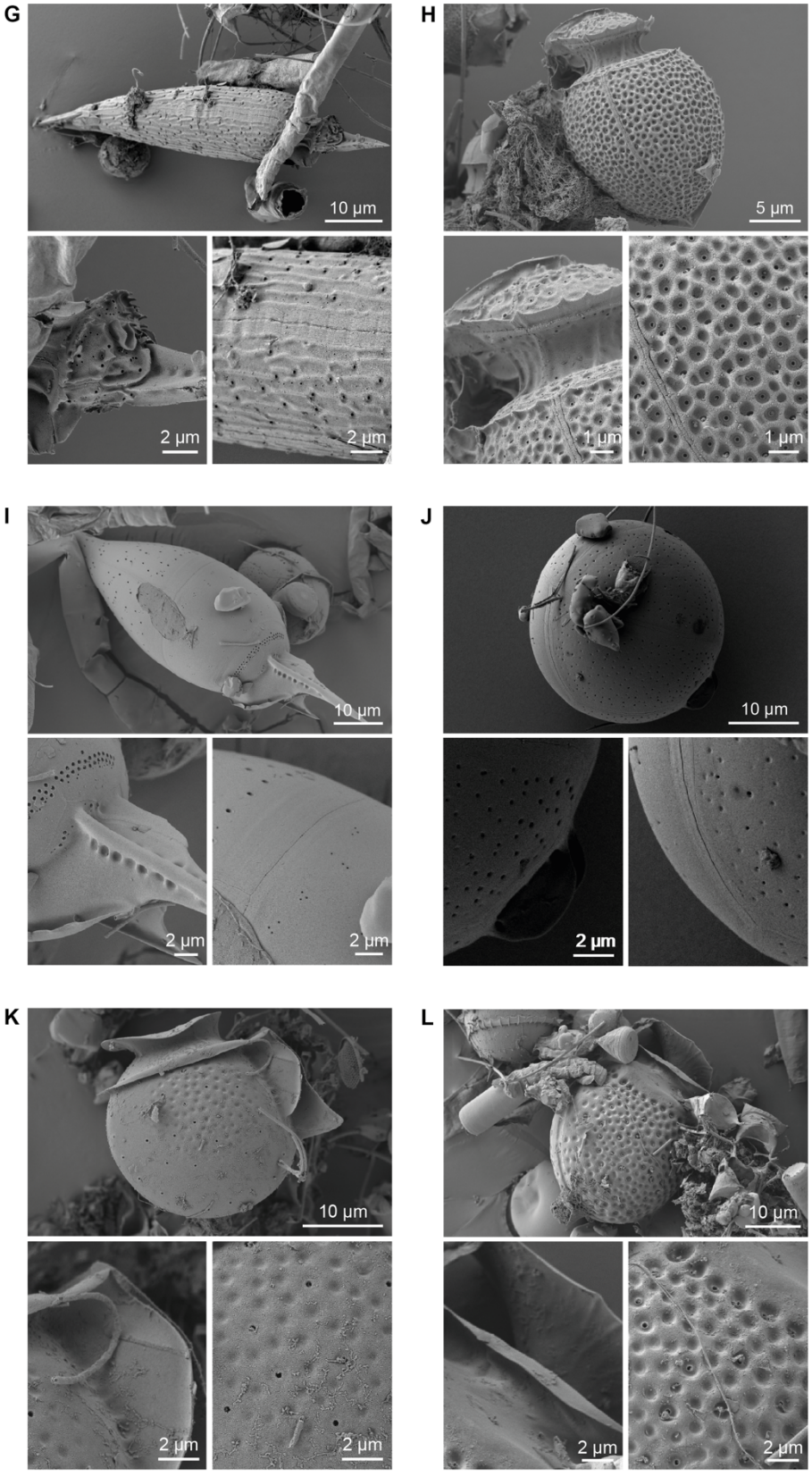

Figure 3: Micrographs from the SEM screen performed on parallelly processed samples. A-B) Species from the genus *Prorocentrum*, A was identified as *Prorocentrum cf. gracile***.** C) *Triadinium cf. sphaericum***,** D) *Paleophalacroma sp*, E-F) Species from the genus *Protoperidinium*, G-H) Species from the genus *Oxytoxum*, I) *Podolompas cf. palmipes*, J) *Pseudalatosphaera cf*

corsica. Nov, K-L) Species from the genus *Dinophysis*. The different close up allow to visualize details of the thecal ornamentation and pore arrangement, as well as details of the cingulum, sulcus area or apical pore complex.

For each micrograph from the TEM screen, I then annotated the occurrence of 18 different categories of organelles present in the cells (Fig. 4). The organelles annotated were chosen for their repeated presence in multiple cells and the possibility to identify them based on their morphology.

I annotated the presence for a dinoflagellate nucleus, trichocysts and pusule as they possess characteristic ultrastructure in the class of dinoflagellate (Fig. 4). Note that since this analysis was done on thin (70 nm) 2D sections, the imaged plan of a given cell would not systematically pass through the nucleus. Yet, it was still possible to identify Dinoflagellates for the presence of other characteristic organelles (as the theca or trichocysts for instance). As some pusule types have been described to be associated to particular genera (Dodge, 1971), I was interested to have a broad overview of pusule subcellular organization across my screen.

In addition, I measured the thickness of the cell covering and annotated the 2D profile of its exterior, as these elements can give additional information on the taxonomic nature of cells (Fig. 4). Indeed, in my screen, cells presenting a thick theca could then easily be affiliated to the class Dinophyceae. Furthermore, as described in Chapter I (3.1.1 Thecate dinoflagellate), past observations showed that when dinoflagellate cells present fewer thecal plates, these plates would usually be thicker and vice versa (Dodge and Crawford, 1970; Taylor, 1980). As the number of thecal plates and their arrangement is giving information of the taxonomy, this measurement of the outer cell covering thickness could indirectly allow to investigate whether distinctive thecal thickness can in some cases be associated to certain genus or species.

Furthermore, I annotated indicators of trophic modes as the presence or absence of chloroplast and food vacuole (Fig. 4), giving indication on whether the cell is potentially phototrophic, mixotrophic or heterotrophic. Over the 12 sampling sessions, in average 59.2% (sd ±11.3%) of dinoflagellates presented chloroplasts. Furthermore, in average 16.9% (sd ±6.8%) of dinoflagellates presented a food vacuole. Note that for various organelles, the probability of observing their occurrence can be higher if they are distributed throughout the cell (as chloroplast) or present a large volume compared to smaller and more rarely occurring organelles. Thus, it is possible that more cells than what I estimated present a food vacuole for instance.

The presence of putative starch (Fig. 4), and more precisely categories based on the number of putative starch granule present in each micrograph, were also annotated. From the 12 samplings, 31.4% (sd ±16.5%) of dinoflagellates presented starch. Thus far, starch has been identified based on the appearance of the granules described in the literature for dinoflagellate and other cell type (Decelle et al., 2021; LeKieffre et al., 2018; Seo and Fritz, 2002). Importantly, the nature of these granules will have to be validated by using a strategy such as PATAg which can stain starch granules in plant systems (Jordy et al., 1998).

Crystalline compartments (Fig. 4), previously described in the Chapter I (3.10.4 Crystalline inclusions), which were reported to be present in various genera of dinoflagellates were annotated as well. Over the 12 samplings, 31.7% (sd ± 10.0%) of the cells presented this compartment. As mentioned previously, the crystals seem to dissolve (probably on water, while sectioning) and thus appear as holes in the resin sections. This compartment presents a variety of internal organization, with seemingly different size and abundance of crystals depending on the cells. Generally, this compartment was localized close to the cell cortex, however it could present ramifications toward the internal part of the cell.

The presence of a large vacuole (Fig. 4) was annotated as well. The nature of this vacuole is unknown to me and can potentially be different between genera or species.

The presence of a basal body or flagella was annotated (Fig. 4). Indeed, the presence of basal bodies within a section allow to gain information on the plane of this section within a cell volume. Noting the presence of a flagella in 2D sections was interesting to me as I noticed that even though these structures are supposed to wrap the classical dinokont cells (presenting a cingulum and a sulcus), I very often could not observe their presence (n=36 dinoflagellates observed with flagella out of 727 imaged in the screen). Additionally, when present, I often could visualize them underneath the theca which was surprising (n=35 flagella within the theca or pellicle). The loss of the flagella, or its presence under the thecal wall, could potentially be caused by the sample preparation of the cells as mentioned in Chapter II.

Interestingly, I could visualize a number of cells presenting another organism within their cytoplasm or nucleus (presenting another type of nucleus, cytoplasm and mitochondria with a different electron density and organisation). I thus annotated these events as potentially symbiotic or parasitic associations (Fig. 4). Furthermore, I also indicated when cells show signs of kleptoplastidy. This could be visualized by the presence of additional membranes or cytoplasm around the chloroplast(s), which additionally tend to group on one side of the cell.

Over the 12 samples, in average 5% (sd ±3.4%) of dinoflagellates showed the presence of a compartments from another microorganism.

The presence of a “reticulated network” was annotated (Fig. 4). Indeed, this compartment was visible in a large proportion of dinoflagellates (mean 45.1%, sd ± 15.69%) and appears to be wrapping or closely associated to numerous organelles. Note that the electron density of this compartment presented variations between cells. Furthermore, this large compartment showed freezing damage in some cases.

Furthermore, electron dense sheets (Fig. 4) were observed in average in 27.4% (sd ±11.52) of dinoflagellates. These structures were also described as membrane like lamellae (MLL) or crystalline rods previously (see Chapter I, 3.11 Crystalline rods).

Interesting and intriguing tubular structures (Fig. 4), presenting diverse electron densities were observed in average in 20.7% (sd ±10.3%) in dinoflagellates over the 12 samplings. While to my best knowledge there has not been any description of these structures, I could visualize them on micrographs from Spector, Himes and Beam of *Cryphtecodinium cohnii* (Spector, 1984, p.193).

As I’m very interested in the dinoflagellate eyespot and the diversity of their structures (Described in Chapter I, 3.8.2 Eyespot), I annotated the presence of eyespots (Fig. 4). They were present in average in 9.1% (sd ±4.5%) of 2D sections of dinoflagellates. This low abundance reflects more the probability to find a discrete organelle in a 2D section rather than the actual occurrence of the eyespot in dinoflagellates.

Additionally, the presence of rhadbosomes, and rhabdosome like organelles (Fig. 4), were recorded. In average, they occurred in a small fraction of dinoflagellates (2.5%, sd ±2.7%). Rhabodosomes have been described in dinoflagellates from the genus *Dinophysis* (Vesk and Lucas, 1986). These structures are described as cylindrical, they can measure several microns in length (4µm were reported in *Dinophysis accuminata*, Vesk and Lucas, 1986) and present a diameter of approximately 150 nm (Vesk and Lucas, 1986). These structures, which can occur in very large amounts within a cell (Vesk and Lucas, 1986), have been described for form bundles that show a general radial distribution (Berland et al., 1995).

Lastly, a category of “non-identified” organelles was annotated. The various structures are shown in Fig. 5. Interestingly, some of these structures seem highly characteristic of certain genus (Fig. 10). Most of these structures presented an amphora or oval shape in 2D sections

and depending on the section, these organelles could be visualized close to the cell cortex. This led to the hypothesis that some of these structures could be mucocysts (See Chapter I, 3.4.2 Mucocysts). Indeed, some of these organelles (Fig. 5t) presented a fibro-granular structures or a paracrystalline (Fig. 5p) arrangement as described in Cachon et al., 1975. Note that some of these organelles possess similarities with previously described compartments. For instance, the organelle represented in Fig. 5s resembles the polyvesicular bodies described to be present at the cell periphery in *Gonyaulax polyedra* (=Now *Lingulodinium polyedra*, Schmitter, 1971). Additionally, the fibrous organelles shown in Fig. 5b, which I associated to belonging to the genus *Prorocentrum* based on the two thick thecal plates observed in cross section and a spine in some sections (Fig. 10A), were described previously the genus *Prorocentrum* as well (Bouck and Sweeney, 1966; Roberts et al., 1995).

The results of the TEM screen concerning the organelles occurrence in morning and afternoon samples are described in the following sections. Furthermore, for a subset of organelles, I also could compare their occurrence or level of occurrence between cells presenting chloroplast (potentially phototrophic or mixotrophic) or devoid of chloroplasts (potentially heterotrophic). Lastly, I also could associate the presence of a subset of “non-identified” organelles to certain genus, particularly if these cells presented a characteristic morphology.

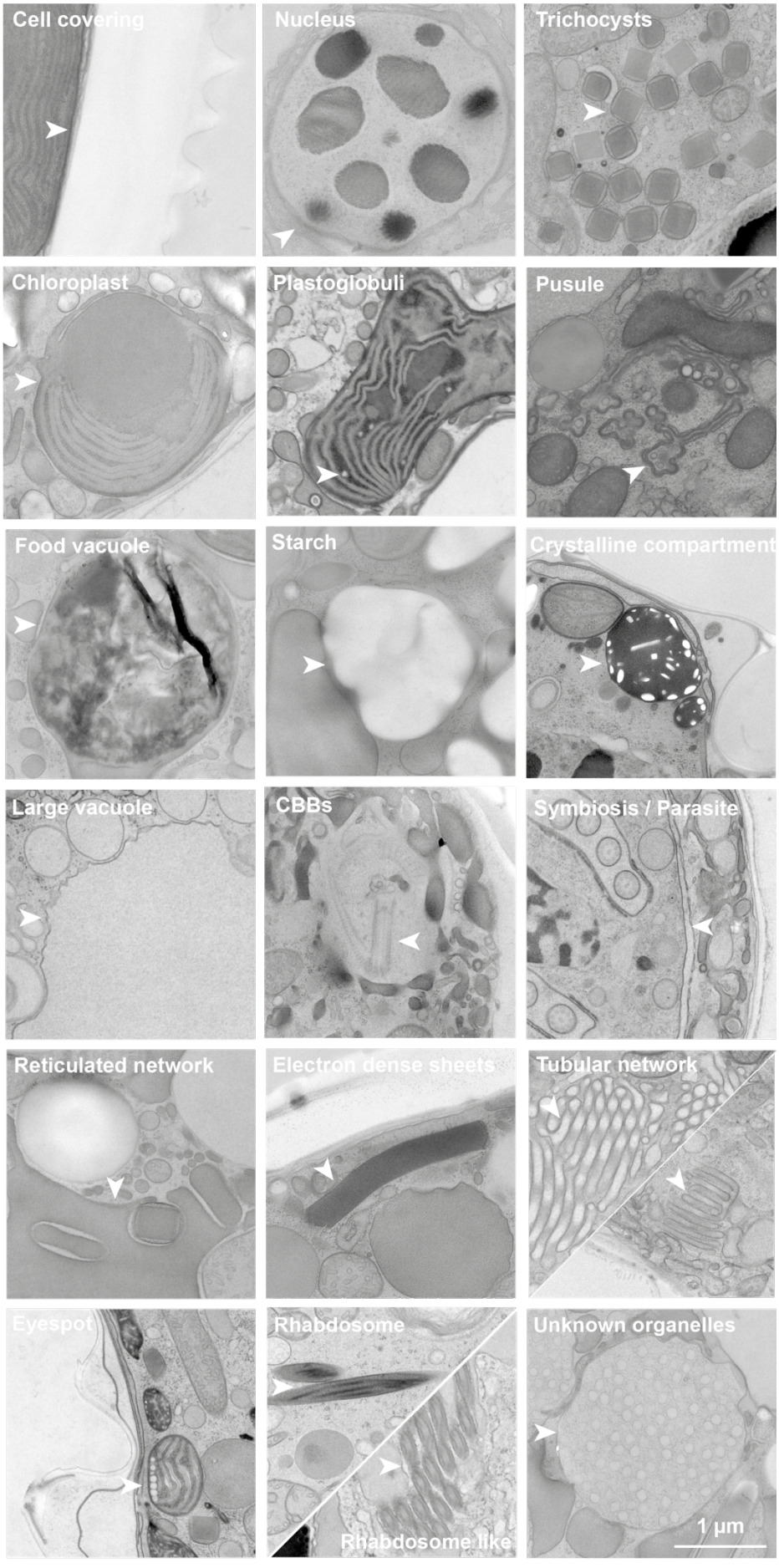
Cell covering
Nucleus
Trichocysts
Chloroplast
Plastoglobuli
Pusule
Food vacuole
Starch
Crystalline compartment
Large vacuole
CBBs
Symbiosis / Parasite
Reticulated network
Electron dense sheets
Tubular network
Eyespot
Rhabdosome
Rhabdosome like
Unknown organelles
1 µm

Figure 4: Categories of annotated organelles. Micrographs of representative aspect of the annotated organelles, respectively the theca or cell outer layer, nucleus, trichocyst, chloroplast, plastoglobuli, pusule, food vacuole, starch, crystalline compartment, large vacuole, basal body or flagellar apparatus (CBBs), Symbiosis or parasitism, reticulated network, electron dense sheets, tubular networks, eyespot, rhabdosome and rhabdosome like organelle, and a class of unknown organelles.

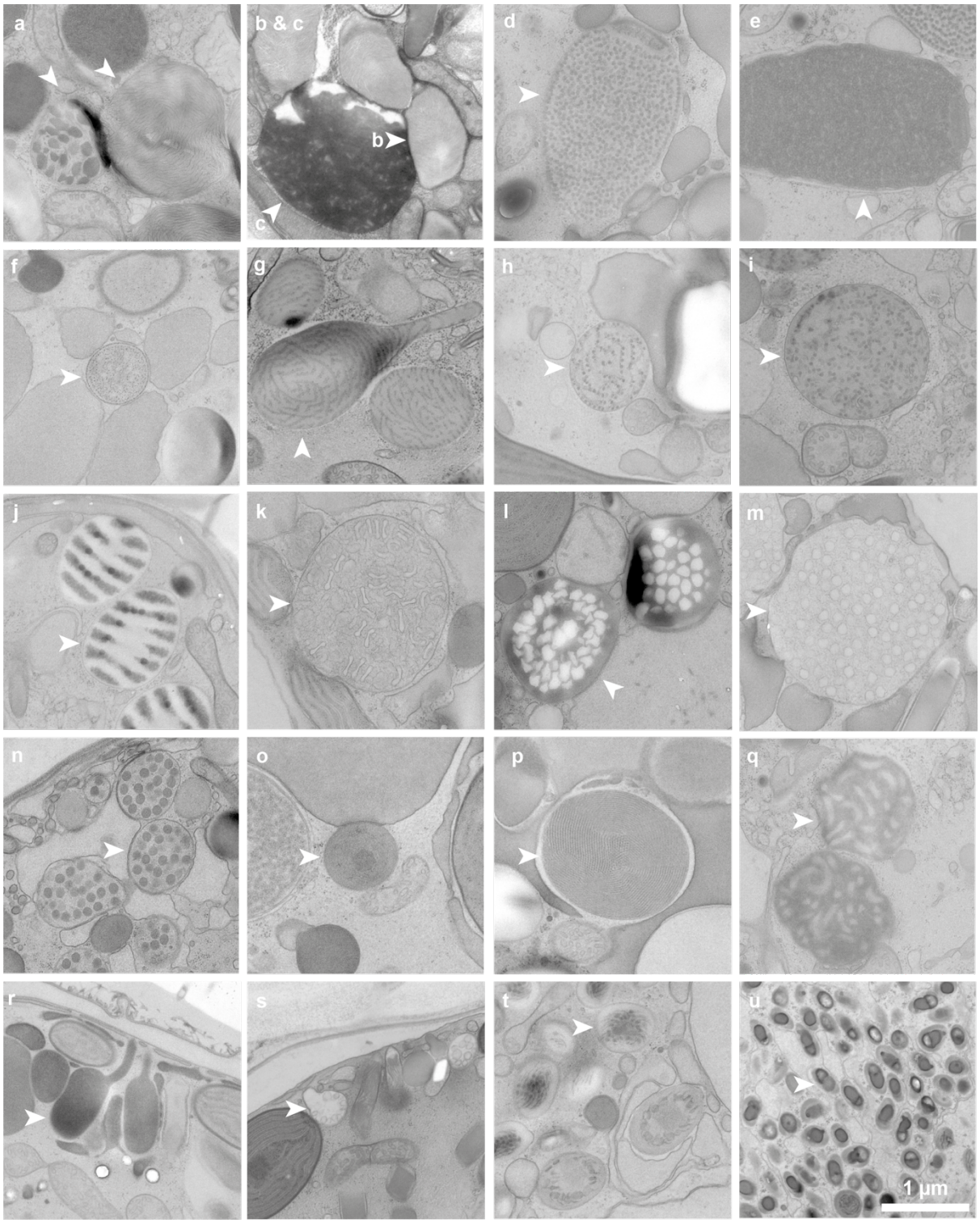

Figure 5: Representative micrographs of each organelle annotated in the "non-identified" category of the TEM screen (a-u).

4.2- A subset of organelles presents higher occurrence in the afternoon compared to the morning samples.

After the TEM screen annotation, I could compare the occurrence of chloroplasts, plastoglobuli, starch, food vacuole, crystalline compartment, reticulated network, tubular network and electron dense sheets between samples collected in the morning or during the afternoon. After analysis, across 2020 and 2021 the occurrence of plastoglobuli within plastid bearing cells was statistically higher in dinoflagellates collected from the afternoon compared to dinoflagellate cells collected in the morning (multiple unpaired t-test, P value = 0.00018). Furthermore, the occurrence of starch was also significantly higher in cells collected in the afternoon, compared to morning collection (multiple unpaired t-test, P value = 0.00010). The occurrence of chloroplast, food vacuole, crystalline compartment, reticulated and tubular network and electron dense sheets were not significantly different between cells collected in the morning or afternoons of 2020 and 2021 (multiple unpaired t-test, P value > 0.001).

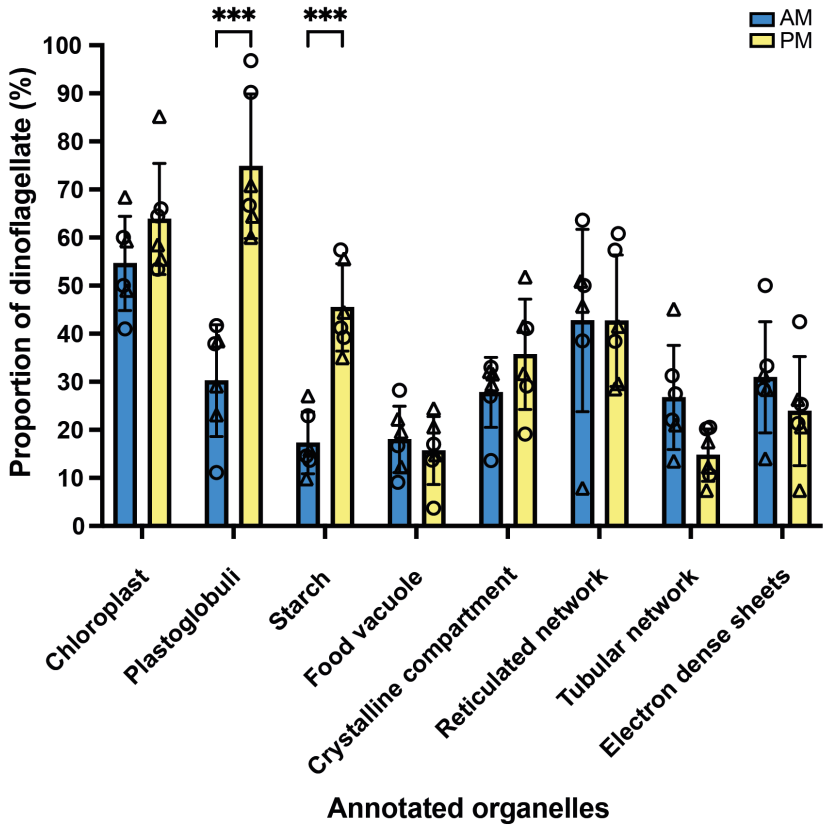

Figure 6: Morning and afternoon distribution of the annotated organelles for the year 2020 and 2021. The round symbols stand the average of respectively each morning and afternoon samples from 2020. The triangle symbols stand the average of respectively each morning and afternoon samples from 2021. Only P values < 0.001 were considered, statistical significance are shown by *** stars on the graph. There is a statistically significant difference between morning and afternoon conditions for the occurrence of starch and plastoglobuli in dinoflagellates from my TEM screen.

I then further analysed the variation of starch content (Fig. 7), and plastoglobuli within plastid bearing dinoflagellates (Fig. 8), between morning and afternoon conditions of 2020 and 2021.

The proportion of dinoflagellates presenting starch granules was 17.3 % in morning samples, compared to 46. 5% in afternoon samples (Fig. 7). Furthermore, classes representing the number of starch granules per 2D sections were analysed (Fig. 7B). The proportion of cells from the mornings samplings of 2020 and 2021 not presenting starch was significantly higher than in the afternoons. Furthermore, the average of dinoflagellates presenting between 6-20 starch granules in the afternoons of 2020 and 2021 was significantly higher than in the afternoons. This more detailed analysis was performed to get a more comprehensive understanding as some cell types or stages seemed to present a large amount of starch granule independently of the sampling condition, as in cysts for instance. Overall, this difference in starch occurrence at the population level between dark and light periods was consistent with previous observations (Loeblich, 1977; Seo and Fritz, 2002).

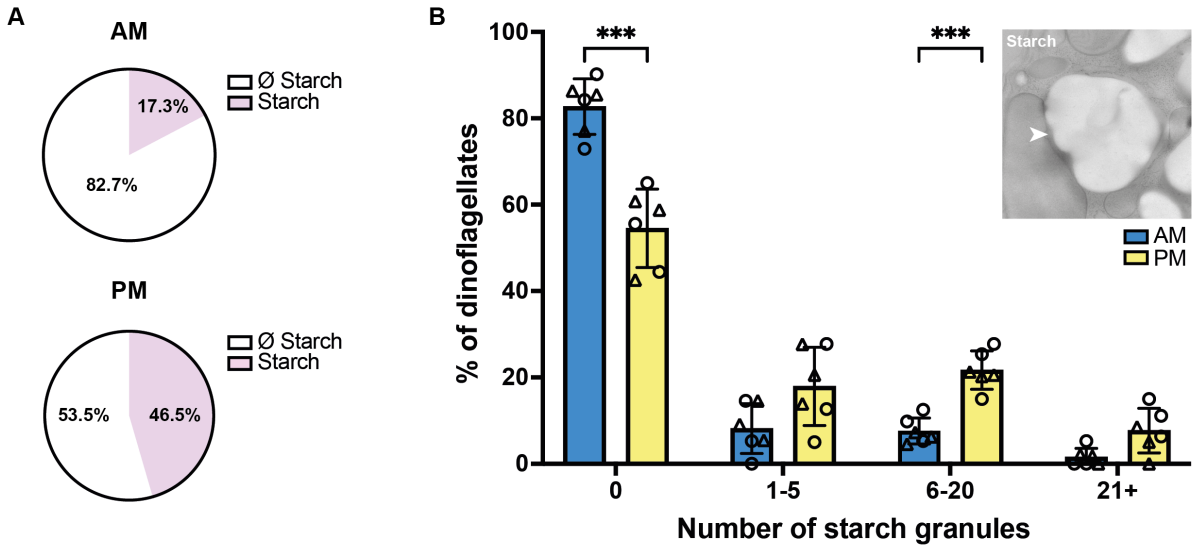

Figure 7: Starch granules quantification and comparison between morning (AM) and afternoon (PM) samplings of 2020 and 2021. A) Shows the global proportion (%) of dinoflagellates presenting or not starch in the morning and afternoon samples. B) Shows the AM and PM average distribution of dinoflagellates presenting either none, between 1 and 5, between 6 and 20 and more than 21 starch granules per 2D section. The round and triangle symbols show the average for each time point of respectively 2020 and 2021. *** stands for a P value < 0.001, measured with the multiple unpaired t-test.

The proportion of plastid bearing dinoflagellates presenting plastoglobuli was of 40% in the samples collected in the mornings, compared to 74.8% in samples collected from the afternoon (Fig. 8A). As for the starch, the number of occurrence of plastoglobuli were divided in four classes (in Fig. 8B, 0= not occurring, 1= occurring between 1-5 times, 2= occurring between 6-11 times and 3= occurring more than 11 times). After analysis, I could observe a significantly lower amount of plastid bearing dinoflagellates devoid of plastoglobuli as seen before in the general analysis (Fig. 6). The class 1, representing the average of cells presenting between 1-5 plastoglobuli in their chloroplast, was significantly higher in the samples collected in the afternoon compared to the morning (multiple unpaired t-test, p-value). This variation did not seem to be associated to a difference in sample composition as in species which could be identified from 2D sections, I could observe the same results as in the global analysis. Interestingly, the average of cells presenting a higher number of plastoglobuli (6-10 and 11+) did not show significant variations between morning and afternoon samplings (multiple unpaired t-test, P value > 0.001). A large amount of plastoglobuli could thus potentially be related to a specific physiological state of cells, independent of the morning or afternoon condition.

In plant systems, as described in Chapter I (3.7.4 Plastoglobuli), the number of plastoglobuli has been shown to increase in stress response including when there are temperature variations or the presence of high light (Venzhik et al., 2019). Interestingly, this would be consistent with my analysis which shows a statistically higher number of plastoglobuli in the afternoon, when high light levels were present. In plants, these structures have been described to play a protective role for the photosynthetic apparatus in these stress conditions. It is possible that these structures could play a similar role in algae, however to confirm this hypothesis further analysis including proteomics studies should be performed.

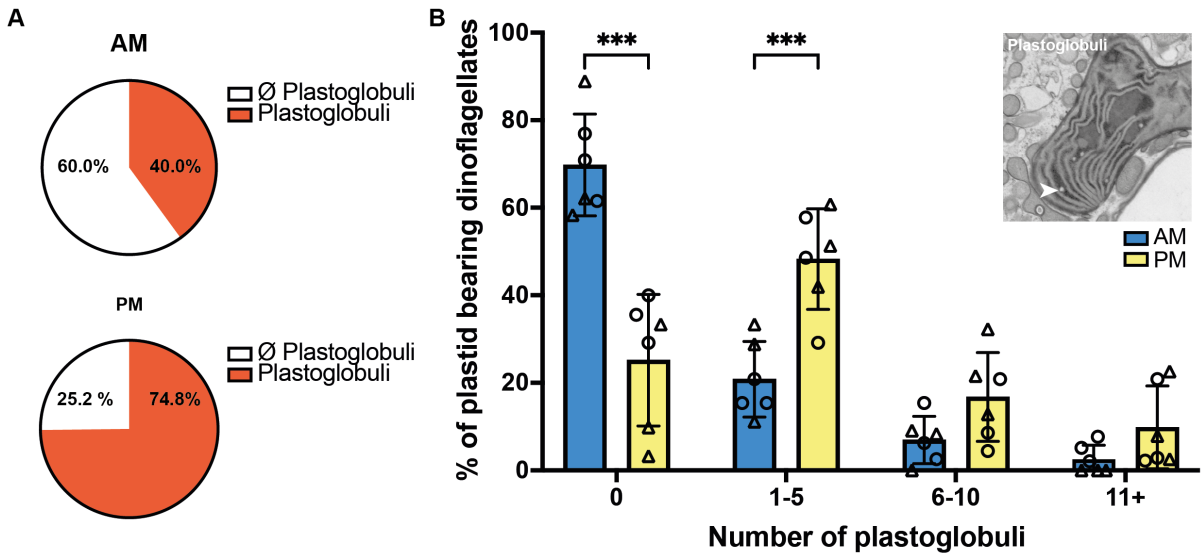

Figure 8: Plastoglobuli quantification and comparison between morning (AM) and afternoon (PM) samplings of 2020 and 2021. A) Shows the global proportion (%) of plastid bearing dinoflagellates presenting or not plastoglobuli in the morning and afternoon samples. B) Shows the AM and PM average distribution of plastid bearing dinoflagellates presenting either none, between 1 and 5, between 6 and 10 and more than 11 plastoglobuli per 2D section. The round and triangle symbols show the average for each time point of respectively 2020 and 2021. *** stands for a P value < 0.001, measured with the multiple unpaired t-test.

4.3- A subset of organelles occurs particularly in heterotrophic dinoflagellates

During the TEM annotations I realized that some the tubular network and the electron dense sheets seemed to occur principally in dinoflagellates not bearing plastids. Thus, from the tables annotated for each sample, I analysed the distribution of the occurrence of a subset of organelles (Food vacuole, crystalline compartment, reticulated network, tubular network and electron dense sheets) in plastid bearing versus non plastid bearing dinoflagellates (Fig. 9). While the occurrence of the food vacuole and reticulated network did not show a statistical difference in their presence for heterotrophic and plastid bearing dinoflagellates (multiple unpaired t-test, P value > 0.001), the crystalline compartment occurrence was significantly higher (multiple unpaired t-test, P value = 0.000054) in cells with chloroplasts (Fig. 9).

Consistently with my general observation, the tubular networks and electron dense rods were significantly more present in cells not possessing chloroplasts (multiple unpaired t-test, P value < 0.000001, Fig. 9). Concerning the electron dense rods, this is consistent with the previous reports of this organelle (Chapter I, 3.11 Crystalline rods / Membrane like lamellae), which was only described in heterotrophic dinoflagellates so far (Calado and Moestrup, 1997; Jacobson and Anderson, 1992; Jeong et al., 2014; Kang et al., 2011; Wedemayer and Wilcox,

1984).

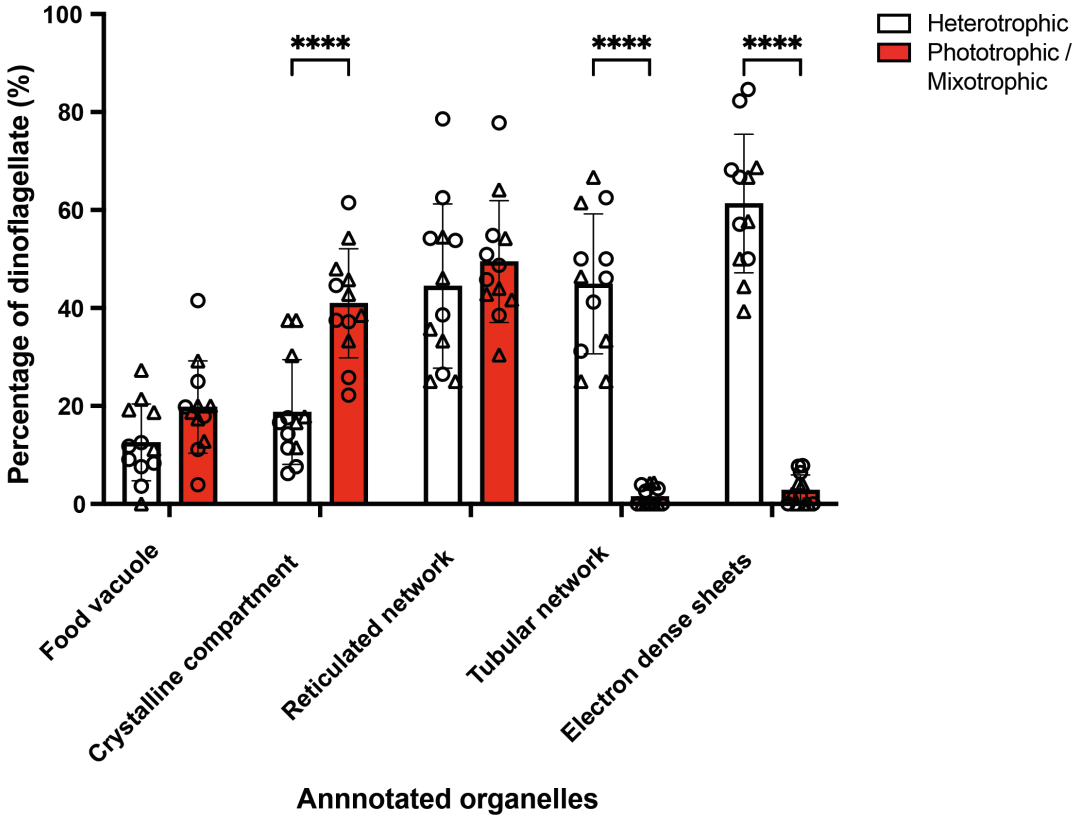

Figure 9: Occurrence analysis of a subset of organelles in dinoflagellates bearing plastids (Phototrophic or mixotrophic, in red) or not (heterotrophic, in white). The subset of organelle analysed here were the food vacuole, crystalline compartment, reticulated network, tubular network and electron dense sheets. The round and triangle symbols show the average for each time point of respectively 2020 and 2021. **** stands for a P value < 0.0001, measured with the multiple unpaired t-test.

4.4- A subset of organelles seems to be associated to specific genus

Interestingly, some organelles were recurrently found in cells with very similar morphologies, leading to the hypothesis that some organelles are specific to genus. This is already known for some organelles as rhabdosomes, present in the genus *Dinophysis* (Berland et al., 1995; Vesk and Lucas, 1986). By combining the images presenting the same organelle, I could have an idea about whether this cell was very represented in the sample, the general cell shape, whether the theca would be smooth or present ornamentation and whether a lot or very few thecal pores were present (Fig. 10). Based on these indications and frequently occurring cells in the SEM screen, I could formulate hypothesis of associations between certain organelles and genus and species. In order to investigate this further, I aimed to perform targeted vEM acquisition of a subset of the cells presented in Fig. 10 (Chapter IV and V).

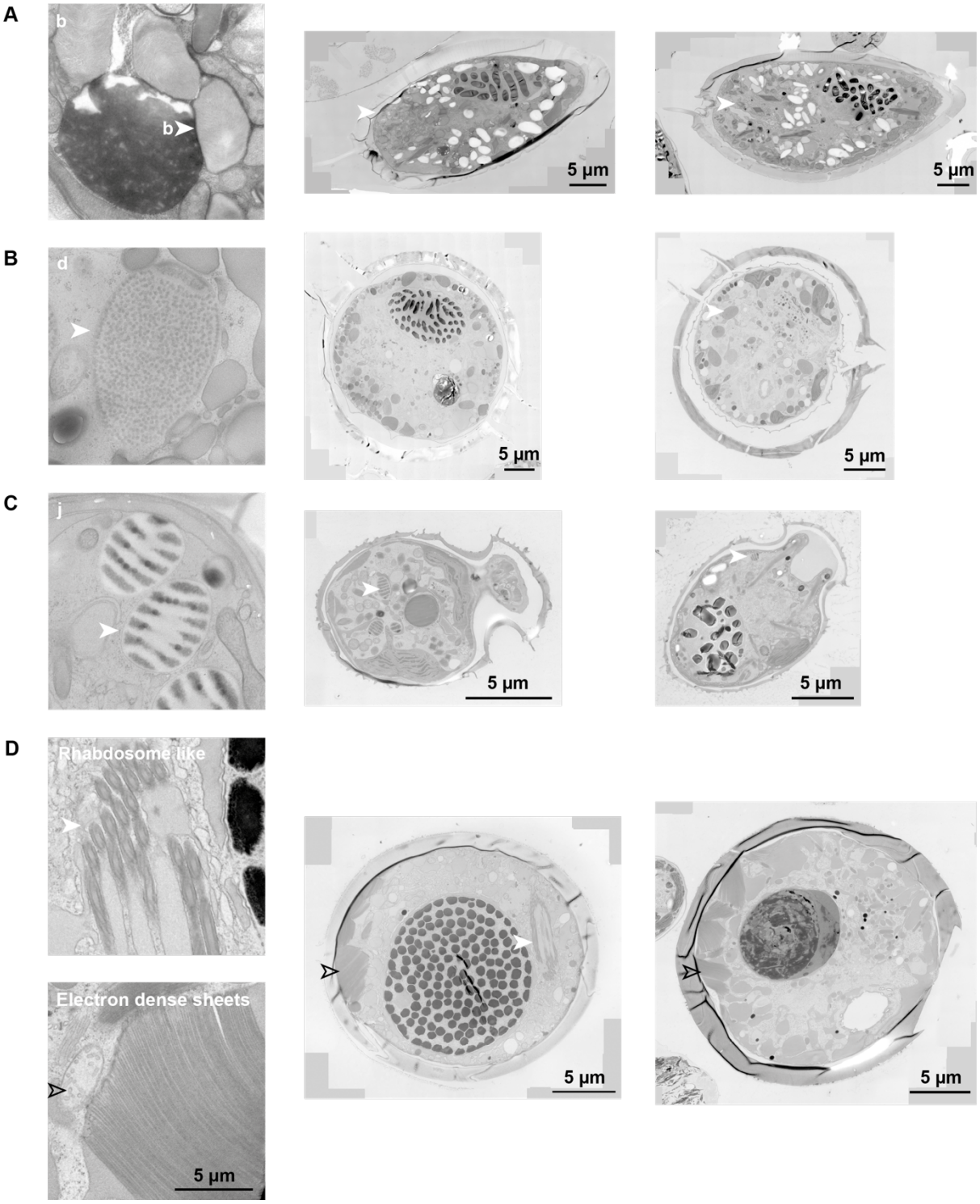

Figure 10: Subset of organelles identified as associated to specific genus or species. A) Fibrous bodies seemed to be present particularly in *Prorocentrum cf. gracile*. On the left is a close up of fibrous bodies, and on the right are examples of TEM micrographs allowing to identify the genus by the cell shape, presence of two main thecal plates, as well as the presence of a spine (which were similar to observations in Fig. 3A). B) The organelle "d" (left) seemed to be particularly associated to rounded cells presenting a wide cingulum (right), these looked similar to the species *Triadinium cf. sphaericum* identified from the SEM screen (Fig. 3C). C) The organelle "j" seemed to be associated to cells from the genus *Oxytoxum.* Indeed, these cells presented diamond like shapes in 2D sections resembling cells identified as *Oxytoxum* from the SEM screen, Fig. 3H. D) The rhabdosome like organelle, and a different organisation of electron dense sheets (present on

one side of the cell), seemed to be associated to a specific genus unidentified yet from the TEM screen.

5- Discussion

This TEM screen allowed to investigate, at the population level, ultrastructural variations associated to early morning or afternoon sampling conditions. Combining this type of approach with proteomics, metabolomics and lipidomics studies to further understand the physiological variations associated to the ultrastructural differences observed would be very powerful. Additionally, developing strategies to stain specifically starch or lipids on fresh or fixed samples could allow to perform high throughput LM screens and thus to perform comparisons between conditions as morning and afternoon or other gradients.

Furthermore, this 2D subcellular screen allowed to start associating structures to specific genera. Taxonomical assignation has been evolving for decades, due to the progressive homogenisation between classification systems and development of molecular tools. Having a range of identification factors obtained through diverse modalities (18S, SEM, LM and TEM) could allow for more precise genus or species assignation. This is ultimately important when it comes to performing research on a specific genus or species for instance, as a lot of information might be lost if they present multiple taxonomical assignations. Thus, possessing information on subcellular structures associated to certain genus could help in providing extra indication for taxonomical identification, as we would use the tabulation determined by SEM for instance (Chapter I, 3.1 Cell covering).

Based on this large environmental ultrastructure study, I could identify structures that seem to be characteristic of heterotrophic microorganisms as the MLL or the tubular network (Fig. 9). This result as well as the identification of compartments potentially specific to certain genus (Fig. 10) lead to set a 3D ultrastructural investigation on a subset of organisms of interest. As the HPF samples I possess are heterogeneous and complex, targeting was necessary in order to perform vEM acquisition (which has a dramatically lower throughput than TEM). The development of this strategy will be described in the next chapter.

This 2D TEM screen was principally descriptive study, however it rose a wide variety of questions concerning the nature of some subcellular compartment identified. It thus would be very interesting to further the analysis of this subset of structures, for example by determining the atomic composition by EDX, in order to better understand their potential function. Furthermore, finding or establishing cultures of cells presenting some of these structures

would be extremely valuable as one could interfere with the culture system and tackle more specific, mechanistic questions informing on the cells' physiology.

One complex factor in this study also remains the complexity in confirming the genus identification, which is until now performed subjectively based on a set of morphological criteria. A link between morphological and genomic taxonomy is thus needed. This confirmation could be done by developing a method to perform in situ hybridization on resin sections, to specifically label targeted taxa, as in Jahn et al., 2016. This would require basal knowledge of organisms that could be present in the sample, which could be done by performing metabarcoding. From knowing which are abundant species within the mix, one could design probes targeting a region of 18S ribosomal RNA for these species and perform this type of on-section FISH-CLEM experiments.

6- References

Berland, B. R., Maestrini, S. Y., Grzebyk, D. and Thomas, P. (1995). Recent aspects of nutrition in the dinoflagellate *Dinophysis cf. acuminata. Aquat. Microb. Ecol.* **9**, 191–198.

Bouck, G. B. and Sweeney, B. M. (1966). The fine structure and ontogeny of trichocysts in marine dinoflagellates. *Protoplasma* **61**, 205–223.

Cachon, J., Cachon, M. and Greuet, C. (1975). *Les "mucocystes"des Péridiniens. Constitution, évolution des structures et comparison avec celles des trichocystes.*

Calado, A. J. and Moestrup, Ø. (1997). Feeding in *Peridiniopsis berolinensis* (Dinophyceae): new observations on tube feeding by an omnivorous, heterotrophic dinoflagellate. *Phycologia*.

Decelle, J., Veronesi, G., LeKieffre, C., Gallet, B., Chevalier, F., Stryhanyuk, H., Marro, S., Ravanel, S., Tucoulou, R., Schieber, N., et al. (2021). Subcellular architecture and metabolic connection in the planktonic photosymbiosis between Collodaria (radiolarians) and their microalgae. *Environ. Microbiol.* **23**, 6569–6586.

Dodge, J. D. (1971). Fine Structure of the Pyrrophyta. *Bot. Rev.* **37**, 481–508.

Dodge, J. D. and Crawford, R. M. (1970). A survey of thecal fine structure in the Dinophyceae. *Bot. J. Linn. Soc.* **63**, 53–67.

Jacobson, M. and Anderson, D. M. (1992). Ultrastructure of the feeding apparatus and myonemal system of the heterotrophic dinoflagellate Protoperidinium spinulosum. *J. Phycol.* 5–24.

Jahn, M. T., Markert, S. M., Ryu, T., Ravasi, T., Stigloher, C., Hentschel, U. and Moitinho-Silva, L. (2016). Shedding light on cell compartmentation in the candidate phylum Poribacteria by high resolution visualisation and transcriptional profiling. *Sci. Rep.* **6**, 1–

9.

Jeong, H. J., Jang, S. H., Moestrup, Ø., Kang, N. S., Lee, S. Y., Potvin, É. and Noh, J. H. (2014). *Ansanella granifera* gen. et sp. nov. (Dinophyceae), a new dinoflagellate from the coastal waters of Korea. *Algae* **29**, 75–99.

Jordy, M. N., Azémar-Lorentz, S., Brun, A., Botton, B. and Pargney, J. C. (1998). Cytolocalization of glycogen, starch, and other insoluble polysaccharides during ontogeny of Paxillus involutus-Betula pendula ectomycorrhizas. *New Phytol.* **140**, 331–341.

Kang, N. S., Jeong, H. J., Moestrup, Ø. and Park, T. G. (2011). *Gyrodiniellum shiwhaense* n. gen., n. sp., a new planktonic heterotrophic dinoflagellate from the coastal waters of western Korea: Morphology and ribosomal DNA gene sequence. *J. Eukaryot. Microbiol.* **58**, 284–309.

LeKieffre, C., Spero, H. J., Russell, A. D., Fehrenbacher, J. S., Geslin, E. and Meibom, A. (2018). Assimilation, translocation, and utilization of carbon between photosynthetic symbiotic dinoflagellates and their planktic foraminifera host. *Mar. Biol.* **165**, 1–15.

Loeblich, A. R. (1977). Studies on synchronously dividing populations of Cachonianiei, a marine dinoflagellate. *Bull. Japanese Soc. Phycol.* **25**, 118–128.

Mocaer, K., Mizzon, G., Gunkel, M., Halavatyi, A., Steyer, A., Oorschot, V., Schorb, M., Kieffre, C. Le, Yee, D. P., Chevalier, F., et al. (2023). Targeted volume Correlative Light and Electron Microscopy of an environmental marine microorganism. *J. Cell Sci.* **c**, 2023.01.27.525698.

Montanaro, J., Gruber, D. and Leisch, N. (2016). Improved ultrastructure of marine invertebrates using non-toxic buffers. *PeerJ* **2016**, 1–15.

Roberts, K. R., Heimann, K. and Wetherbee, R. (1995). The flagellar apparatus and canal structure in *Prorocentrum micans* (Dinophyceae). *Phycologia* **34**, 313–322.

Schmitter, R. E. (1971). The fine structure of *Gonyaulax polyedra*, a bioluminescent marine dinoflagellate. *J. Cell Sci.* **9**, 147–173.

Seo, K. S. and Fritz, L. (2002). Diel changes in pyrenoid and starch reserves in dinoflagellates. *Phycologia* **41**, 22–28.

Spector, D. L. (1984). *Dinoflagellates*.

Taylor, F. J. R. (1980). On dinoflagellate evolution. *BioSystems* **13**, 65–108.

Venzhik, Y. V., Shchyogolev, S. Y. and Dykman, L. A. (2019). Ultrastructural Reorganization of Chloroplasts during Plant Adaptation to Abiotic Stress Factors. *Russ. J. Plant Physiol.* **66**, 850–863.

Vesk, M. and Lucas, I. A. N. (1986). The rhabdosome: a new type of organelle in the dinoflagellate *Dinophysis*. *Protoplasma* **134**, 62–64.

Wedemayer, G. J. and Wilcox, L. W. (1984). The Ultrastructure of the Freshwater, Colorless

Dinoflagellate *Peridiniopsis berolinense* (Lemm.) Bourrelly (Mastigophora, Dinoflagellida). *J. Protozool.* **31**, 444–453.

Chapter IV: Development of a workflow to study a subset of cells of interest from a heterogeneous sample

1- Introduction

As the TEM screen revealed potential correlations between the occurrence of certain organelles and specific genera, one aim was then to be able to precisely acquire a subset of selected microorganisms using vEM.

vEM comprises a range of techniques that have the common aim to study the ultrastructure of a sample in 3D. The sample is either in the form of serial consecutive sections (collected on grids or on tape for TEM imaging; or substrates for SEM imaging) or a full block where the surface is iteratively shoved precisely and imaged by SEM (the surface is removed by a focused Ion Beam for FIB-SEM, or a diamond knife within the chamber for SBF-BEM). Each of these techniques present their advantages and limitations, as they can offer various resolutions, field of imaging and throughput.

Until now, vEM techniques have rarely been applied to small marine microorganisms. Further characterization of the overall subcellular organization of these organisms, as well as the distribution and quantitative description of their organelles shall permit a better understanding of their cell biology.

To this day, most subcellular descriptions of dinoflagellates were derived from TEM studies. There are a few exceptions where vEM was performed on cultured dinoflagellates (Decelle et al., 2022; Gavelis et al., 2017; Gavelis et al., 2019; Uwizeye et al., 2021b) or from isolates from the environment (Decelle et al., 2021; Uwizeye et al., 2021a). However, our 2D and 3D understanding of most genera organization is still largely missing both in cultures and from native ecosystems. Furthermore, as only a fraction of species can be cultured in the laboratory (Dixon and Syrett, 1988; Oliveira et al., 2020), only a subset of organisms have been thoroughly investigated. Additionally, it has been shown that some cells can lose structures in vitro, as their photosensitive apparatus in prolonged monocultures (Moldrup et al., 2013). Thus, even though information exists from past EM studies on the subcellular characteristics of dinoflagellate, there is a need for new systematic methods to characterize these cells from their native environment.

In the case of this study, Focused Ion Beam-Scanning Electron Microscopy (FIB-SEM) was the method of choice for vEM imaging. Indeed, as our samples are environmental, they can include material such as silica (e.g. from diatom frustules) which are detrimental to the diamond knifes used in volume imaging strategies such as SBEM or array tomography. Furthermore, as we were interested in imaging relatively small volumes at quite high resolution in a sample presenting sparse cell distribution, FIB-SEM was the preferred technique.

One limit of vEM techniques in general is their low throughput. Indeed, the volume of sample that can be acquired is generally technically restricted, and image acquisition presents an important cost both in time and resources. Thus, it is quite important to be able to limit as much as possible the imaged volume to be able to further scale up the number of acquisitions to targeted cells and reach representative numbers. Note that here, the heterogeneity of the environmental sample adds to the already existing technical challenge of implementing a targeted approach.

In this chapter, the developed workflow to target specific cells from a complex environmental community is presented. This method is based on a specific EM sample preparation, compatible with both light and vEM imaging adapted from Ronchi et al., 2021. This workflow allows the identification of a genus of interest from a complex community presenting hundreds of different species. The identification is performed using the fluorescence pattern as well as the shape of the cells using fluorescence excitation and transmitted light respectively. This correlative approach then allows to acquire precisely the corresponding cell by FIB-SEM. The 3D subcellular analysis allows to understand the intracellular organelle distribution and morphologies, providing useful information on the biology of dinoflagellates.

The proof of principle for the method shown in this chapter not only provides insights in dinoflagellates biology but demonstrates its power for targeted subcellular analyses of environmental microorganisms from complex communities.

2- Contributors

This work was done in close collaboration with Paolo Ronchi from the EMCF at EMBL Heidelberg as well as the team of Johan Decelle at Grenoble CEA. The conceptualization for this work was done with Johan Decelle, Yannick Schwab and Paolo Ronchi. Giulia Mizzon, Manuel Gunkel, Aliaksandr Halavatyi, Viola Oorschot, Martin Schorb, Benoit Gallet and Paolo Ronchi contributed to the methodology. Anna Steyer, Charlotte LeKieffre, Daniel. P. Yee, Fabien Chevalier and Paolo Ronchi participated in the investigation. Martin Schorb contributed

in software and visualization development for this project. Kenneth Mertens, Nicolas Chomerat, Raffaele Siano, Hugo Berthelot and Mona Hoppenrath helped in the taxonomic identification.

3- Material and methods[1]

[1]The content of this section has been copied or mildly adapted from my first author publication (Mocaer et al., 2023)

3.1- Sample collection

Sampling of marine plankton was performed by towing at slow speed (around 2 knots) a net of 5-10 µm mesh size (Aquatic Research Instruments, Hope, ID, USA) for 10 minutes in surface waters of the Villefranche-sur-Mer bay (France). Sampling was performed in 2021/09/14 in the early morning. Samples were filtered through serial sieves (Retsch GmbH, Haan, Germany) to collect cells measuring less than 40 µm in diameter. The fraction obtained (5 to 40µm) was kept in Nalgene plastic bottles and placed in a closed cooler filled with sea water to preserve them at sea temperature and in darkness until further processing. The sample was then concentrated on a 1.2 µm size meshed mixed cellulose ester membrane (Merk, Darmstadt, Germany) and pelleted using centrifugation for 5 minutes at 1000G and 20°C with a swinging bucket centrifuge (Eppendorf 5427R, Hamburg, Germany).

3.2- High-pressure freezing (HPF) and Freeze substitution (FS)

After the collection described above, 1.2 µl of the sample pellet was loaded in a HPF type A gold coated copper carrier (200 µm deep and 3 mm wide, Leica microsystems, Wetzlar, Germany) and topped with the flat side of an aluminium type B carrier (Leica microsystems). HPF was performed using an EM ICE (Leica microsystems). To allow for a very rapid freezing of the sample upon collection at sea, the instrument was set up meters away from the peer at the Institut de la mer in Villefranche-sur-Mer (France). Samples presented here were frozen within a time window of less than 2 hours after being collected at sea. Cryoimmobilized samples were then shipped to EMBL at cryogenic temperatures using a dry-shipper and underwent freeze-substitution (FS, EM-AFS2, Leica microsystems) following a protocol adapted from Ronchi et al., 2021. Briefly, the samples were incubated in the FS cocktail (0.1% UA (Agar Scientific, Stansted, UK) in dry acetone (EMS, Hatfield, PA, USA)) for 69h at -90°C. Temperature was raised to -45°C over 15h (3°C/h) and then the samples were further

incubated for 5h at -45°C. After rinsing with acetone, the infiltration with Lowicryl HM20 (Polysciences, Warrington, PA, USA) was performed using increasing resin concentration in steps of 6h each. During infiltration the temperature was increased gradually to -25°C. Three infiltration steps using 100% Lowicryl were done at -25°C for 6h, 17h and 10h respectively. Polymerization was performed using UV at -25°C for 48h followed by raising the temperature to 20°C.

3.3- Targeting strategy

In order to target the cell of interest, we generated a 3D map of the block using confocal microscopy (Ronchi et al., 2021). For this, the sample was mounted face down on a glass bottom dish (glass thickness 17µm MatTek, Ashland, MA, USA) on a drop of water. Acquisition and laser branding were done using a Zeiss LSM 780 NLO microscope equipped with a pulsed near infrared (NIR) laser used in 2-photon microscopy and a 25x/0.8NA multi-immersion objective (LD-LCI Plan-Apochromat, Zeiss, Jena, Germany). The following channels were acquired: two color channels detecting the autofluorescence signal of the sample, exciting autofluorescence at 488nm and 633nm respectively. Together with the 488nm excitation channel, an image of the transmitted laser light was generated using the T-PMT detector of the microscope. Additionally, a reflection signal was recorded to visualize the surface of the resin block. For this, the main beamsplitter was changed to a T80/R20 filter reflecting 80% of the incident light and transmitting 20%. The reflection of a 633nm laser at low intensity was measured with a MA-PMT at low gain. Reflection protection for all laser lines was removed in the beam path of the microscope. The interface between water and resin was visible as bright reflection signal in this channel, and could be used to determine the axial position of the autofluorescent structures within the block.
For laser branding, the bleaching functionality of the microscope was used, by which specific regions within an image can be selectively illuminated. For these regions the NIR laser was set to a wavelength of 850 nm. Laser power was tuned to achieve efficient branding while avoiding blebbing of the resin. With our system, we achieved this at values around 12% of the maximum power.

3.4- Sample mounting and FIB-SEM acquisition

The base of the block was cut parallel to its surface in order to be 2-3 mm high, and mounted on an SEM stub (Agar scientific) using a 1:1 mix of superglue (Loctite precision max, Henkel Corp., Rocky Hill, CT, USA) and silver paint (EM-Tec AG44, Micro to Nano, Haarlem,

Netherlands). Silver paint was further added to the edges of the block. The sample underwent gold sputtering for 180 s at 30 mA (Q150RS, Quorum, Laughton, UK) before insertion in the FIB-SEM chamber. FIB-SEM imaging was performed using a Zeiss Crossbeam 550, following the Atlas 3D workflow. FIB milling was performed at 1.5 nA. SEM imaging was done with an acceleration voltage of 1.5 kV and a current of 750 pA using an ESB detector (ESB grid 1100V). Volume imaging of the planktonic cell was done using an 8 nm isotropic voxel size with a dwell time of 9 µs. Post-acquisition dataset alignment was performed using the automated AMST procedure from Hennies et al., 2020.

3.5- Volume analysis and quantification

Overlay of the EM and LM data (Fig. 4) and most of the segmentations (Fig. 7A,B,C,D,E) were done using Amira (Thermo Fisher Scientific, Waltham, MA, USA). The segmentation of the theca, nucleolus, chromosomes, starch, mitochondrion, mucocysts, trichocysts, eyespot and flagellar apparatus were done using the thresholding and interpolation tools. The result of this semi-automated procedure was further manually proofread. The nucleus (nuclear envelope) was manually segmented using interpolation. The segmentation of the chloroplast was performed using Microscopy Image Browser (Belevich et al, 2016) by manually annotating and interpolating (Fig. 7C). In total, the segmentation of the various organelles took 72h. Volume quantifications were performed on segmented organelles using the Amira (Thermo Fisher Scientific) label analysis tool. Lengths of the trichocysts were measured using the Amira measurement tool.

3.6- SEM

Part of the sample collected as described above was fixed with 2% formaldehyde (EMS) and 0.5% glutaraldehyde (EMS) in 0.1M marPHEM (Montanaro et al., 2016) for 6h at 4°C. The sample was then transferred to 0.1M PHEM containing 1% formaldehyde and preserved at 4°C until further processing. The sample was then rinsed once using 0.1M PHEM at 4°C and dehydrated at 4°C using the following (v/v) acetone/water series: 30%, 50%, 70%, 80%, 90%, followed by two pure acetone steps. Samples were left to sediment for a duration of 3 to 12h before each exchange to avoid loss of material. The sample was then critically point dried (CPD300, Leica microsystems) in small containers (1-1.6 µm pore size, Vitrapore ROBU, Hattert, Germany). In the CPD program, 30 slow exchange steps were used. CPD dried plankton were then distributed on carbon tape placed on an SEM stub (Agar scientific) before further gold sputtering (Quorum Q150RS). SEM imaging was performed using a Zeiss

Crossbeam 540 with an acceleration voltage of 1.5 kV and a current of 700 pA and a Secondary Electron Secondary Ion (SESI) detector.

4- Results

4.1- Workflow overview, sample preparation and cell identification

One very crucial step for electron microscopy subcellular analysis is the initial fixation which greatly impacts the preservation of ultrastructural features. Generally, samples can be preserved in two ways, respectively chemical fixation or cryo-immobilization. While chemical fixation is easily available and present lower costs, it usually leads to the introduction of some artifacts (Gautier et al., 1986; Szczesny et al., 1996). Cryo-immobilization via high-pressure freezing is on the other hand usually less accessible, however it usually allows to preserve structure of the samples closer to their native state.

Ultrastructure preservation for EM analysis of environmental marine microorganisms is complex. Indeed, their preparation for good subcellular preservation is time sensitive and they can be affected by distortions before or during chemical fixation (Truby, 1997). During the course of my thesis, the first steps of the workflow thus consisted in sample collection at sea followed by subsequential fractionation, concentration and cryo–immobilization within 2h after collection (See material and method, Fig. 1A-C).

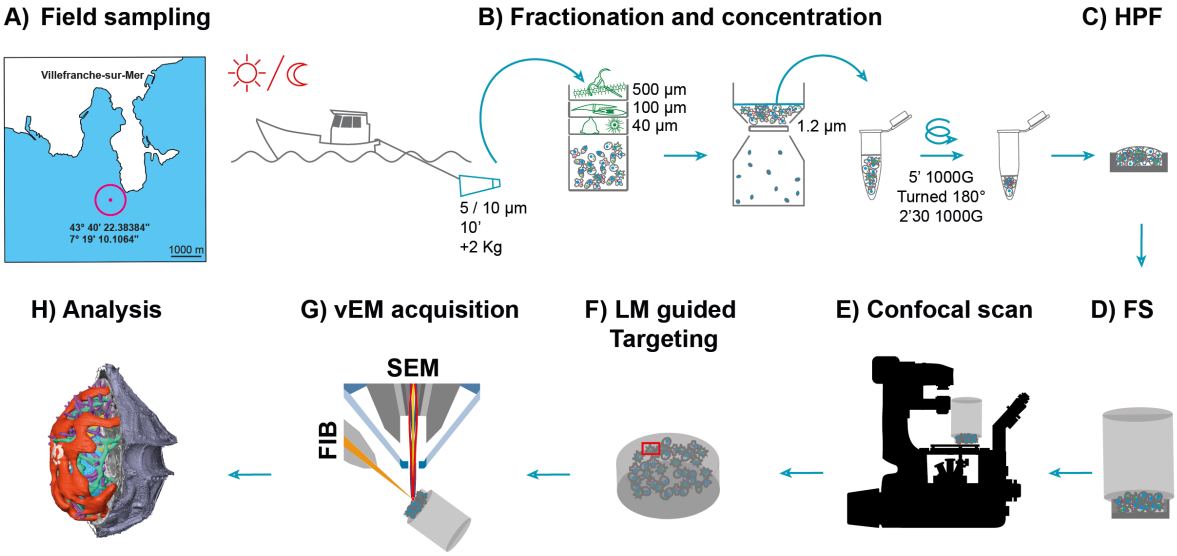

Figure 1: Description of the workflow for vEM targeting of an environmental dinoflagellate. A) Sampling in Villefranche-sur-mer in the early morning and afternoon, B) Fractionation and concentration of the samples on board and at the marine station respectively, C) High-Pressure

Freezing (HPF) of the cell pellet, within 2h after collection in a custom set up at the marine station, D) Freeze-substitution (FS) at EMBL Heidelberg, E) Creation of a confocal map of the block, F) Targeting guided by light microscopy consisting in a succession of trimming step and the branding of the block's surface around the cell of interest, G) FIB-SEM acquisition of the cell of interest and H) Segmentation, rendering and morphometric analysis.

The samples were then further freeze-substituted and embedded in resin following Ronchi et al., 2021 (Fig. 1D). This protocol was selected as it allows for the preservation of the fluorescence signal within the block. Indeed, it presents low amounts of heavy metals and uses a special resin (Lowicryl HM20) that crosslinks differently than classical resin, and polymerizes at sub-zero temperature.

As the samples were solely size-fractionated and concentrated, they contain a complex combination of organisms from widely various species. However, many microorganisms can be recognized thanks to their shape using transmitted light, and they can present a specific autofluorescence signature. Indeed, photosynthetic dinoflagellates present autofluorescence from chlorophyll and its associated pigments, as well as other autofluorescence patterns called "Green autofluorescence" (GAF, Ying and Dobbs, 2007). Thus, after acquiring a 3D map of the entire block, using both transmitted and fluorescent signals, it is then possible to identify diverse organisms as well as to discriminate between genera of dinoflagellate (Fig. 1E).

The endogenous autofluorescence was preserved throughout the depth of the specimen (200µm). The block was imaged by using transmitted light as well as fluorescence by exciting at 488 nm, in order to obtain the GAF, and at 633 nm (Hense et al., 2008), which corresponds to the excitation for the most common type of chlorophyll in dinoflagellates, namely chlorophyll a. This allowed to identify multiple microorganisms, as well as different genera of dinoflagellates (Fig. 2). Interestingly, damaged cells were also possible to identify, allowing to avoid investing imaging efforts on dead organisms.

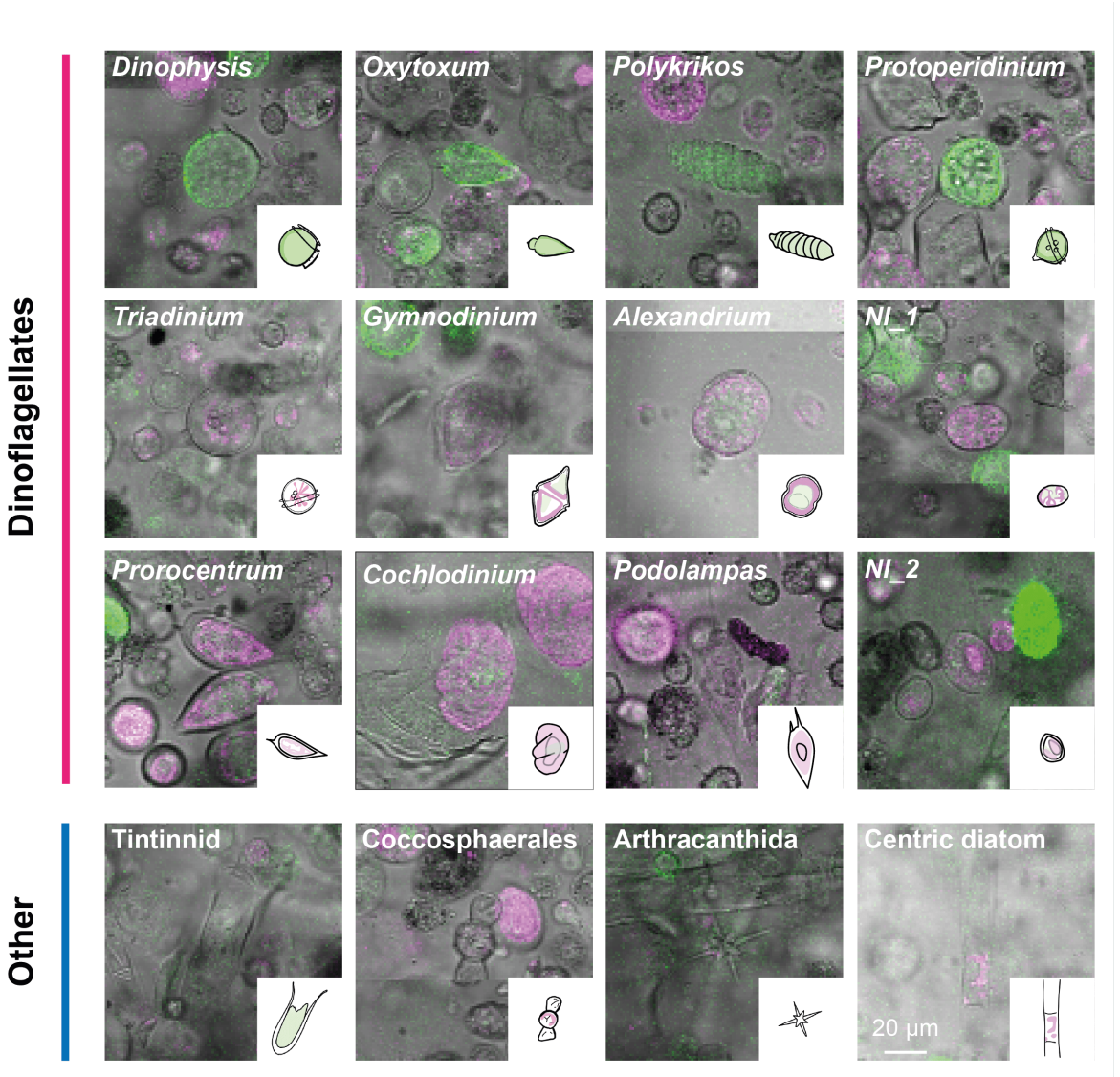

Figure 2: Identification of diverse organisms within the resin block. Overlay of a single slice of the transmitted light and the maximum intensity projection of the confocal stacks of the two-fluorescence channel. The imaging settings are the same for each cell in the different channels. The identification was done using the shape of the cells as well as their autofluorescence profile. The dinoflagellates are identified at the genus level and the other microorganisms at the order level. (NI = Non identified). Figure inspired from figure S1 from Mocaer et al., 2023.

Once a target has been identified, the LM dataset is used to find its x,y and z coordinates (in relation to the block's surface). Unwanted resin on top of the sample is then trimmed away, the target is then close to the surface and marks are branded around it to allow for its precise acquisition using FIB-SEM (Fig.1F). After FIB-SEM imaging (Fig. 1G), the dataset is aligned, followed by segmentation and ultimately visualization and morphometric analysis are possible (Fig. 1H).

4.2- Cell targeting and acquisition

For this first case study, I targeted a small marine dinoflagellate. This cell was identified as belonging to Dinophyceae as it had a transversal groove as well as a longitudinal one (Chapter I, Fig. 2).

Furthermore, it potentially carries chloroplasts, as it presented a far red signal when excited at 633 nm. Interestingly, the endogenous signal was located both at the center of the cell as well as in patches at the cell inner periphery (Fig. 4). The signal located at the cell periphery corresponded to what was expected for the localization of plastid(s).

The targeting workflow for vEM imaging via FIB-SEM, optimized from the method described by Ronchi et al., 2021, consisted in mainly two steps. While acquiring the confocal stack of the block, an extra channel was added in order to image the reflection of the laser light at the interface between the block's surface and the mounting medium, which possess different refractive index (water is used as a mounting medium and the block is made of Lowicryl (Fig. 3C,D arrowhead). This allows to estimate the distance between the cell of interest and the block's surface.

For FIB-SEM imaging, in order to get an even and stable milling and imaging, it is preferable to dispose the region of interest (ROI) as close as possible to the block's surface. Thus, the next step consists in trimming away the resin located above the cell using a diamond knife mounted on an ultramicrotome. This step of trimming and imaging is preferably performed iteratively as the measured distance between the cell and the surface of the block is an estimation. Indeed, the index mismatch present when using the laser reflection for measurement must be taken into account.

When the cell is located close to the surface, landmarks are branded onto the surface of the block around the ROI using a near infrared laser (NIR). These landmarks will later be visible in the SEM view, allowing to determine the area to prepare and acquire via FIB-SEM. The sample preparation for FIB-SEM acquisition consists in depositing protective layers of platinum and carbon above the ROI and opening a trench on one side of the ROI. The acquisition window could then be placed accordingly to the predictions done using the confocal stack.

The entire cell was then acquired using FIB-SEM automated imaging at 8nm isotropic voxel size. This complete dataset and associated segmentation are available on EMPIAR (EMPIAR -11399) and can be visualized and interacted with using the MoBIE plugin in Fiji (https://github.com/mobie/environmental-dinoflagellate-vCLEM).

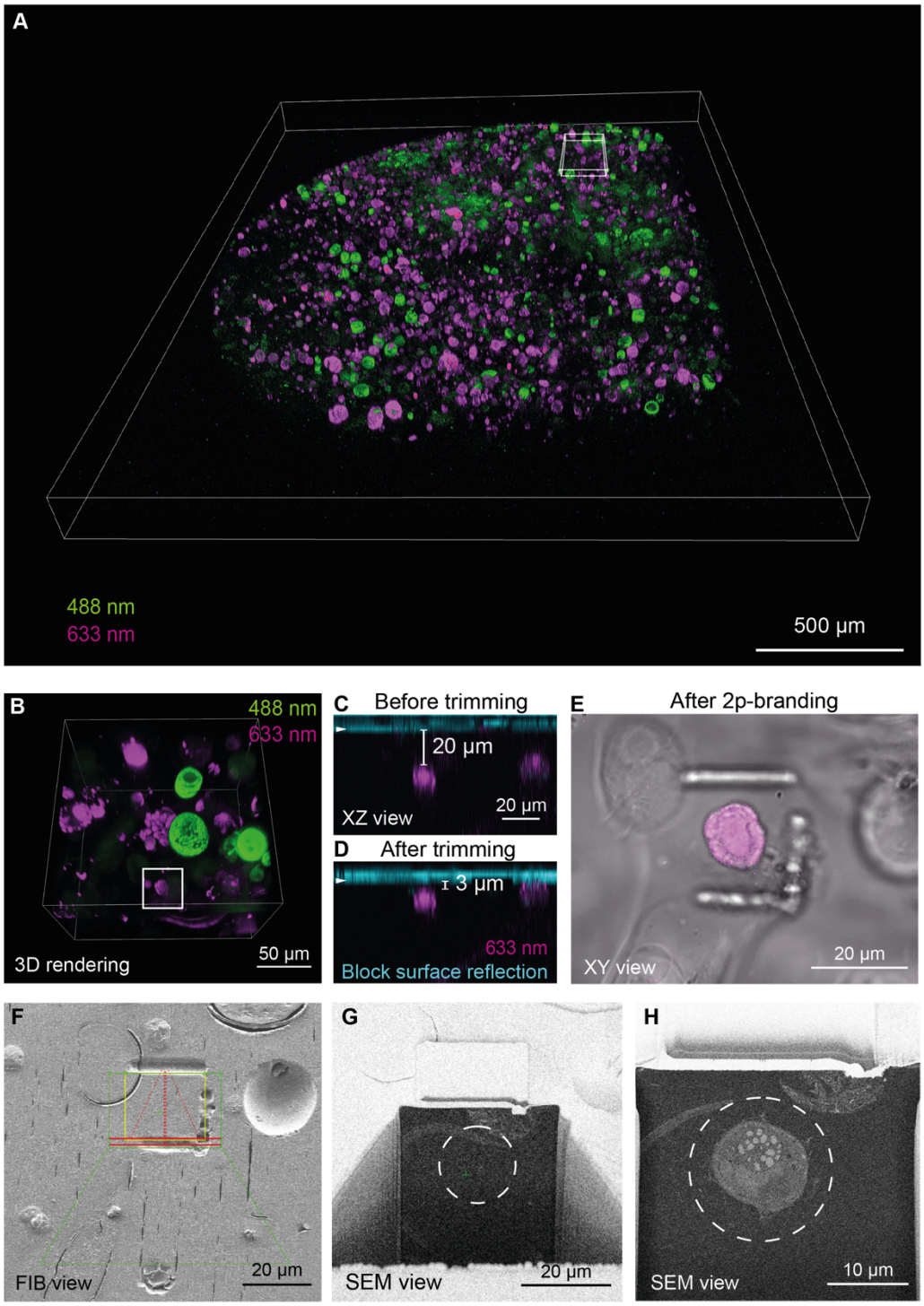

Figure 3: Targeting of a plastid bearing dinoflagellate from an heterogeneous mix of organisms. A) 3D rendering of a dual colour low-resolution tiled z-stack of the entire resin block acquired by confocal imaging. The small box represents the area shown in B. B) 3D rendering of a higher resolution z-stack of the area of interest. The square shows the targeted cell. C-D) Orthogonal view showing the distance between the cell of interest and the surface of the block before (C) and after (D) trimming. E) Landmarks branded by a NIR laser around the cell of interest. F) FIB view of the landmark shown in E, allowing to find the area of interest and prepare it for vEM imaging. G) SEM view of the area ready for FIB-SEM imaging, the dashed circle shows where the cell is expected. H) SEM overview taken during FIB-SEM imaging showing the precision of the acquisition prediction. The dashed circle is in the same position as in G. Figure adapted from figures 2 and 3 from Mocaer et al., 2023.

In order to verify whether the autofluorescence signal was corresponding to the position of the chloroplast, the LM and vEM dataset were overlayed. The far red signal colocalized with the chloroplast (Fig. 13), as expected by the presence of chlorophyll (Hense et al., 2008) confirming the possible use of the far red signal for the identification of species presenting plastid. However, a far red signal was also visible where the nucleus is positioned, which I could not find explanations for (Fig. 4).

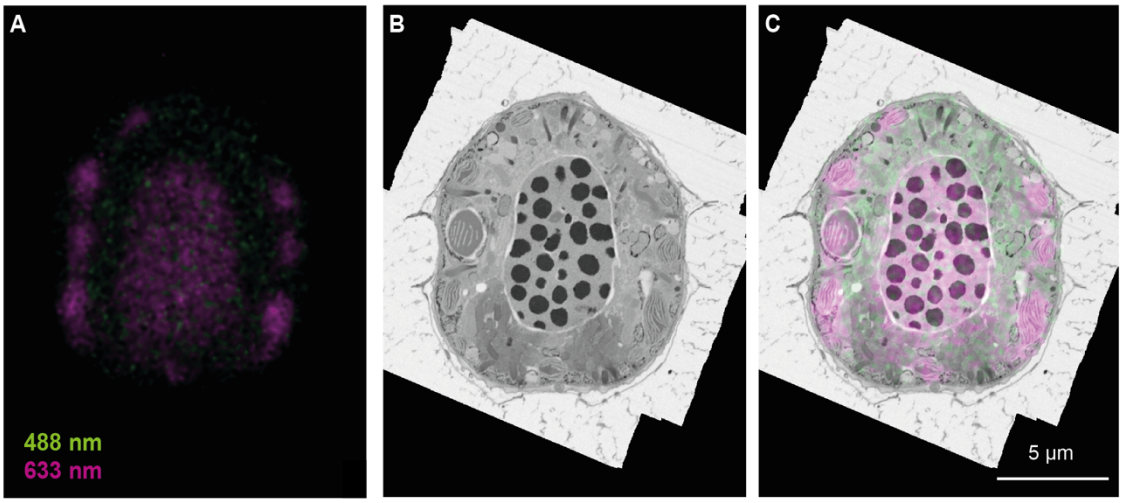

Figure 4: Overlay of the endogenous fluorescence and subcellular morphology. A) Autofluorescence signal of the cell of interest when excited at 633 nm and 488 nm. The image thickness of this slice is 2.2 µm. B) Slice from the FIB-SEM dataset in the same region than the LM slice shown in A. C) Overlay of the LM signal on the slice from the vEM dataset. Figure inspired from figure 4 from Mocaer et al., 2021 (https://github.com/mobie/environmental-dinoflagellate-vCLEM).

4.3 Ultrastructural characterization

4.3.1 Outer cell morphology

From the FIB-SEM acquisition, I segmented a subset of organelles for further 3D visualization and morphometric characterization. First, the outer cell wall was segmented, allowing to determine an overall cellular volume of 1009 µm3. From apex to antiapex, the cell measures 16 µm and its diameter is 13.5 µm. It presents a wide cingulum, dividing the cell between a conical epitheca and a more rounded hypotheca (Fig. 5, Fig. 7A). The cell also presents a sulcus, where the flagellar pores are visible (Fig. 7A, empty black arrows).

In addition to the volumetric information, the 3D rendering of the theca permitted to establish the tabulation for this cell which was important for taxonomical identification (see Chapter I). Traditionally, the plate arrangement was determined using light microscopy and a stain for the cellulosic plates (as calcofluor white) or using SEM. With this method, we show that we can now obtain the thecal arrangement using the reconstruction of the FIB-SEM volume as well.

According to the Kofoidian system (Fensome, 1993), the thecal arrangement is the following: x, 4‘, 3a, 7’’, 4c+T, 5’’’, 2’’’’. Based on the tabulation, size and outer morphology, this cell was identified with the help of Dr Kenneth Mertens, Dr Nicolas Chomerat, Dr Raffaele Siano, Dr Hugo Berthelot and Prof. Dr Mona Hoppenrath as *Ensiculifera tyrrhenica*, from the order *Peridiniales* (= *Pentapharsodinium tyrrhenicum* (Balech)). The same species was identified in samples collected in parallel that were processed for topography SEM (Fig. 5C,D).

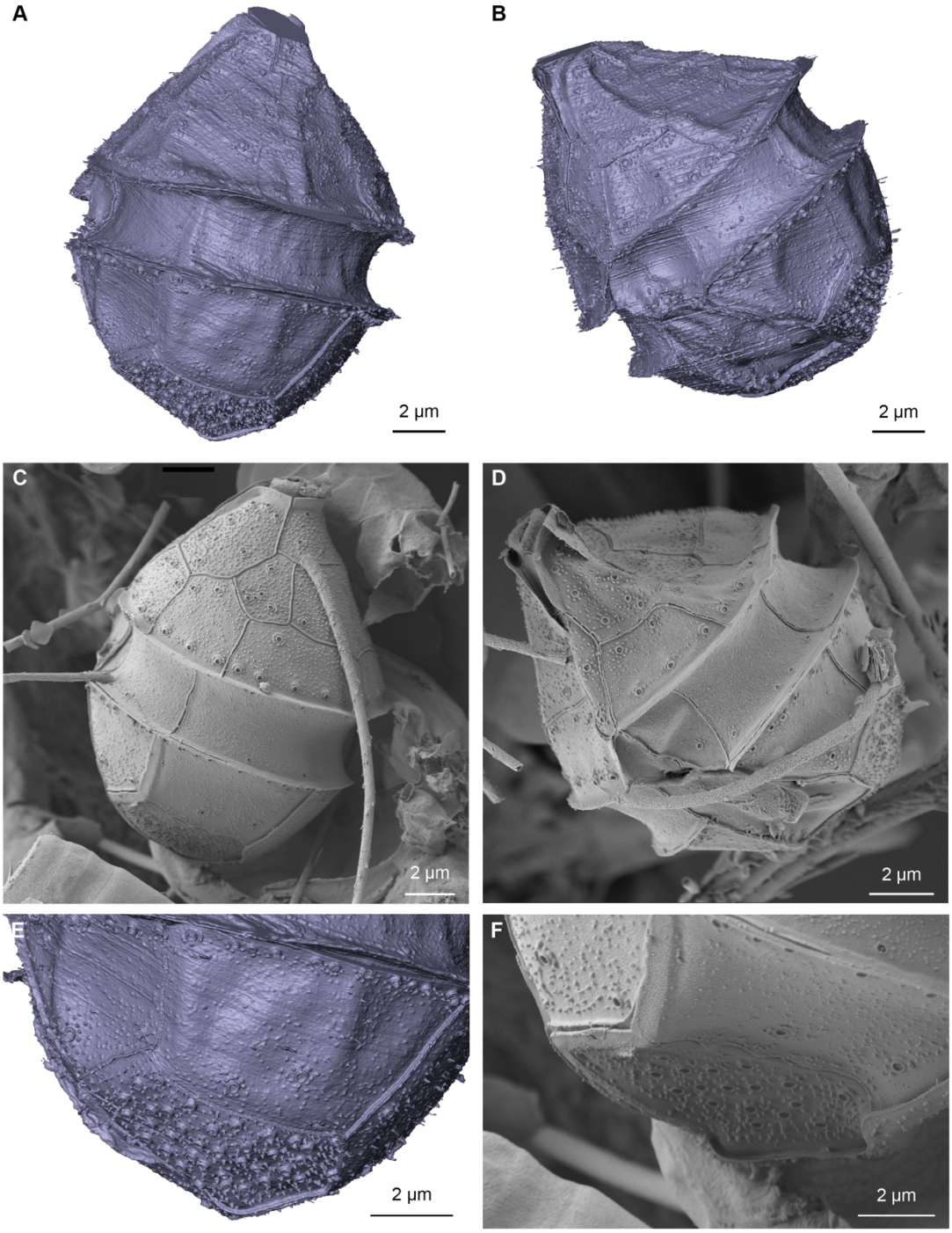

Figure 5: Thecal shape and ornamentation, visualized from the reconstruction of the segmentation of the vEM data and compared to SEM analysis of the same species. A-B) 3D rendering of the segmentation of the theca from the FIB-SEM dataset, in similar orientation as in

C-D. C-D) Topography SEM of cells that we believe are from the same species, collected in parallel to the sample possessed for FIB-SEM imaging. E) Close up of the rendering of the segmentation of the theca showing the ornamentation of the thecal plate and the high concentration of pore on the lower antiapical plates. F) Higher magnification micrograph of the cell shown in C, matching the orientation in E. Figure inspired from figure S2 from Mocaer et al., 2023.

As the cell surface was nicely preserved in our vEM dataset, the thecal ornamentation (small knobs) as well as the thecal pores were easily distinguishable. The pores are not distributed homogeneously between the plates. Interestingly, they are positioned in a linear arrangement apically and antiapically to the cingulum, and have a higher density on the two antiapical plates (Fig. 5, Fig. 6, Fig. 7A). This distribution was similar with the one of cells from the same species imaged in SEM (Fig. 5C, D, F).

4.3.2 Intracellular morphology

vEM not only permits to visualize the outer morphology, but also allows to gain insights on the intracellular structure of the cell with great details. Thus, the next step was to segment a subset of intracellular organelles of interest, allowing to assess their localization, as well as morphometric information (Fig. 7)

The nucleus, possessing an elliptical shape, is positioned centrally in the dorsal part of the cell, and is representing 14.3% of the cell's volume (Fig. 7B,H) The 12 stacks of Golgi apparatus (Fig. 7A,B) are distributed hemispherically close to the apex of the nucleus (Fig. 7B), they occupy 0.02% of the cell's volume (Fig. 7H).

The chloroplast is distributed along the cell periphery and represented a quite important part of the cell volume (9%, Fig. Fig. 7C,H). Contrary to previous observations by light microscopy or 2D TEM analysis of the genus *Ensiculifera* that reported the presence of reticulated chloroplasts (Li et al., 2020a), the chloroplast observed here consists in a single convoluted structure. This shows the potential benefice of using vEM to unambiguously resolve the 3D distribution of a complex convoluted organelle. Furthermore, thanks to the good preservation of our sample and the high resolution of our FIB-SEM dataset acquisition, we could visualize the thylakoid and pyrenoid distribution (Fig. 11C,D). On each sides of the pyrenoid, we can observe a starch sheet (Fig. 11C,D), which represents 0.12% of the cell volume (Fig. 7C,H). As this cell was collected in the early morning, the low amount of starch observed here is consistent with previous reports of low amount of starch during dark phases in dinoflagellates (Seo and Fritz, 2002).

The mitochondrion, which forms an intricated network, is also located in close proximity to the chloroplast. This is also observed in vEM dataset of other algae (Uwizeye et al., 2021b). This organelle occupies 2.37% of the cell volume (Fig. 7D,H).

Additionally, I segmented the trichocysts (Fig. 11E,F). These structures are numerous (n=138) and occupy an important fraction of the cell volume (5.61%, Fig. 7F,H). From the 3D analysis of these organelles, we can visualize two types of sizes and localization for these structures. One group of trichocysts is shorter (2.04 ± 0.92 µm, Fig. 7G), presents the typical straight rod like structure, and they are distributed orthogonally to the plasma membrane, close to the cell cortex in the apical part of the cell. A second group is organized in a bundle of longer (14.17 ± 1.61 µm, Fig. 7G) twisted structures that are ranging from the Golgi area to the antiapical part of the cell. Interestingly, the trichocysts (short or long) are not aligned with the circular openings (Fig. 6).

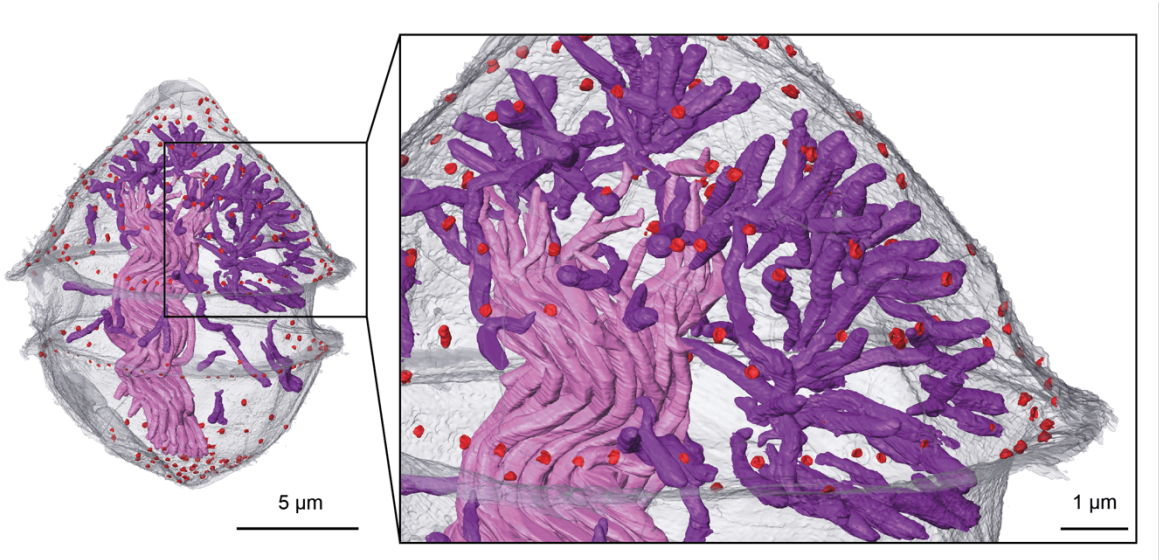

Figure 6: Thecal pores and trichocysts localization. The panel on the right is a close up from the left panel showing that the trichocysts do not seem to align with the thecal pores.

The mucocysts, described as secretory organelles, were also segmented and represent 0.13% of the volume of the cell (Fig. 7E,H). They are distributed as 30 amphora shaped organelles (Fig. 11G,H), and present a volume of 0.046 ± 0.017 μm^3 (Fig. 7H) They are located as a cluster under the plasma membrane in the posterior apical region of the cell.

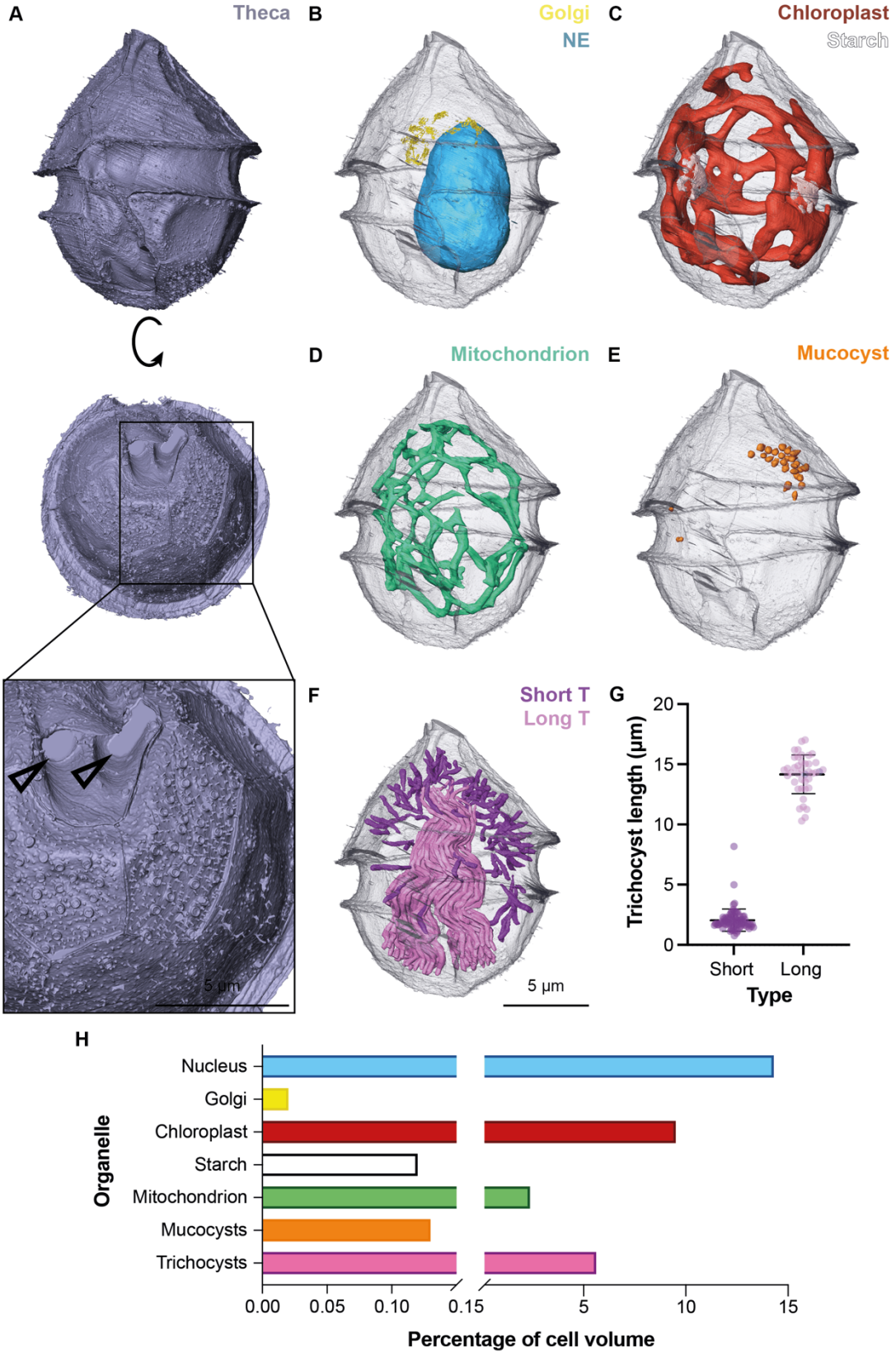

Figure 7: Morphometrics of a subset of organelles from the targeted dinoflagellate. A) Rendering of the segmentation of the theca in a ventral (top) and an antiapical view (center), the bottom image is an enlargement of the antiapical plates showing the pores and small spines. The empty arrows indicate the flagellar pores. B-E) The panels are in the same orientation as the cell

shown in the top A panel. B) Rendering of the segmentation of the nuclear envelope (NE, in blue) and Golgi apparatus (yellow). C) Rendering of the segmentation of the chloroplast (red) and starch (white). D) Rendering of the segmentation of the mitochondrion. E) Rendering of the segmentation of the mucocysts (orange). F) Rendering of the segmentation of the trichocysts, the long trichocysts (Long T) are shown in light pink and the short (short T) ones in darker pink. G) Size distribution of the long and short classes of trichocysts (n=80 for the short T, n= 41 for the long T, mean and standard deviation are shown in the graph). H) Morphometric of the different organelles, their volume in µm3 is expressed as relative of the entire cell volume (1008.76 μm^3). Figure inspired from figure 5 from Mocaer et al., 2021.

We then focused on the internal organisation of nuclear components. Segmentation of the chromatin revealed the presence of 105 condensed chromosomes (Fig. 8A) which possess an averaged volume of 0.510 μm^3 ± 0.162 μm^3. The nucleolus has a volume of 2.308 μm^3. Notably, two small chromosomes (respectively 0.025 μm^3 and 0.004 μm^3) are located in close proximity of the nucleolus (Fig. 8A,B). Further analysis of this area revealed threads originating from the chromosomes and ranging toward the inner part of the nucleolus (Fig. 8C,D). The intensity profile of these threads, which is highly similar to the one of chromosomes, suggests that they could be of chromatin nature in an intermediate compaction state (Fig. 8C).

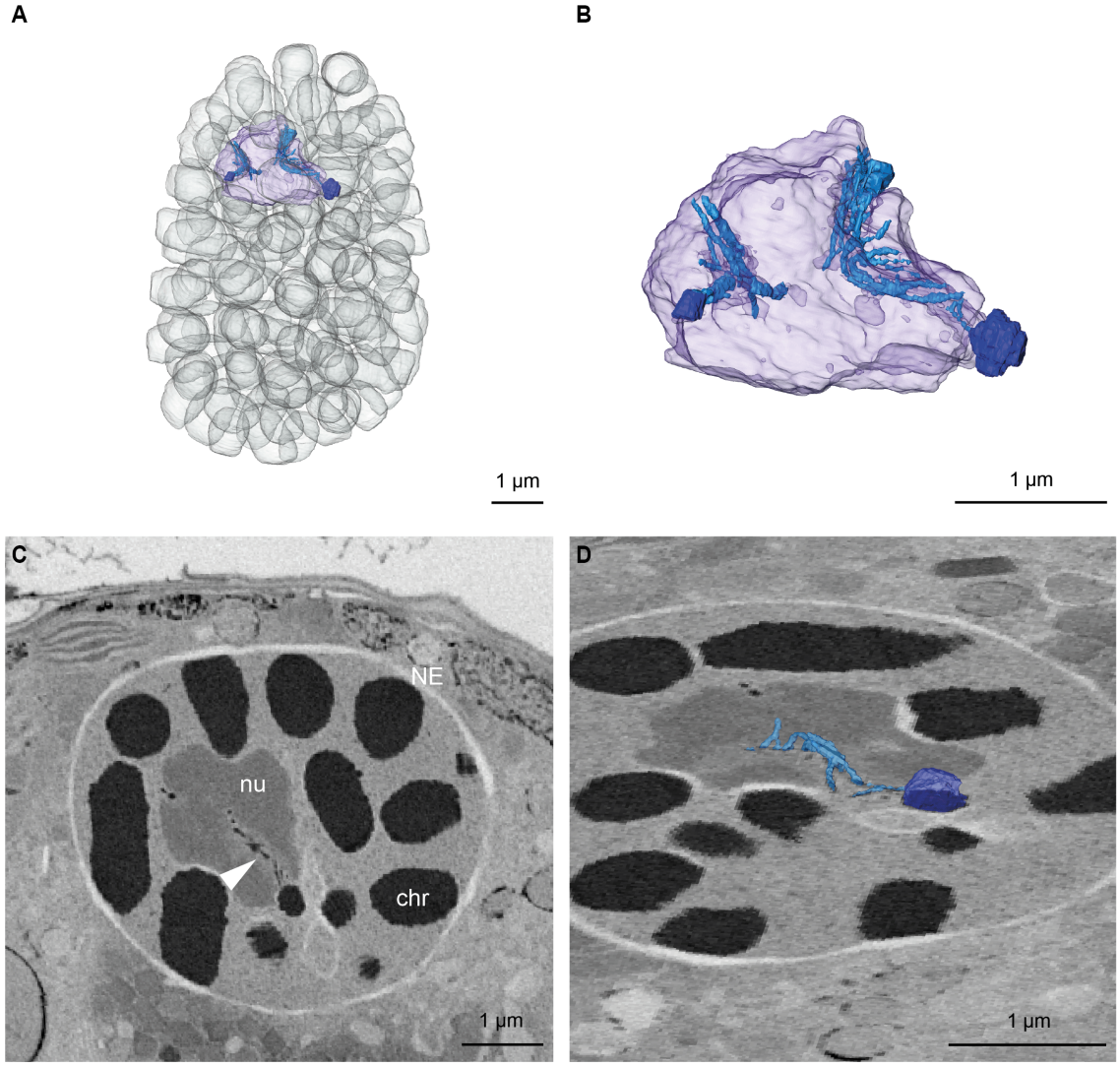

Figure 8: Nucleolar and chromosomal organisation within the nucleus. A) Rendering of the segmentation of the chromosomes (transparent grey), nucleolus (transparent purple) and small chromosomes (dark blue) with their associated filaments (light blue). B) Close up on the rendering of the segmentation of the nucleolus (transparent purple) and small chromosomes (dark blue) with their associated filaments (light blue). C) Slice from the FIB-SEM volume going through the nucleolar region (NE = nuclear envelope, nu = nucleolus, chr = chromosome). The white arrow indicates the filament originating from the small chromosome and extending in the nucleolus. D) Rendering of the segmentation of one of the small chromosomes with its associated filamentous structure overlayed with a slice of the FIB-SEM volume. Figure inspired from figure 6 from Mocaer et al., 2021.

Finally, the flagellar area was analysed. The basal bodies, flagella, microtubular arrays as well as the eyespot were segmented (Fig. 9B, E, F). The cell presents 2 flagella, originating from basal bodies placed under the intersection of the cingulum and sulcus (Fig. 9B). These structures are protruding in the space between the cell body and the theca (Fig. 9C). While the longitudinal flagellum is long and following half of the cell perimeter, the transverse flagella is short and might have been affected during sample collection or shredded by the cell itself (Kofoid, 1908).

The eyespot of this organism is present within the chloroplast, and is organized as a single layer of globules distributed on the side of the chloroplast facing the exterior (Fig. 9A, B,E,F). Its arrangement seems to indicate that it is part of the category I(A) of the eyespot classification from Hoppenrath., 2017 (See Chapter I, Fig. 8). The type I(A) of eyespot has been seen in other members of the Peridiniaceae (Calado et al., 1999; Messer and Ben-Shaul, 1969; Moestrup and Daugbjerg, 2007). It is located behind the sulcus groove, as previously seen in the order *Peridiniales* (Dodge, 1984; Li et al., 2020b).

Part of the microtubule arrays could be resolved, as microtubules are at the limit of what we could resolve in our FIB-SEM imaging conditions. While one of the arrays is starting close to the basal body of the longitudinal flagellum, and is following the plasma membrane's curvature with a direction towards the cell surface (Fig. 9C,D,E,F). The second array is originating close to the basal body of the transversal flagella and is directed towards the inner part of the cell (Fig. 9C,E,F).

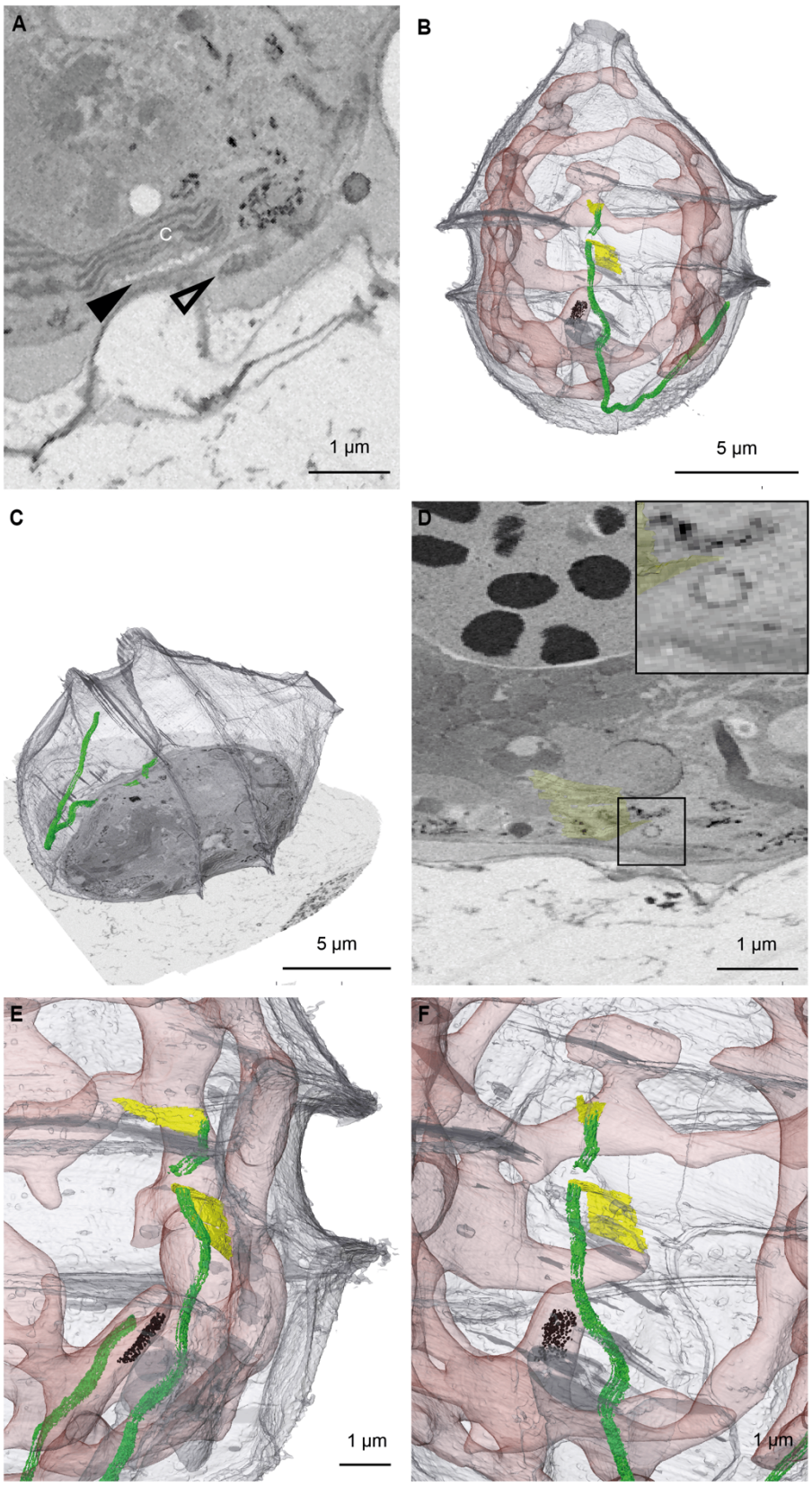

Figure 9: Organisation of the flagellar apparatus and eyespot. A) FIB-SEM slice through the eyespot (pointed by the full black arrow) and the longitudinal flagella (pointed by the empty black arrow). C = Chloroplast. B) 3D visualization of the segmentation of the theca (transparent grey), chloroplast (transparent red), flagella (green), microtubule arrays (yellow) and eyespot (black)

ventrally under the intersection of the cingulum and sulcal groove. C) 3D Rendering from the segmentation of theca (light grey) and the flagella (green), which is positioned under thecal arrangement. The two renderings are overlayed with a slice from the FIB-SEM volume. D) Rendering of the segmentation of the microtubule array (transparent yellow) overlayed with a slice from the FIB-SEM volume. The black box underlines the basal body of the longitudinal flagella, also shown as a close up in the upper right corner. E-F) Zoomed in views of the rendering of the segmentations of the flagella (green), microtubule arrays (yellow), chloroplast (transparent red) and eyespot located inside the chloroplast (black). Figure inspired from figure 7 from Mocaer et al., 2021.

Lastly, I segmented the crystalline inclusions (CI) that were distributed throughout the cell volume. Even though the membranes are complex to resolve in this dataset, these inclusions appear to be located in defined reticulated compartments, spanning throughout the cell volume. Interestingly, the inclusions seem to be distributed on the outer part of the cell and are often located in close proximity to the chloroplasts (Fig. 10)

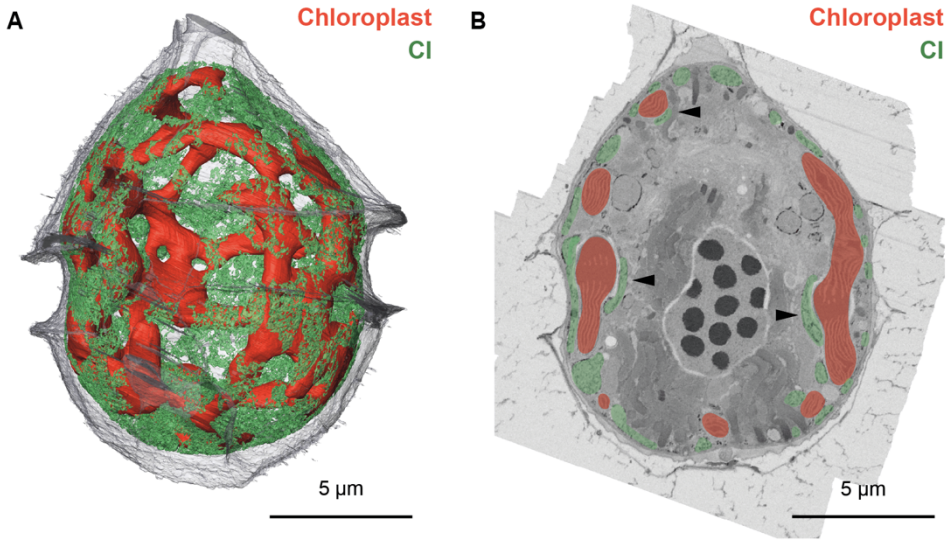

Figure 10: Crystalline inclusions distribution. A) Crystalline inclusions (CI) localisation within the cell and distribution of chloroplast. B) Micrograph from the FIB-SEM volume showing the distribution of the crystalline inclusions and the localisation of the chloroplast. The arrows show the proximity of some CI compartments to the chloroplast.

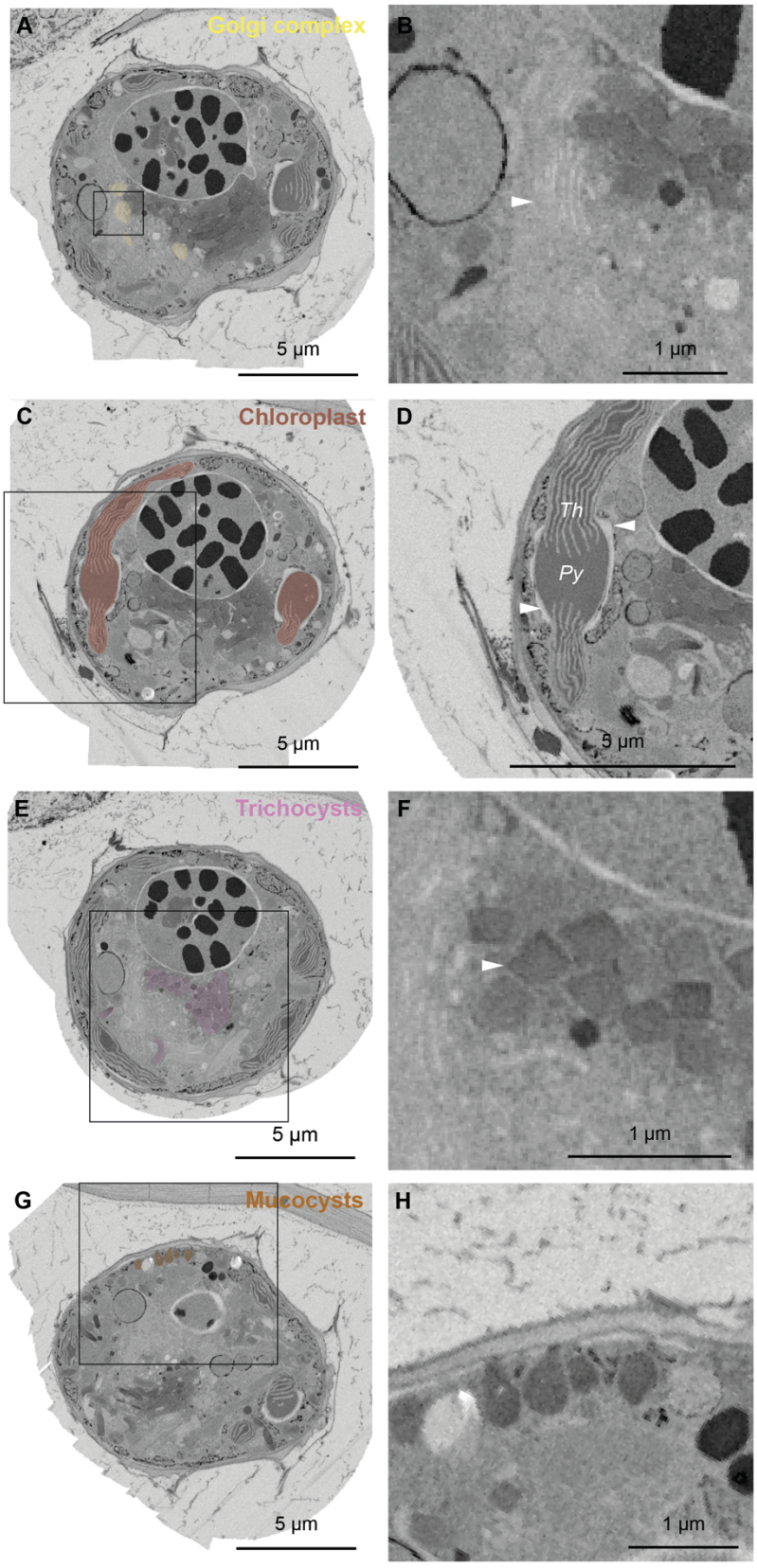

Figure 11: Raw images from the FIB-SEM dataset showing the subcellular details of different organelles. On the left is a low magnification image with a square and a colour overlayed for each organelle shown as a close up on the left panel. A-B) Golgi apparatus, in B two Golgi stacks are visible. C-D) Chloroplast, in D the pyrenoid (Py) and thylakoid (Th) membranes are

shown. The arrowheads point at the starch sheets around the pyrenoid area. E-F) Trichocysts, F shows their squared profile in cross section. G-H) Mucocysts, F shows their typical amphora shape. Figure inspired from figure S3 from Mocaer et al., 2021.

5- Discussion

In this chapter, I described a correlative method, based on light microscopy to allow targeted vEM imaging and subcellular analysis of a specific microorganism from an environmental population.

Previous methods were developed to target expressed fluorescence proteins (Ronchi et al., 2021) or small molecule live dyes (Imprima et al., 2023). Here, we show the opportunity to use the preserved endogenous fluorescence to navigate to targets of interest within an heterogeneous sample. This is especially important in the case of heterogeneous environmental sample where finding replicates of specific cell for a representative description of its ultrastructure can represent a complex challenge. This opens a range of possibilities for ultrastructural environmental studies.

vEM can allow to comprehend the organisation of subcellular compartments, in relation to each other, within a volume. This approach is thus very powerful, however the throughput of this technique is limited. Therefore, methods that can allow to restrict the time of acquisition by efficiently finding and acquiring precise regions of interest are valuable as it can allow to scale up this type of study. As a matter of fact, a lower precision in targeting would lead to the preparation and acquisition of a larger region (to allow for buffer around the subject of interest), leading to longer processing time by FIB-SEM.

In the case of my small dinoflagellate (~15 µm diameter), the entire volume could be acquired in less than 48h. Note that depending of the volume to image, for a similar resolution, the imaging time will of course vary. For some of the larger cells found in my dataset (examples shown in Fig. 11), acquisition of a full cell would take approximately in 5 days when using the same imaging settings. Interestingly, in the case of microorganisms presenting an autofluorescence profile, this method could be scaled up by imaging only a smaller targeted subcellular region. For instance, this could allow to investigate, in various marine microorganisms, the ultrastructure associated to GAF or other compartments known to be autofluorescent as the eyespot or accumulation body (Ying and Dobbs, 2007).

Another bottleneck for a high throughput in this type of study is the segmentation time. As one gains experience, this process becomes more efficient and here the mostly manual approach took 72h. Developments of artificial intelligence will probably help in making this step more automatic, thus decreasing the analysis time substantially and permitting ultimately analysis of a wider number of specimen (Heinrich et al., 2021).

In addition to be a methodological proof of concept, the study described in this chapter is one of the first examples of 3D ultrastructural analysis on environmental samples. The transmitted LM signal in combination with autofluorescence signature of the cells permitted here to target a small plastid bearing thecate dinoflagellate, which we could identify thanks to the FIB-SEM dataset as *Ensiculifera tyrrhenica (*synonym to *Pentapharsodinium tyrrhenicum (Balech),* Montresor et al., 1994, order *Peridiniales*). In combination to the details of the cell surface, this approach allows to reveal the subcellular architecture of the cell. This type of datasets is rare and precious for the community, and it is very important to make them available. The raw data and the segmentation are available on EMPIAR (ID 11399) as well as in the Mobie plugin (https://github.com/mobie/environmental-dinoflagellate-vCLEM) in Fiji (Pape et al., 2022).

The vEM analysis allowed to visualize the position of organelles relative to one another. This was particularly valuable for the eyespot, flagella and microtubule arrays, where the combination of these structures could have a role in phototaxis. Additionally, we could visualize the 3D organization of the nucleus, permitting to notice filamentous structures localized in the nucleolar space which were extending from small chromosomes. Based on the filaments appearance, they seem to be of chromatin nature in an intermediate folding state. This is very interesting as dinoflagellates chromosomes are permanently condensed (Gautier et al., 1986), which always raised questions concerning the mechanism of their genome's transcription. Past studies hypothesized that DNA structures protruding from the chromosome core are implicated in RNA transcription (Rizzo, 1991; Sigee, 1983; Sigee, 1984; Soyer-Gobillard et al., 1990). These type of structures, emanating from the chromosomes have been seen in diverse dinoflagellates (Bhaud et al., 2000; Decelle et al., 2021; Soyer-Gobillard et al., 1990). Furthermore, as the nucleolus is an important localization for the biogenesis of ribosomes in eukaryotes (Hadjiolov, 1980), and genes of rRNA have been situated at the nucleolus/chromatin interface in dinoflagellate (Géraud et al., 1991), the arrangement visible in *E. tyrrhenica* would be consistent with a previously proposed intranucleolar transcriptional activity (Géraud et al., 1991).

From the subcellular analysis of *Ensiculifera tyrrhenica*, we could infer that the cell is polarized. Raising questions for the general organisation of other dinoflagellates (see chapter 4). Indeed,

certain organelles are densely present in the apical region of the cell, such as the mucocysts or the Golgi apparatus. The short trichocysts also have a distinct distribution, as they are radiating from the Golgi area, and are directed towards the apical inner cell membrane. This organization suggests that they could be mature and ready for extrusion.

Altogether, this chapter shows here the potential of using vCLEM for subcellular exploration of a targeted organism from marine complex environmental samples.

6- References

Belevich, I., Joensuu, M., Kumar, D., Vihinen, H. and Jokitalo, E. (2016). Microscopy Image Browser: A Platform for Segmentation and Analysis of Multidimensional Datasets. *PLoS Biol.* **14**, 1–13.

Bhaud, Y., Guillebault, D., Lennon, J. F., Defacque, H., Soyer-Gobillard, M. O. and Moreau, H. (2000). Morphology and behaviour of dinoflagellate chromosomes during the cell cycle and mitosis. *J. Cell Sci.* **113**, 1231–1239.

Calado, A. J., Hansen, G. and Moestrup, Ø. (1999). Architecture of the flagellar apparatus and related structures in the type species of *Peridinium, p. cinctum* (dinophyceae). *Eur. J. Phycol.* **34**, 179–191.

Decelle, J., Veronesi, G., LeKieffre, C., Gallet, B., Chevalier, F., Stryhanyuk, H., Marro, S., Ravanel, S., Tucoulou, R., Schieber, N., et al. (2021). Subcellular architecture and metabolic connection in the planktonic photosymbiosis between Collodaria (radiolarians) and their microalgae. *Environ. Microbiol.* **23**, 6569–6586.

Decelle, J., Kayal, E., Bigeard, E., Gallet, B., Bougoure, J., Clode, P., Schieber, N., Templin, R., Hehenberger, E., Prensier, G., et al. (2022). Intracellular development and impact of a marine eukaryotic parasite on its zombified microalgal host. *ISME J.* **16**, 2348–2359.

Dixon, G. K. and Syrett, P. J. (1988). The growth of dinoflagellates in laboratory cultures. *New Phytol.* **109**, 297–302.

Dodge, J. D. (1984). The functional and phylogenetic significance of dinoflagellate eyespots. *BioSystems* **16**, 259–267.

Fensome, R. A. (1993). *A classification of living and fossil dinoflagellates*. Micropaleontology

Press, American Museum of Natural History.

Gautier, A., Michel-Salamin, L., Tosi-Couture, E., McDowall, A. W. and Dubochet, J. (1986). Electron microscopy of the chromosomes of dinoflagellates in situ: confirmation of Bouligand's liquid crystal hypothesis. *J. Ultrastruct. Res. Mol. Struct. Res.* **97**, 10–30.

Gavelis, G. S., Wakeman, K. C., Tillmann, U., Ripken, C., Mitarai, S., Herranz, M., Özbek, S., Holstein, T., Keeling, P. J. and Leander, B. S. (2017). Microbial arms race: Ballistic "nematocysts" in dinoflagellates represent a new extreme in organelle complexity. *Sci. Adv.* **3**,.

Gavelis, G. S., Herranz, M., Wakeman, K. C., Ripken, C., Mitarai, S., Gile, G. H., Keeling, P. J. and Leander, B. S. (2019). Dinoflagellate nucleus contains an extensive endomembrane network, the nuclear net. *Sci. Rep.* **9**, 1–9.

Géraud, M. L., Herzog, M. and Soyer-Gobillard, M. O. (1991). Nucleolar localization of rRNA coding sequences in *Prorocentrum micans* Ehr. (dinomastigote, kingdom Protoctist) by in situ hybridization. *BioSystems* **26**, 61–74.

Hadjiolov, A. A. (1980). Biogenesis of Ribosomes in Eukaryotes. In *Subcellular Biochemistry: Volume 7* (ed. Roodyn, D. B.), pp. 1–80. Boston, MA: Springer US.

Heinrich, L., Bennett, D., Ackerman, D., Park, W., Bogovic, J., Eckstein, N., Petruncio, A., Clements, J., Pang, S., Xu, C. S., et al. (2021). Whole-cell organelle segmentation in volume electron microscopy. *Nature* **599**, 141–146.

Hennies, J., Lleti, J. M. S., Schieber, N. L., Templin, R. M., Steyer, A. M. and Schwab, Y. (2020). AMST: Alignment to Median Smoothed Template for Focused Ion Beam Scanning Electron Microscopy Image Stacks. *Sci. Rep.* **10**, 1–10.

Hense, B. A., Gais, P., Jütting, U., Scherb, H. and Rodenacker, K. (2008). Use of fluorescence information for automated phytoplankton investigation by image analysis. *J. Plankton Res.* **30**, 587–606.

Hoppenrath, M. (2017). Dinoflagellate taxonomy — a review and proposal of a revised classification. *Mar. Biodivers.* **47**, 381–403.

Imprima, E. D., Gawrzak, S., Schwab, Y., Jechlinger, M., Mahamid, J., Montero, M. G., Gawrzak, S., Ronchi, P. and Zagoriy, I. (2023). Technology Light and electron microscopy continuum-resolution imaging of 3D cell cultures II Light and electron

microscopy continuum-resolution imaging of 3D cell cultures. *Dev. Cell* **58**, 616-632.e6.

Kofoid, C. . (1908). *Exuviation, Autotomy and Regeneration in Ceratium*. Berkeley, The University Press.

Li, Z., Mertens, K. N., Gottschling, M., Gu, H., Söhner, S., Price, A. M., Marret, F., Pospelova, V., Smith, K. F., Carbonell-Moore, C., et al. (2020a). Taxonomy and Molecular Phylogenetics of *Ensiculiferaceae, fam. nov.* (Peridiniales, Dinophyceae), with Consideration of their Life-history. *Protist* **171**,.

Messer, G. and Ben-Shaul, Y. (1969). Fine Structure of Peridinium westii Lemm., a Freshwater Dinoflagellate. *J. Protozool.* **16**, 272–280.

Mocaer, K., Mizzon, G., Gunkel, M., Halavatyi, A., Steyer, A., Oorschot, V., Schorb, M., Kieffre, C. Le, Yee, D. P., Chevalier, F., et al. (2023). Targeted volume Correlative Light and Electron Microscopy of an environmental marine microorganism. *J. Cell Sci.* **c**, 2023.01.27.525698.

Moestrup, Ø. and Daugbjerg, N. (2007). On dinoflagellate phylogeny and classification. 215–230.

Moldrup, M., Moestrup, Ø. and Hansen, P. J. (2013). Loss of phototaxis and degeneration of an eyespot in long-term algal cultures: Evidence from ultrastructure and behaviour in the dinoflagellate *Kryptoperidinium foliaceum. J. Eukaryot. Microbiol.* **60**, 327–334.

Montanaro, J., Gruber, D. and Leisch, N. (2016). Improved ultrastructure of marine invertebrates using non-toxic buffers. *PeerJ* **2016**, 1–15.

Montresor, M., Montesarchio, E., Marino, D. and Zingone, A. (1994). Calcareous dinoflagellate cysts in marine sediments of the Gulf of Naples (Mediterranean Sea). *Rev. Palaeobot. Palynol.* **84**, 45–56.

Oliveira, C. Y. B., Oliveira, C. D. L., Müller, M. N., Santos, E. P., Dantas, D. M. M. and Gálvez, A. O. (2020). A Scientometric Overview of Global Dinoflagellate Research. *Publications* **8**, 50.

Pape, C., Meechan, K., Moreva, E., Schorb, M., Chiaruttini, N., Zinchenko, V., Vergara, H., Mizzon, G., Moore, J., Arendt, D., et al. (2022). MoBIE: A Fiji plugin for sharing and exploration of multi-modal cloud-hosted big image data. *Nat. Methods* **20**, 2022.05.27.493763.

Rizzo, P. J. (1991). The Enigma of the Dinoflagellate Chromosome. *J. Protozool.* **38**, 246–252.

Ronchi, P., Mizzon, G., Machado, P., D'imprima, E., Best, B. T., Cassella, L., Schnorrenberg, S., Montero, M. G., Jechlinger, M., Ephrussi, A., et al. (2021). High-precision targeting workflow for volume electron microscopy. *J. Cell Biol.* **220**,.

Seo, K. S. and Fritz, L. (2002). Diel changes in pyrenoid and starch reserves in dinoflagellates. *Phycologia* **41**, 22–28.

Sigee, D. C. (1983). Structural DNA and genetically active DNA in dinoflagellate chromosomes. *BioSystems* **16**, 203–210.

Sigee, D. C. (1984). Some observations on the structure, cation content and possible evolutionary status of dinoflagellate chromosomes. *Bot. J. Linn. Soc.* **88**, 127–147.

Soyer-Gobillard, M. O., Geraud, M. L., Coulaud, D., Barray, M., Theveny, B., Revet, B. and Delain, E. (1990). Location of B- and Z-DNA in the chromosomes of a primitive eukaryote dinoflagellate. *J. Cell Biol.* **111**, 293–308.

Szczesny, P. J., Walther, P. and Müller, M. (1996). Light damage in rod outer segments: The effects of fixation on ultrastructural alterations. *Curr. Eye Res.* **15**, 807–814.

Truby, E. W. (1997). Preparation of single-celled marine dinoflagellates for electron microscopy. *Microsc. Res. Tech.* **36**, 337–340.

Uwizeye, C., Brisbin, M. M., Gallet, B., Chevalier, F., LeKieffre, C., Schieber, N. L., Falconet, D., Wangpraseurt, D., Schertel, L., Stryhanyuk, H., et al. (2021a). Cytoklepty in the plankton: A host strategy to optimize the bioenergetic machinery of endosymbiotic algae. *Proc. Natl. Acad. Sci. U. S. A.* **118**,.

Uwizeye, C., Decelle, J., Jouneau, P.-H., Flori, S., Gallet, B., Keck, J.-B., Bo, D. D., Moriscot, C., Seydoux, C., Chevalier, F., et al. (2021b). Morphological bases of phytoplankton energy management and physiological responses unveiled by 3D subcellular imaging. *Nat. Commun.* **12**, 1049.

Ying, Z. T. and Dobbs, F. C. (2007). Green autofluorescence in dinoflagellates, diatoms, and other microalgae and its implications for vital staining and morphological studies. *Appl. Environ. Microbiol.* **73**, 2306–2313.

Chapter V: Targeted vEM of a subset of cells reveals their ultrastructure

1- Introduction

Following the vEM targeting strategy described in Chapter IV, acquisition of a subset of dinoflagellates species was performed. These specific organisms were selected based on the hypothesis that they would possess particular subcellular features identified in the TEM screen (described in Chapter II). In fact, as some organelles seemed to consistently occur in a subset of similar looking organisms, based on their abundance of 2D profiles, I could get an idea concerning their potential cell morphology. Knowing which genera were particularly abundant in my samples, thanks to the LM and SEM data, I could precisely choose targets of interest for which I investigated the presence of specific organelles.

In this chapter, the ultrastructure of *Triadinium cf sphaericum*, *Prorocentrum cf gracile* and *Pseudalatosphaera cf corsica* will be described. Furthermore, I will show that morphological variations previously observed in the TEM screen between samples collected in the early morning or the afternoon could be recapitulated in the acquired volumes.

To the best of my knowledge, these cells have not been investigated neither by TEM nor vEM so far. Thus, very little is known about their subcellular organisation. Interestingly, these three species of dinoflagellate each seemed to present a stereotypic arrangement. Indeed, for each n=2 described below, the localisation of the nucleus, pusule and more specific organelles as the electron dense compartment in *Pseudalatosphaera cf corsica* were preserved. Note that in this study, as the number of vEM datasets is rather low (n=2 per species), the cellular organisation could be different according to phases of the cell cycle or in varying conditions. However, I hope that these volumetric and morphometric information, which I aim to make available publicly, can help further investigate the biology of these complex microorganisms.

Additionally, I investigated the autofluorescence profile of the electron dense sheets compartment present in *Pseudalatosphaera cf corsica* in lowicryl HM20. Possessing further information on autofluorescence profile of various species can potentially contribute to a finer targeting, ultimately allowing to increase the throughput of this targeting approach.

2- Contributors

Sample collection for this work was done in collaboration with the team of Johan Decelle at Grenoble CEA (Johan Decelle, Charlotte LeKieffre, Daniel. P. Yee, Fabien Chevalier) and Anna Steyer (Mattei Group, EMBL Heidelberg). The conceptualization for this work was done with Yannick Schwab.

Paolo Ronchi (EMCF Heidelberg), Benoit Gallet (IBS Grenoble) and Anna Steyer (Mattei Group, IC Heidelberg) contributed to the methodology. Julian Hennies (Mattei Group, IC Heidelberg) contributed in the alignment of the FIB-SEM dataset. Martin Schorb (EMCF Heidelberg) contributed in software and visualization development for this project. Kenneth Mertens, Nicolas Chomerat, Raffaele Siano, Hugo Berthelot and Mona Hoppenrath helped in the taxonomic identification.

Martin Fritsch (Leica Microsystems) and Dietrich Walsh (Zimmerman Group, IC Heidelberg) contributed in the characterization of the autofluorescence profile.

3- Material and methods

See Chapter III, 3- Material and methods for details on collection, processing for EM, targeting strategy, volume acquisition and analysis.

3.1 Characterization of the autofluorescence profile

In order to investigate and acquire the emission spectrum of the autofluorescent compartment present in *Pseudalatosphaera cf corsica*, the Stellaris microscope (Leica Microsystems) was used with the help of Martin Fritsch and Dietrich Walsh. The cell shown in Fig. 5 was acquired using an HC PL APO CS2 40x/1.10 water objective and excited at 490 nm (the excitation wavelength was determined thanks to the previous acquisition of an excitation / emission scan for this cell type). The emission scan was acquired with steps of 6.38 nm and a bandwidth of 5 nm. The pixel size for the acquisition was 168 nm.

4- Results

4.1- Prorocentrum cf gracile

Dinoflagellates from the genus *Prorocentrum* are distributed worldwide (Hoppenrath et al., 2013). There are approximately 60 species described, all of them phototrophic (Hoppenrath et al., 2013). Cells from this genus have the specificity of presenting two main thecal plates separated by a sagittal suture, having an apical flagellar insertion and not possessing either a cingulum or a sulcus (Chapter I, Fig. 2F).

The taxonomy of cells from this genus is based on the cell shape and size, presence of an apical spine, and the positioning of pores on the theca as well as the thecal ornamentation (Cohen-Fernandez et al., 2006).

Based on the morphological features observed using LM, SEM and vEM of *Prorocentrum* cells found in my sample, on the literature (Cohen-Fernandez et al., 2006) and with the help of Pr. Dr. Mona Hoppenrath, I could identify the cells acquired here by vEM as *Prorocentrum. cf. gracile* (order Prorocentrales).

Note that *Prorocentrum micans*, *Prorocentrum gracile* and *Prorocentrum sigmoide* can be very similar in appearance, making it generally complex when it comes to identification (Cohen-Fernandez et al., 2006).

This cell was targeted as I was interested in confirming the presence of the fibrous organelle “b” described in the TEM screen (Chapter III, Fig 5). As in the TEM screen, these organelles were present in a “leaf” shaped cell and showed the presence of chloroplast, I targeted for a cell presenting this overall “leaf” morphology and which presented an autofluorescence signal when excited at 633 nm (Chapter IV, Fig. 11 *Prorocentrum*). The following paragraph describes the results concerning the cells organization as well as the morphometric parameters in *Prorocentrum cf. gracile* imaged respectively from a morning and an afternoon sample.

4.1.1 Description of the cell volume and morphometric analysis

The cells from morning and afternoon samples measured respectively approximately 44 µm in length and 13 µm at its maxima in width, and 50 µm in length and 17µm at its maxima in width. The whole cell, and the cytoplasm volumes were respectively 4518.94 μm^3 and 2777.47 μm^3 for the cell collected in the morning, and 7616.27 μm^3 and 4382.36 μm^3 for the cell collected in the afternoon.

The two large thecal plates of *Prorocentrum cf. gracile*, as well as the acquired part of its spine, were segmented and rendered (Fig. 1iA,iiA). The theca presents a foveate type ornamentation as well as thecal pores (Fig. 1iA,iiA).

Prorocentrum cf. gracile cells present a nucleus located at the posterior region (Fig. 1iB,iiB). Interestingly, in cell from the early morning sampling, the chromosomes are all connected suggesting that the cell might be in the replication phase of its cell cycle. In the second cell, collected in the afternoon, I could distinguish approximately 77 chromosomes with an average volume of 4.03 μm^3 per chromosome (± 2.44 μm^3). The volume of chromatin is similar for both cells, suggesting that the morning cell is potentially is starting its S phase and did not replicate its DNA yet. For the afternoon cell, the nucleus presented a "U" shape as described for species from the genus, *Prorocentrum micans* (Soyer-Gobillard and Geraud, 1992). The nucleus, in both cases, represents an important part of the cell's volume, respectively 20.64% and 13.45% of the cell's cytoplasm (Fig. 1iH,iiH).

For both cells, the Golgi apparatus is located anterior to the nucleus (Fig. 1iB,iiB), forming a hemispherical structure, as described for other species (Dodge, 1971).

Both of the acquired cells presented a single convoluted chloroplast (Fig. 1iC,iiC), representing respectively 12.13% (AM, Fig. 1iH) and 6.77% (PM, Fig. 1iH) of the cytoplasm volumes respectively. Each chloroplast is distributed along the cellular periphery. This is consistent with the reticulated nature and peripheral disposition of the plastid in other species of *Prorocentrum,* as *Prorocentrum lima* and *Prorocentrum maculosum,* (Zhou and Fritz, 1993).

Consistently with our global TEM analysis, the cell from the afternoon sampling session presents numerous putative starch granules. These large granules are located in close proximity with the chloroplast and occupy close to 32.41% of the cell volume (Fig. 1iiC,H). Interestingly, no starch was observed in the cell from the morning sampling (Fig. 1iC,H). These observation would be consistent with the suggested model of dinoflagellates building starch reserved during the day (Loeblich, 1977; Seo and Fritz, 2002).

The non-identified organelle, previously called "b" (Chapter III, Fig. 5), presenting fibrous structures within their lumen were segmented and rendered (Fig. 1iD,iiD). These subcellular compartments are localized at the anterior end of the cell in both morning and afternoon cells. They represent 0.74% and 0.69% of the cytoplasm volume (Fig. 1iH,iiH). Note that this compartment did present some infiltration artifacts using Lowicryl HM20, in comparison to Epon Hard embedding.

Interestingly, the morning and afternoon cells presented a reticulated network (Fig. 1iE,iiE, Chapter III, Fig. 4). In both cases, this compartment is principally localized at the cell periphery, but presents some protrusions towards the cell center. However, in the morning cell, I could note the presence of crystalline inclusions in this compartment, which I had initially identified as reticulated network based on its organization and appearance. Relating back to the TEM screen analysis, it could be possible that the crystalline compartment and reticulated network could be the same subcellular structure. According to this hypothesis, the reticulated network could potentially present crystalline inclusions in some physiological stages or cell cycle stages for instance. In the morning and afternoon cells, this compartment represents respectively 18.10% and 9.66% of the cytoplasm volume (Fig. 1iH,iiH).

The pusule (Fig. 1iF,iiF), positioned at the anterior end of the cell, represents respectively 0.51% of the cytoplasm volume in the morning and 0.16% in the cytoplasm volume in the afternoon cell (Fig. 1iH,iiH). In both *Prorocentrum cf. gracile* cells, the pusule presented a intricated sheet like organization (Fig. 1iF,iiF).

The cells both present two types of trichocysts, that we divided in length classes as previously in Mocaer et al., 2023. The long trichocysts measure in average 14.9 µm (sd ±3.4 µm, n=3) in the morning sample and 12 µm (sd ± 1.5 µm, n=5) in the afternoon sample in length and in both cells they are emanating from the Golgi area (Fig. 1iG,iJ,iiG,iJ). The shorter trichocysts are more abundant and present a similar size between the two cells. They measured in average 3.8 µm (sd ± 1.0 µm, n=19) in the morning cell and 3.5 µm (sd ± 0.8 µm, n=33) in the afternoon cell (Fig. 1iG,iJ,iiG,iJ). They are distributed at the cell periphery, pointing towards the cell surface (Fig. 1iG,iiG). Note that the short trichocysts were present in higher proportions in the afternoon, compared to the morning cell (Fig. 1iG,iiG). Overall, the trichocysts represented 1.38% and 2.07% of the cytoplasm volume (Fig. 1iH,iiH).

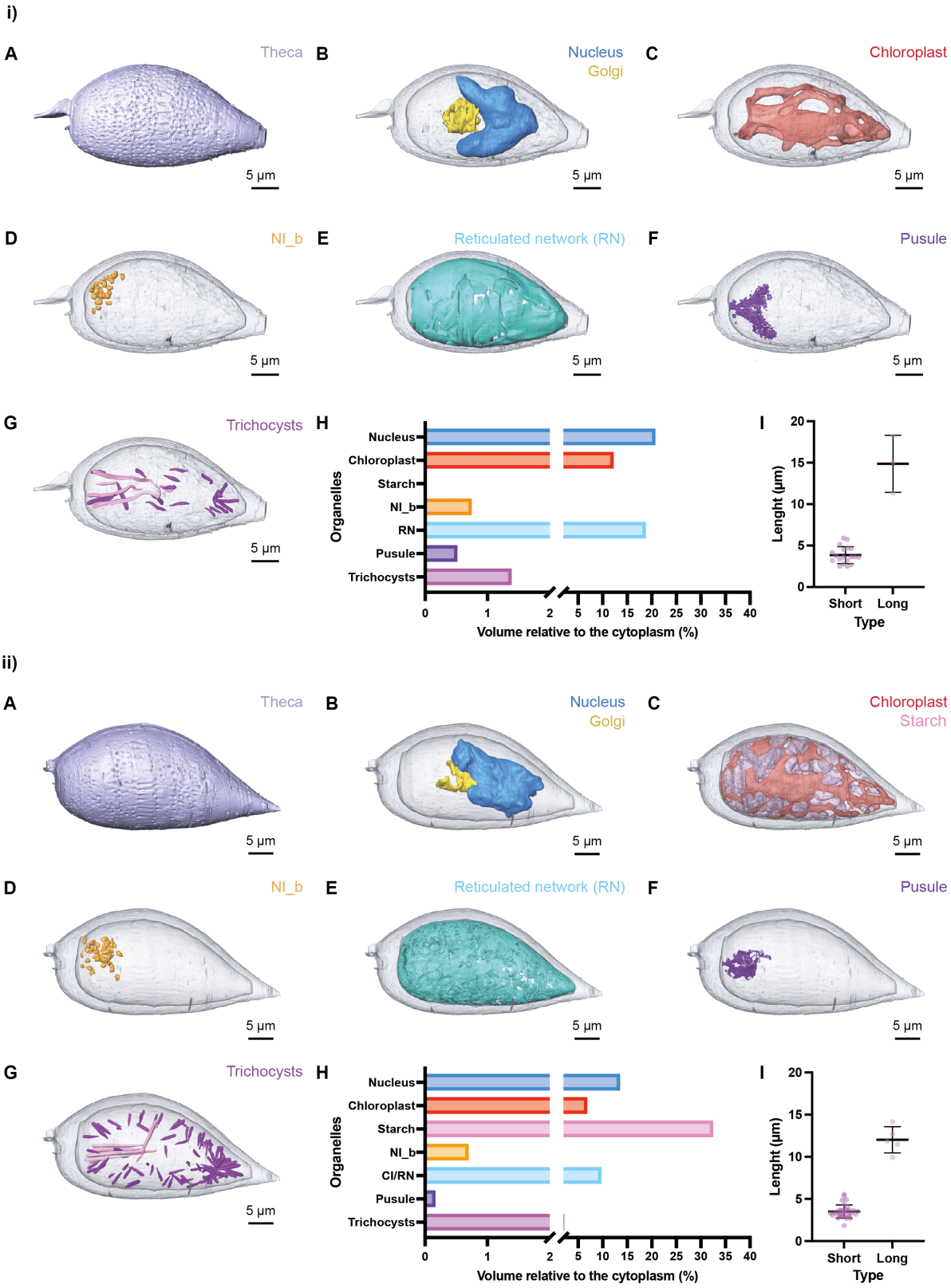

Figure 3: Morphometric analysis of a subset organelles from morning sampled and afternoon sampled *Prorocentrum cf gracile.* i) Volume rendering and morphometrics of *Prorocentrum cf gracile* collected in the morning. ii) Volume rendering and morphometrics of

Prorocentrum cf gracile collected in the afternoon. i-ii) A) Rendering of the segmentation of the theca in ventral view (blue-grey), B-G) The panels are in the same orientation as the cell shown in the top A panel, the outline of the theca and cytoplasm are visible in light grey transparency. B) Rendering of the segmentation of the nuclear envelope (NE, in blue) and Golgi apparatus (yellow). C) Rendering of the segmentation of the chloroplast (red in transparency) and starch (light pink in transparency). D) Rendering of the segmentation of the classes of "non identified organelles b"(Chapter III, Fig5. b) (orange). E) Rendering of the segmentation of the reticulated network (RN, light blue). Crystalline inclusions were observed in this compartment in the morning cell (called CI/RN in the panel H). F) Rendering of the segmentation of the pusule (purple). G) Rendering of the segmentation of the trichocysts, the class of long trichocysts is shown in light pink and the class of short trichocyst in darker pink, H) Morphometric of the different organelles, their volume in μm^3 is expressed as relative of the entire cytoplasm volume, respectively 2777.47 μm^3 for the upper panel and 4382.36 μm^3 for the lower panel. I) Size distribution of the trichocysts (i) n=3 long and n=18 short trichocysts, ii) n=4 long and n=32 short trichocysts, the mean and standard deviation are shown in the graph).

4.2- Triadinium cf. sphaericum

This cell was targeted as I was interested in confirming the presence of the granular organelle "d" and the organelle "o" described in the TEM screen (Chapter III, Fig 5). As in the TEM screen, these organelles were present in a round shaped cell, presenting a wide and distinguishable cingulum and which showed the presence of radially organized chloroplast, I targeted for a cell presenting this overall morphology and which presented an autofluorescence signal when excited at 633 nm (Chapter IV, Fig. 11 *Triadinium*). The following paragraph describes the results concerning the cells organization as well as the morphometric parameters in *Triadinium* imaged respectively from a morning and an afternoon sample.

4.2.1 Description of the cell volume and morphometric analysis

The cells from morning and afternoon samples both measured approximately 30 µm in diameter. The cells appeared spherical and presented the following tabulation 3',6'', 6c, 5''', 2p, 1''''. Note that thus far I could not resolve the sulcal plates from my SEM and vEM dataset. From the tabulation, as well as micrographs from the SEM screen and the precious help of Prof. Dr. Hoppenrath, Dr. Kenneth Mertens and Dr. Nicolas Chomerat, I could identify this cell as *Triadinum cf. sphaericum* (Previously *Goniodoma sphaericum,* order Gonyaulacales*,* Murray and Whitting, 1899). The whole cells, and the cytoplasm volumes were respectively 15416 μm^3 and 9898 μm^3 for the cell collected in the morning, and 14793 μm^3 and 8508 μm^3 for the cell collected in the afternoon. Note that microorganisms from this genus are generally lacking morpho-molecular information.

The theca of both *Triadinium cf. sphaericum* cells were segmented and rendered (Fig. 2iA,iiA). The cells, of spherical shape, present a large and prominent cingulum dividing the cell in two approximately centrally, as reported in Murray and Whitting, 1899. Numerous thecal pores are visible and distributed homogeneously across the thecal plates (Fig. 2iA).

Both cells, from the morning and afternoon collection, present a large nucleus, positioned in the right bottom quadrant (Fig. 2iC,iiC). The nucleus each occupy respectively 13.25% and 12.21% of the morning and afternoon cell's cytoplasm (Fig. 2iI,iiI). The morning cell presents n= 81 chromosomes of an average volume of 5.96 μm^3 (sd ± 9.82 μm^3), and the afternoon one shows n=73 chromosomes with had an average volume of 5.98 μm^3 (sd ± 1.01 μm^3).

The Golgi Apparatus, divided in approximately 40 stacks is located close to the nucleus, and present a hemispherical shape (Fig. 2iC,iiC).

Triadinium cf sphaericum cells present a chloroplast with a radial distribution. While larger lobes were present close to the cell cortex, fine structures were spanning through the cell centers forming connections throughout the cell volume (Fig. 2iC,iiC). The chloroplasts represent respectively 9.47 and 9.16% of the cytoplasm volume from the cell collected in the morning and the afternoon (Fig. 2iI,iiI).

Interestingly, both cells presented a food vacuole (Fig. 2iD,iiD). The food vacuoles occupy respectively 0.39% of the morning cell cytoplasm volume and 0.19% of the afternoon cell cytoplasm volume (Fig. 2iI,iiI). The presence of this structure suggests that *Triadinium cf sphaericum* could be mixotrophic and not only phototrophic.

The cell collected in the afternoon presented structures identified as putative starch granules (Fig. 2iD). However, the cell collected in the morning did not show these structures (Fig. iiD). This observation is similar to what was observed in *Prorocentrum cf. gracile*, and is consistent with results of the TEM screen analysis. For *Triadinium cf. sphaericum* collected in the afternoon, the putative starch granules represent 0.95% of the cell's cytoplasm volume (Fig. 2iI,iiI).

Both cells presented the "non-indentified" organelles "d" and "o" that had been associated to this cell type in the TEM screen previously. In both morning and afternoon cells, these organelles are localized mostly in the apical part of the cell (Fig. 2iD,iiD). They represent respectively 0.90% and 1.42% of the cell's cytoplasm for "d", and 0.10% and 0.33% of the cells cytoplasm for "o".

Morning and afternoon cells of *Triadinium cf. sphaericum* presented a reticulated network. Differently than in *Prorocentrum cf. gracile* this structure was spanning throughout the cell volume and enveloping most cellular structures as for instance the pusule or the nucleus (Fig. 2iF,iiF). In both cases, these structures occupy a significant part of the cytoplasm volume, respectively 19.94% in the cell from the morning sampling and 7.78% in the cell from the afternoon sampling (Fig. 2iI,iiI).

Both cells presented a pusule, these pusular systems present a large spherical shape. In the case of the morning cell, it also presents some protrusions spanning through the cytoplasm (Fig. 2iG,iiG). These protrusions were not observed in the cell collected in the afternoon, however, the pusule structure was a bit damaged in this cell and I can't exclude that it is not present. Overall, these structures represent 1.27% of the cytoplasm volume in the cell collected from the morning and 7.75% of the cytoplasm volume from the cell collected from the afternoon (Fig. 2iI,iiI).

Interestingly, *Triadinium cf sphaericum* only presented one size class of trichocysts in both morning and afternoon cells. For both cells, 40 trichocysts were measured. In average, they measure 2.7 (sd ±0.5 µm) for the cell collected in the morning and 2.6 µm (sd ±0.3 µm) in the cell collected in the afternoon (Fig. 2iJ,iiJ). As for *Prorocentrum cf. gracile*, *both Triadinium cf sphaericum* cells present a similar average size for their trichocyst.

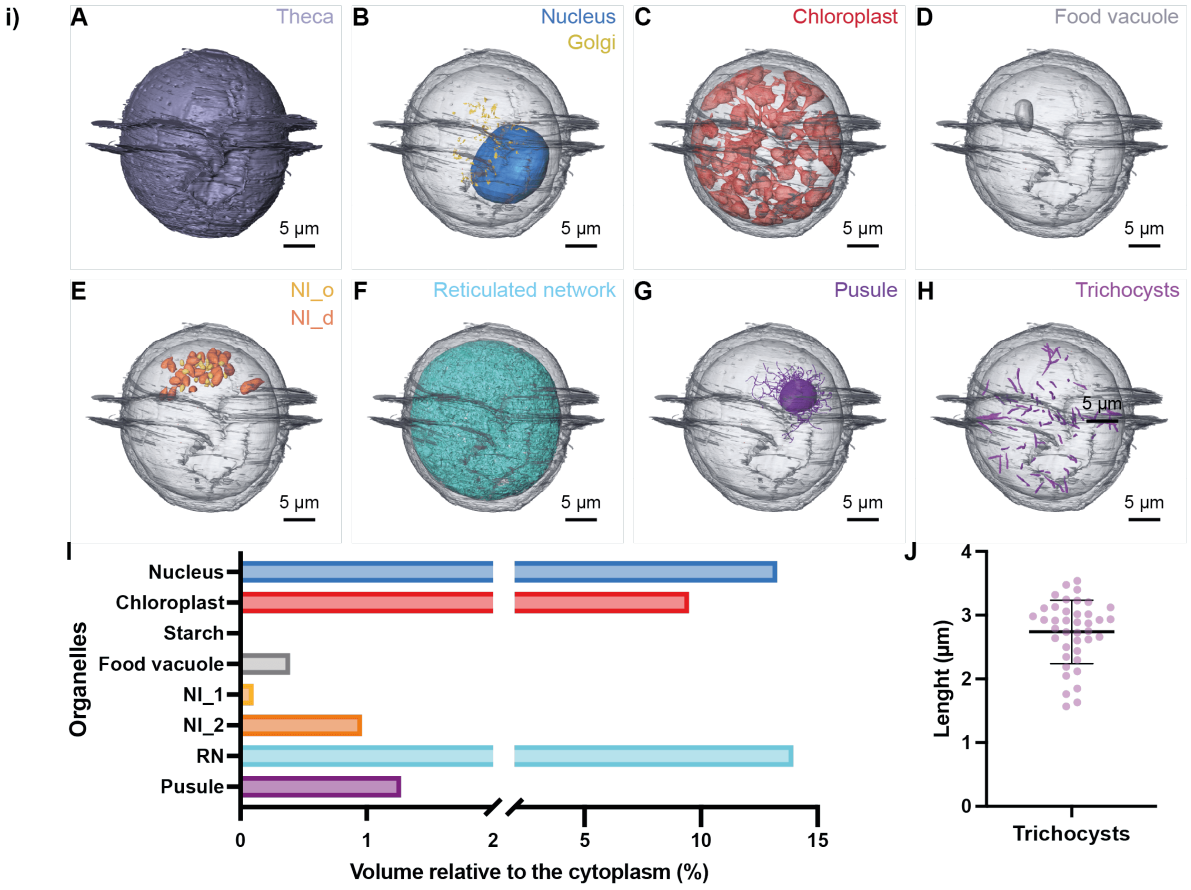
i)
A
Theca
B
Nucleus
Golgi
C
Chloroplast
D
Food vacuole
E
NI_o
NI_d
F
Reticulated network
G
Pusule
H
Trichocysts
5 µm
I
Nucleus
Chloroplast
Starch
Food vacuole
NI_1
NI_2
RN
Pusule
Organelles
0
1
2
5
10
15
Volume relative to the cytoplasm (%)
J
Lenght (µm)
0
1
2
3
4
Trichocysts

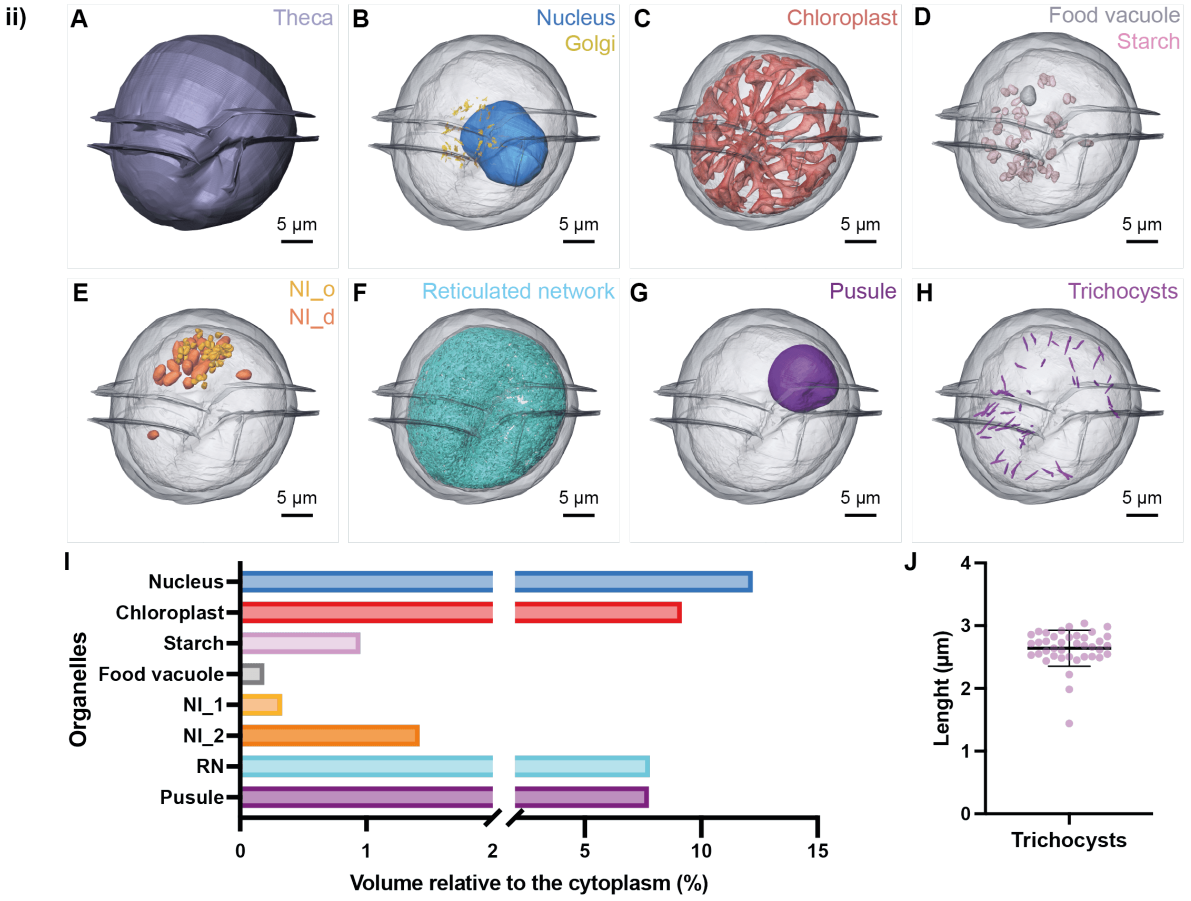
ii)
A
Theca
B
Nucleus
Golgi
C
Chloroplast
D
Food vacuole
Starch
E
NI_o
NI_d
F
Reticulated network
G
Pusule
H
Trichocysts
5 µm
I
Nucleus
Chloroplast
Starch
Food vacuole
NI_1
NI_2
RN
Pusule
Organelles
0
1
2
5
10
15
Volume relative to the cytoplasm (%)
J
Lenght (µm)
0
1
2
3
4
Trichocysts

Figure 2: Morphometric analysis of a subset organelles from morning sampled and afternoon sampled *Triadinium cf sphaericum.* i) Volume rendering and morphometrics of *Triadinium cf sphaericum* collected in the morning. ii) Volume rendering and morphometrics of *Triadinium cf sphaericum* collected in the afternoon. i-ii) A) Rendering of the segmentation of the theca in ventral view (blue-grey), B-H) The panels are in the same orientation as the cell shown in the top A panel, the outline of the theca and cytoplasm are visible in light grey transparency. B) Rendering of the segmentation of the nuclear envelope (NE, in blue) and Golgi apparatus (yellow). C) Rendering of the segmentation of the chloroplast (red in transparency). D) Rendering of the segmentation of the putative starch granules (light pink) and food vacuole (grey). E) Rendering of the segmentation of the classes of "non identified organelles o and d" (Chapter III, Fig5. d-o) (orange). F) Rendering of the segmentation of the reticulated network (RN, light blue). G) Rendering of the segmentation of the pusule (purple). H) Rendering of the segmentation of the trichocysts (pink), I) Morphometric of the different organelles, their volume in μm^3 is expressed as relative of the entire cytoplasm volume, respectively 9898.25 for the upper panel and 8508.09 μm^3 for the lower panel. J) Size distribution of the trichocysts (n=40, mean and standard deviation are shown in the graph).

4.3 Photosynthetic dinoflagellates collected in the afternoon presented more plastoglobuli in the vEM datasets compared to the morning

After analysis of the TEM screen, one result was the presence of a higher abundance of plastoglobuli in plastid bearing dinoflagellates in samples collected in the afternoon compared to the morning (Chapter III, Fig. 6, Fig. 8). Thus, in my vEM datasets, I segmented and analysed the amount of plastloglobuli present in *Prorocentrum cf. gracile* and *Triadinium cf. sphaericum* from both morning and afternoon samples (Fig. 4). Interestingly, the results recapitulated the population wide observations made in the TEM screen. As a matter of fact, while *Prorocentrum cf. gracile* and *Triadinium cf. sphaericum* from the morning sampling session presented respectively 15 and 13 plastoglobuli (Fig. 3A-B, upper panels), the same species collected in the afternoon presented each 401 plastoglobuli (Fig. 3A-B, lower panels).

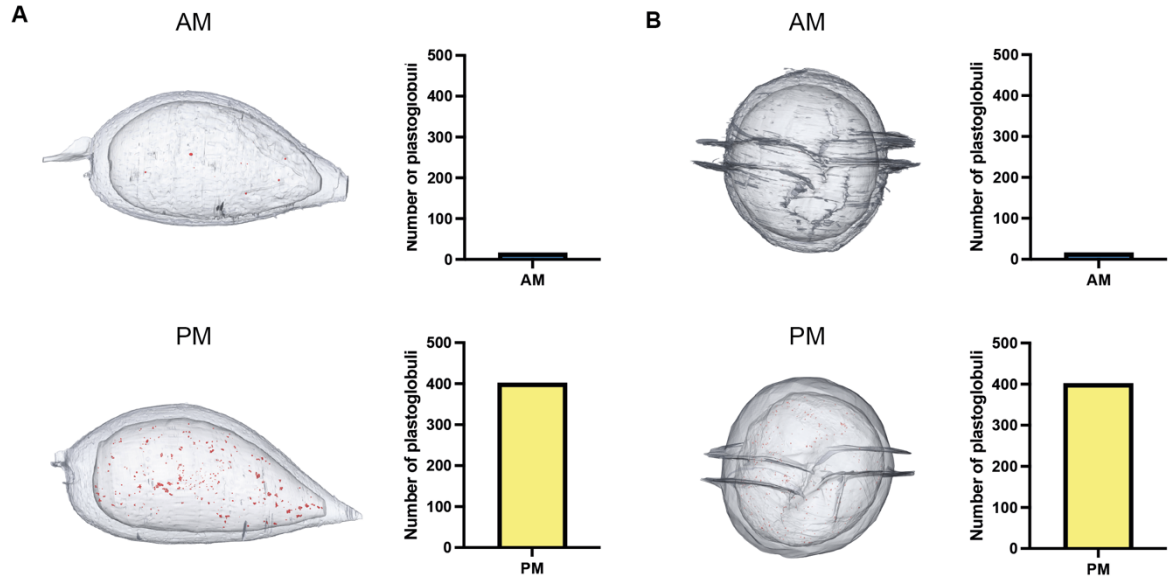

Figure 3: Distribution of plastoglobuli in *Prorocentrum cf. gracile* and *Triadinium cf sphaericum* collected in the morning and the afternoon. A-B) On the left panels are the rendering of the segmentation of plastoglobuli (in red), as well as of the theca and the cytoplasm for each cell (ventral views). The amount of segmented plastoglobuli is shown on the right panels. A) The morning collected *P. cf. gracile* showed 15 plastoglobuli, and the afternoon *P. cf. gracile* showed 401 plastoglobuli. B) The morning *T. cf. sphaericum* showed 13 plastoglobuli and the afternoon *T. cf. sphaericum* showed 401 plastoglobuli.

4.4- Pseudalatosphaera cf. corsica

This cell was targeted as I was interested in investigating the presence of electron dense sheets, found to be particularly abundant in heterotrophic cells from the TEM screen analysis (Chapter III, Fig 4, Fig. 9). As in the TEM screen, some spherical cells were presenting these electron dense sheets organelles mostly in one part of the cell, and did not present chloroplast I targeted for a cell presenting this overall morphology and which did not present autofluorescence signal when excited at 633 nm (Fig. 5). The following paragraph describes the results concerning the cells organization as well as the morphometric parameters in *Pseudalatosphaera* imaged respectively from two morning samples.

4.4.1 Description of the cell volume and morphometric analysis

The cells acquired by vEM appeared oval (Fig. 4iA,iiA), with a height of respectively 24µm and 29.2µm, and a width of respectively 21.8 and 27.2 µm. The tabulation I could resolve for both cells is 3', 1a, 5'', 3c, 4''', 1iiii. Thanks to the tabulation, the SEM data and the help of Prof. Dr. Mona Hoppenrath, I could resolve this cells as *Pseudalatosphaera cf. corsica* (Carbonell-Moore, Zézan, K.N Mertens and Chomérat *gen. nov,* Mertens et al., 2023). These cells did

not present a cingulum and only presented a small sulcal area. The thecal plates were covered by small pores. Interestingly, in my vEM dataset, both cells presented a layer resembling polysaccharidic material on the cell's surface, which was not visible in the SEM dataset.

The cytoplasm volumes are respectively 4173.84 μm^3 (Cell volume of 6107.11 μm^3) and 7911.59 μm^3 (Cell volume of 1225.65 μm^3)

The cells present a nucleus localized at the antiapical pole of the cell (Fig. 4iB,iiB). The nuclei each represent respectively 13.9% and 11.72% of the cell volume (Fig. 4iH,iiH). Interestingly, in both cases the chromosomes are connected to each other at the nucleus periphery. The chromosomes present a total volume of respectively 298.4 μm^3 and 446.4μm^3.

The Golgi apparatus, organized as a hemisphere, is located in close proximity with the nucleus (Fig. 4iB,iiB).

Both cells show a large food vacuole (Fig. 4iD,iiD), occupying respectively 7.33% and 3.35% of the cytoplasm volume (Fig. 4iH,iiH). Additionally, neither of these cells present a chloroplast. These cells thus belong to the heterotrophic microorganisms.

Furthermore, electron lucent vesicles could be observed in proximity to the food vacuole (Fig. 4iD,iiD). These compartments were identified as "reserves" but their nature needs to be confirmed by further analysis. These compartments represent respectively 0.68 and 0.67% of the cytoplasm volume (Fig. 4iH,iiH).

This cell type, as *Prorocentrum* and *Triadinium* cells described above, presents a reticulated network (Fig. 4iD,iiD). The organization of this network is similar to what is observed in *Triadinium cf. sphaericum* and surrounds most subcellular organelles. It represents 9.88 and 21.71% of the cytoplasm volume for each cell respectively (Fig. 4iH,iiH)..

As visualized in the TEM screen, we could see in this cell an electron dense compartment with very strong striated arrangement distributed on one side of the cell. From the vEM data, I could further identify that these compartments are present at the cell posterior in both cases (Fig. 4iE,iiE). These structures occupy respectively 6.01 % and 5.47 % of the cytoplasm volume (Fig. 4iH,iiH).

Furthermore, a bundle of tubular structure resembling rhabdosomes, also visible in the TEM screen (Chapter III, Fig. 4), could be observed in the antapical part of the cell (Fig. 4iE,iiE). These bundles both have a similar position and orientation. They are spanning from the basal body area along the nuclear region. Their organization differ from what was described for rhabdosomes in *Dinophysis* species for which the distribution was suggested to be radial within the cell (Berland et al., 1995). The nature or function of this organelle is still unknown to the best of my knowledge. These structures occupy respectively 0.16 and 0.08% of each cell's cytoplasm (Fig. 4iH,iiH).

The pusule of these organisms presented two structures. In the first cell, a pusule organized as sheets is visible (Fig. 4iF), when both sheets and a globular organization are present in the second cell (Fig. 4iiF). The pusule volumes represent 0.06% and 2.48% of the cytoplasm volumes respectively (Fig. 4iH,iiH).

Lastly, a number of trichocysts were segmented and rendered for each cells (n= 24 and n=11, Fig. 4iG,iiG). As in *Triadinium cf. sphaericum* only one class of trichocyst was visible. They measured in average 4.2 µm (sd± 0.69 µm) for the first cell and 4.8 µm (sd ± 1.12 µm) for the second cell (Fig. 4iI,iiI).

Pseudalatosphaera cf. corsica, as *Triadinium cf. sphaericum* and *Prorocentrum cf. gracile* presents a highly stereotypical organization (Fig. 4). As a matter of fact, the position of the nucleus (Fig. 4B), food vacuole (Fig.4D), electron dense sheet compartment (Fig. 4E) as well as the trichocysts arrangement (Fig. 4G) was highly similar between the two cells imaged with FIB-SEM. This suggests that cells from these species are polarized, and that this polarization probably has a functional importance.

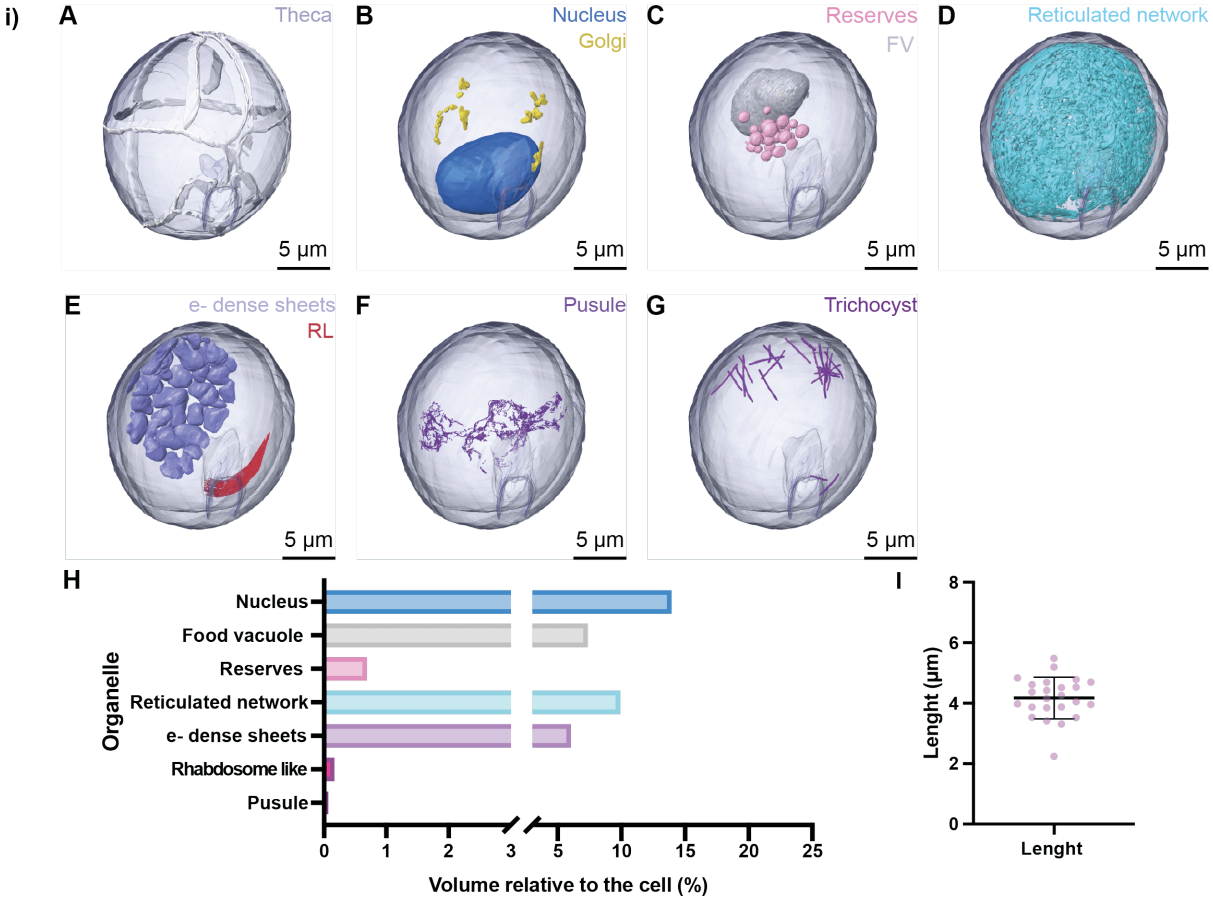
i)
A
Theca
5 µm
B
Nucleus
Golgi
5 µm
C
Reserves
FV
5 µm
D
Reticulated network
5 µm
E
e- dense sheets
RL
5 µm
F
Pusule
5 µm
G
Trichocyst
5 µm
H
Nucleus
Food vacuole
Reserves
Reticulated network
e- dense sheets
Rhabdosome like
Pusule
Organelle
0 1 2 3 5 10 15 20 25
Volume relative to the cell (%)
I
Lenght (µm)
0 2 4 6 8
Lenght

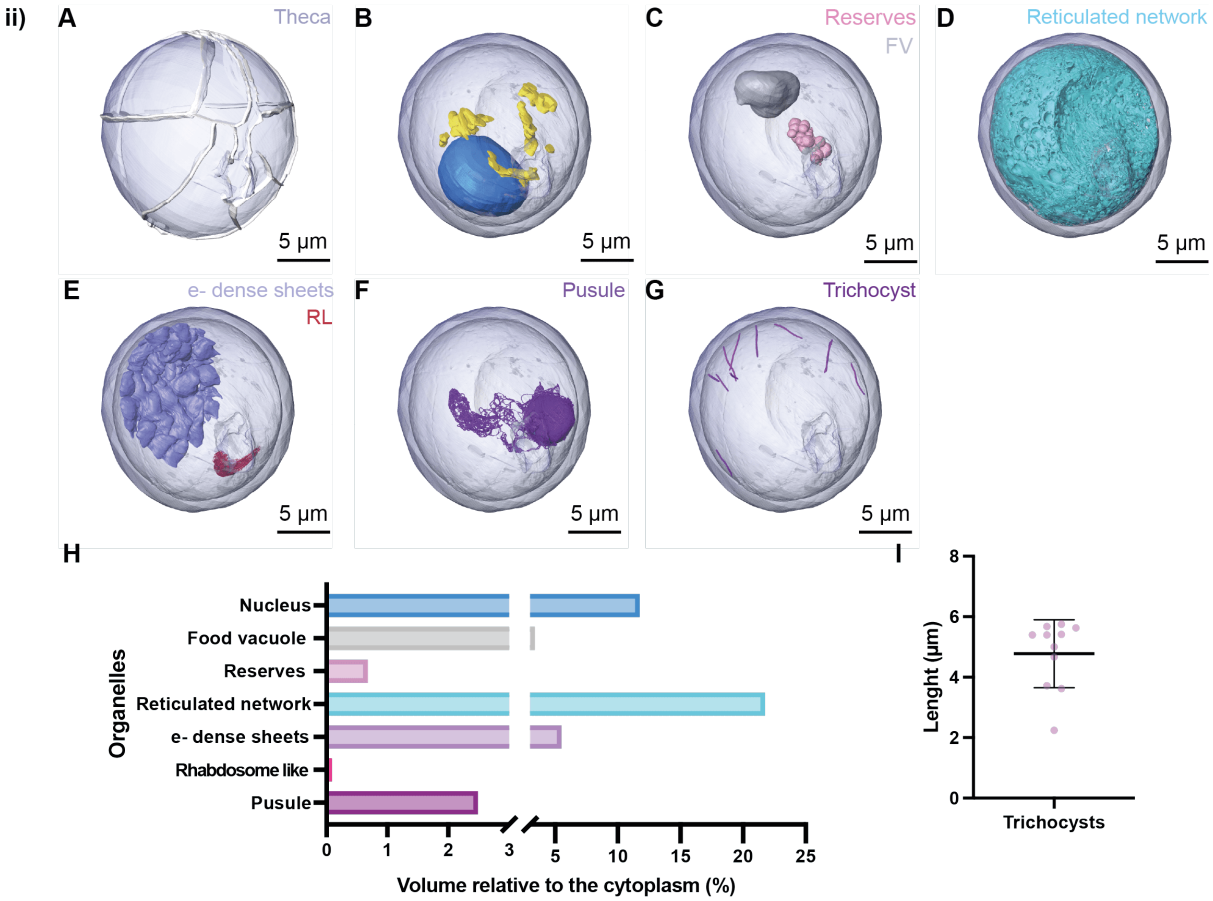
ii)
A
Theca
5 µm
B
5 µm
C
Reserves
FV
5 µm
D
Reticulated network
5 µm
E
e- dense sheets
RL
5 µm
F
Pusule
5 µm
G
Trichocyst
5 µm
H
Nucleus
Food vacuole
Reserves
Reticulated network
e- dense sheets
Rhabdosome like
Pusule
Organelles
0 1 2 3 5 10 15 20 25
Volume relative to the cytoplasm (%)
I
Lenght (µm)
0 2 4 6 8
Trichocysts

Figure 4: Morphometric analysis of a subset organelles from morning sampled and afternoon sampled *Pseudalatosphaera cf. corsica.* i-ii) Volume rendering and morphometrics of *Pseudalatosphaera cf. corsica* collected in the morning. i-ii) A) Rendering of the segmentation of the theca in right lateral/ventral view (blue, in transparency), plates are rendered in white, B-G) The panels are in the same orientation as the cell shown in the top A panel, the outline of the theca and cytoplasm are visible in light grey transparency. B) Rendering of the segmentation of the nuclear envelope (NE, in blue) and Golgi apparatus (yellow). C) Rendering of the segmentation of the "reserves" (light pink) and food vacuole (grey). D) Rendering of the segmentation of the reticulated network (RN, light blue). E) Rendering of the segmentation of the classes of "non identified organelles" (Chapter III, Fig4). The compartment showing electron dense striated structures is shown in purple and "rhabdosome like" structures in red (Chapter III, Fig4). F) Rendering of the segmentation of the pusule (purple). G) Rendering of the segmentation of the trichocysts (pink), H) Morphometric of the different organelles, their volume in μm^3 is expressed as relative of the entire cytoplasm volume, respectively 4173.84 μm^3 for the upper panel and 7911.59 μm^3 for the lower panel. I) Size distribution of the trichocysts (n=24 in the upper panel and n=11 in the lower one, mean and standard deviation are shown in the graph).

4.4.2 Autofluorescence profile of the electron dense striated compartment

After investigating of the autofluorescence profile in HM20 blocks for the cells *Pseudalatosphaera cf. corsica*, I could visualize a signal in the posterior part of the cell when exciting at 490 nm. After performing an emission scan for this excitation on the Leica Stellaris system, I could visualize in the two cells analyzed a pic between 630 and 670 nm (Fig. 5). After imaging a z-stack of this signal, it seems to correspond to the electron dense striated compartment (Fig. 4iE,iiE). Indeed, this correlation between the signal and structure was confirmed by first imaging autofluorescence signal in the second cell (Fig. 5), and further performing FIB-SEM on the same cell (Fig. 5ii).

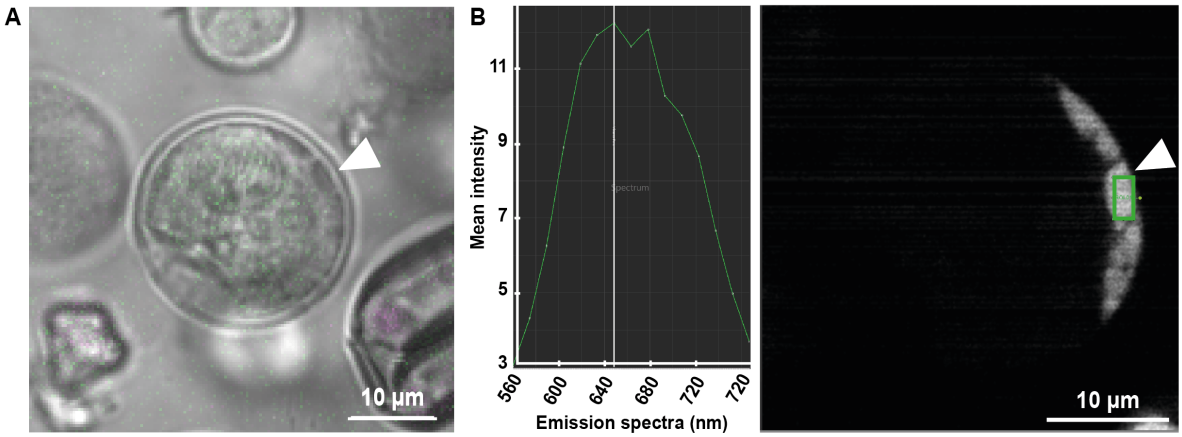

Figure 5: Autofluorescence profile of the electron dense striated compartment of *Pseudalatosphaera cf. corsica*. A-B) The same cell was imaged in HM20 resin with the Zeiss LSM 780 NLO for localization and Stellaris system (Leica Microsystems) to acquire an emission spectrum. A) shows the overlay of a single slice of transmitted light and fluorescence confocal imaging after excitation at 633 nm (magenta) and at 488 nm (green) from *Pseudalatosphaera cf. corsica.* The white arrow indicates a subcellular characteristic allowing to recognize this species, identified as the electron dense striated compartment in vEM. B) shows the emission profile of the autofluorescent compartment (ROI shown in green) after excitation at 490 nm.

5- Discussion

From the TEM screen and thanks to vEM analysis, I identified a set of organelles that seems to be specific to certain genus or trophic modes. Thanks to the vEM imaging and its 3D analysis presented in this chapter, it is possible to better understand the distribution of these organelles within the cell. Interestingly, the dinoflagellate cells analyzed here and in Chapter III seem to present a strong polarity. Overall, this ultrastructural study could help to bring additional information that could be useful for taxonomical identification subcellular features.

Interestingly, the pusule which was previously described as potential taxonomical indicator seems to present various organization depending on the life cycle or conditions cells are living in. This was also described by Abe, 1981. Indeed, in my vEM dataset *Pseudalatosphaera cf.corsica* presented both a globular pusule as well as a sheet-like pusule. Thus, vEM investigations can bring complementary information on the overall organisation and context of specific organelles, not allowed by 2D TEM. Performing vEM more consistently on the studied organisms could help determine further the set of compartments correlated to certain species.

I now characterized the morphology and distribution of a subset of organelles using TEM and vEM. However, in order to study further these organelles and try to understand their potential role in a cellular context, complementary analyses are necessary. One interesting aspect would be to study the elemental or biochemical composition of these organelles thanks to EDX, or on section mass spectrometry. For instance, further investigating the role of the reticular network, found in large portion of dinoflagellates spanning throughout the cytoplasm in close proximity to many organelles, would be very interesting.

Additionally, in order to tackle the physiological role of these subset of organelles, it would be important to study the subset of species analyzed here in cultured conditions. While

Prorocentrum species can be found in culture collections, to the best of my knowledge, the other species are not available in culture systems to this day. One possibility for dinoflagellates not present in cultures could be of isolating and enriching for these cells from collection in Villefranche-sur-mer at a similar time point. This could allow to perform multimodal complementary analysis (such as proteomics, transcriptomics, metabolomics …) in order to investigate further these organisms and their organelles.

Furthermore, if possible, it would be interesting to try to maintain these organisms in cultures in order to be able to study the cells life cycle, being able to tamper with this system and thus tackle more specific questions.

Interestingly, the observations made during the TEM screen concerning the more important number of plastoglobuli in the chloroplast of photosynthetic cells, as well as the higher abundance of starch, could be confirmed in our vEM datasets. This support that the use of TEM screens allows to probe for ultrastructural variations when sampling across different conditions.

6- References

Abe, T. H. (1981). Studies on the Family Peridinidae an Unfinished Monograph on the Armoured Dinoflagellata. *Publ. Seto Mar. Biol. Lab. Spec. Publ. Ser.* **6**, 1–409.

Berland, B. R., Maestrini, S. Y., Grzebyk, D. and Thomas, P. (1995). Recent aspects of nutrition in the dinoflagellate *Dinophysis cf. acuminata*. *Aquat. Microb. Ecol.* **9**, 191–198.

Cohen-Fernandez, E. J., Meave Del Castillo, E., Salgado Ugarte, I. H. and Pedroche, F. F. (2006). Contribution of external morphology in solving a species complex: The case of *Prorocentrum micans, Prorocentrum gracile* and *Prorocentrum sigmoides* (Dinoflagellata) from the Mexican Pacific coast. *Phycol. Res.* **54**, 330–340.

Dodge, J. D. (1971). Fine Structure of the Pyrrophyta. *Bot. Rev.* **37**, 481–508.

Hoppenrath, M., Chomérat, N., Horiguchi, T., Schweikert, M., Nagahama, Y. and Murray, S. (2013). Taxonomy and phylogeny of the benthic *Prorocentrum species* (Dinophyceae)-A proposal and review. *Harmful Algae* **27**, 1–28.

Loeblich, A. R. (1977). Studies on synchronously dividing populations of Cachonianiei, a marine dinoflagellate. *Bull. Japanese Soc. Phycol.* **25**, 118–128.

Mertens, K. N., Carbonell-Moore, M. C., Chomérat, N., Bilien, G., Boulben, S., Guillou, L., Romac, S., Probert, I., Ishikawa, A. and Nézan, E. (2023). Morpho-molecular analysis of podolampadacean dinoflagellates (Dinophyceae), with the description of two new genera. *Phycologia* **62**, 117–135.

Mocaer, K., Mizzon, G., Gunkel, M., Halavatyi, A., Steyer, A., Oorschot, V., Schorb, M., Kieffre, C. Le, Yee, D. P., Chevalier, F., et al. (2023). Targeted volume Correlative Light and Electron Microscopy of an environmental marine microorganism. *bioRxiv* 2023.01.27.525698.

Murray, G. and Whitting, F. G. (1899). New peridiniceae from the Atlantic. *Trans. Linn. Soc. London* **Series 2.**, 321–342, pl.27–33.

Seo, K. S. and Fritz, L. (2002). Diel changes in pyrenoid and starch reserves in dinoflagellates. *Phycologia* **41**, 22–28.

Soyer-Gobillard, M. O. and Geraud, M. L. (1992). Nucleolus behaviour during the cell cycle of a primitive dinoflagellate eukaryote, Prorocentrum micans Ehr., seen by light microscopy and electron microscopy. *J. Cell Sci.* **102**, 475–485.

Zhou, J. and Fritz, L. (1993). Ultrastructure of two marine dinoflagellates, *Prorocentrum lima* and *Prorocentrum maculosum. Phycologia*.

Chapter VI: Discussion

1- Workflows development to investigate environmental microorganisms

During this study, I contributed in developing workflows in order to investigate microorganisms' subcellular morphology from environmental samples.

In this thesis, I described the protocols developed and applied in order to sample the small size fraction of marine microorganisms in Villefranche-sur-Mer and perform both TEM and targeted vEM. Generally, as environmental samples can be influenced by numerous parameters, developing strategies and acquiring tools in order to record further metadata would be crucial for a more exhaustive analysis. As a matter of fact, a better understanding of the chemistry and physical properties of where samples are originating is important to better apprehend potential variations observed at the subcellular level for instance.

Additionally, in the future, coupling this type of ultrastructural screens with further investigations such as genomics, transcriptomics, proteomics or metabolomics studies could allow to get a more comprehensive understanding of these complex microorganisms.

The TEM screens of a mixed population allowed to visualize interesting trends in morphological variations and to have a broad overview of subcellular characteristics present in the sample. Generally, building atlases and having additional taxonomical indicators such as subcellular features can be extremely valuable. In fact, this could be an additional identification tool when investigating new species or species for which the taxonomical identification is still debated. Furthermore, this screen underlined the high distribution of certain structures in heterotrophic cells. As these compartments were often found, in heterotrophs from various species, they most probably have an important functional role for these organisms.

Indeed, while this descriptive study raises various questions concerning the biology of dinoflagellates, performing complementary studies in less heterogeneous system would be very interesting. To this aim, enriching for a fraction of organisms or studying them in culture systems could permit to tackle precise mechanistic questions.

Diverse approaches could be used for enrichment, as manual isolation or developments of sorting methods. Manual isolation is time demanding and can be complex when it comes to

small cells. Moreover, if the purpose is to cryopreserve these cells for subcellular analysis, a long picking of the cells could lead to decrease in viability and thus structural changes. One drawback of cell sorting can be the complexity to select for one cell type, or the presence of strong pressure on the cells in some flow cytometers. However, the latest developments in these technologies presenting very gentle fluidics, as well as their implementation in proximity to sampling sites as done in TREC is very promising.

During the 4 pilot expeditions that I have been involved in, and further working on analysing the cells that I have collected, I realized the great challenge that goes with working on field samples, that are highly heterogeneous. When envisioning a holistic imaging approach is a fair dream, especially considering the ongoing developments in high throughput imaging techniques, I think that an intermediate, pragmatic approach would be to first focus on those organisms that can be cultured. Studies of cells in a culture system can allow to investigate their general behaviour and life cycle, but are also amenable to treatments, interferences that are essential for any further mechanistic studies.

For example, I am particularly interested by key functions of the dinoflagellates, especially swimming patterns, cell cycle stages, ability to form cysts, ability to use specific feeding mechanism or to form of a mucosphere. Accessing those in culture systems would be paramount for isolating the underlying sub-cellular morphologies, and working towards their mechanisms. Additionally, culture studies could allow to investigate the putative function of a subset of structures. For instance, if the cell presents the ability to form mucospheres, one could investigate the aspect and abundance of secretory organelles such as mucocysts by TEM or vEM. Many groups of dinoflagellates establish interactions with other cells or organisms, and we have seen in the introduction that even the feeding behaviour, can vary from one species to the other. Establishing cultures where preys and dinoflagellates can be brought in contact and monitored, one could further investigate the feeding apparatus and target this structure for vEM analysis.

As time of sampling is a sensitive parameter in environmental conditions, performing a more detailed time or condition series to investigate the effects of a gradient on microorganisms can be complex. However, performing preliminary studies in cultured system could help optimizing the experimental design of studies performed in the environment by indicating time points or conditions that might be relevant to examine for instance.

Indeed, while the TEM study allowed to perform global snapshots and assess variations, I would find interesting to investigate further the dynamical aspect of these changes in a subset

of organisms. Additionally, for this subset of organisms, one could perform complementary studies to link morphological results to more physiological information. For instance, proteomic studies on cultures grown in a day night cycle could allow to investigate whether there are there more enzymes degrading starch during the dark period in comparison to day time, or whether there are higher levels of proteins involved in the photosynthetic apparatus during the day. I have been involved in such a study, on polar diatoms, collaborating with the group of Chris Bowler from the ENS, Paris. This was an enlightening experience for me because I could apprehend the power of plankton cultures, even at different scales from lab cultures to mesocosms. This group is also studying field samples and establish frequent crass-talks between wild species and almost clonal cultures, a foundation for hypothesis driven research, keeping a close relation to the environment.

2- TEM screen and observation of organelles potentially associated to certain genera or subcellular variation at the population level

As shown in this thesis, the TEM screen and its analysis can be a powerful tool to assess the diversity of morphologies existing in various microorganisms from their native habitat.

This analysis allowed to observe subcellular variations, at the population level, revealing for example that the starch volume and the number of plastoglobuli in plastids dramatically change in multiple taxa of dinoflagellates. Further assays to better understand metabolic fluctuations in dinoflagellate across the diurnal cycle could allow to better understand the physiology of these microorganisms. While it would be interesting to study starch fluctuations using complementary modalities, I would also be interested in investigating variations in lipid contents which can be lost or badly preserved in preparation for electron microscopy.

This TEM screen revealed a strong correlation between the presence (or absence) of a subset of structures and certain genera. Following up on this TEM screen (Chapter III), whilst many organelles are of known nature, I would find very keen to further characterize the unidentified organelles. Thus, performing elemental analysis of these areas using EdX or using techniques like NanoSIMS on sections to try to identify their composition would allow to draw hypothesis on the potential role of these organelles.

In particular, I would like to investigate the nature of the crystalline inclusions present in various genera (Chapter I, Fig. 12, Chapter III, Fig. 4 and Chapter IV, Fig. 10). Investigating in culture conditions how this compartment fluctuates during the diurnal cycle or the life cycle of various organisms could allow to go towards a better understanding of its potential role within the cell

as a storage compartment or reflectors for photon as described in Chapter I, 3.10.4 Crystalline inclusions (Jantschke et al., 2019; Mojzeš et al., 2020).

Finally, whilst the systematic acquisition of 2D images across the pellet of field samples is powerful to assess the morphologies of the whole community, only a few species can be recognized. In parallel, metabarcoding of the same fractions reveals its biodiversity, and it is for new very challenging to find systematic matches between genomic and morphologic taxonomy. Developing strategies to confirm the identification of species directly on the TEM sections using FISH-CLEM strategies (Jahn et al., 2016) could allow to validate the hypothesized correlations between certain organelles and specific genera.

3- Targeting of organisms for vEM using endogenous fluorescence

As vEM techniques are still limited by the volume that can be imaged, targeting strategies are very valuable tools in order to study a particular event, region of interest or in our case microorganism in a complex, highly heterogenous single cell community. Furthermore, as many microplanktonic cells can't be kept in culture to this day, this strategy allows to study these organisms in a culture free system directly from the environment. Additionally, if the possibility of isolating cells of interest is challenging due to the size of the organism for instance, this type of targeting method permits to postpone the isolation or selection step to a later stage where the cell is preserved within a resin block.

Additionally, I believe that there is more to correlating 3D light and electron microscopy data than just a targeting use. In Chapter IV, it was possible to overlay endogenous autofluorescence signal to a precise ultrastructural region. It is thus within reach to assign a fluorescence pattern to an organelle.

Further studies on the rich and diverse autofluorescence spectra of these marine microorganisms could allow to associate fluorescence profiles to specific organisms. Moreover, it could allow to investigate the origin of each type of endogenous fluorescence by associating them to an ultrastructure permitting a more comprehensive understanding of these structures. Some studies have indeed shown that phytoplankton can present compartments as accumulation bodies, eyespots or other pigmented organelle which present various fluorescence profiles (Ying and Dobbs, 2007). Whether these different autofluorescence profiles are preserved inside the resin block is to be investigated, but if it was the case, multispectral analysis of resin embedded specimens could become an additional mean to investigate field samples.

Finally, I have shown in my thesis work how volume EM can reveal the innermost features of environmental cells. When further analysed, for example by performing semantic, instance segmentation, organelles can be further described, by their complex shapes, volumes and number as well as their mutual interactions. In my thesis, I have performed such segmentation manually, which was a considerable effort, but still at reach because the number of cells that I have investigated was limited. With the constant progress of vEM techniques and their application to field samples, it is obvious that automated, AI-based workflows have to be developed.

4- References

Jahn, M. T., Markert, S. M., Ryu, T., Ravasi, T., Stigloher, C., Hentschel, U. and Moitinho-Silva, L. (2016). Shedding light on cell compartmentation in the candidate phylum Poribacteria by high resolution visualisation and transcriptional profiling. *Sci. Rep.* **6**, 1–9.

Jantschke, A., Pinkas, I., Hirsch, A., Elad, N., Schertel, A., Addadi, L. and Weiner, S. (2019). Anhydrous β-guanine crystals in a marine dinoflagellate: Structure and suggested function. *J. Struct. Biol.* **207**, 12–20.

Mojzeš, P., Gao, L., Ismagulova, T., Pilátová, J., Moudříková, Š., Gorelova, O., Solovchenko, A., Nedbal, L. and Salih, A. (2020). Guanine, a high-capacity and rapid-turnover nitrogen reserve in microalgal cells. *Proc. Natl. Acad. Sci. U. S. A.* **117**, 32722–32730.

Ying, Z. T. and Dobbs, F. C. (2007). Green autofluorescence in dinoflagellates, diatoms, and other microalgae and its implications for vital staining and morphological studies. *Appl. Environ. Microbiol.* **73**, 2306–2313.